Ressources naturelles Canada
Natural Resources Canada

GEOLOGICAL SURVEY OF CANADA
OPEN FILE 8203

Caprock integrity of the Carboniferous Frederick Brook Shale analyzed by oil and gas well logs: McCully gas field and Elgin area, New Brunswick

S. Séjourné

2017

GEOLOGICAL SURVEY OF CANADA
OPEN FILE 8203

Caprock integrity of the Carboniferous Frederick Brook Shale analyzed by oil and gas well logs: McCully gas field and Elgin area, New Brunswick

S. Séjourné[1]

[1] Consulting geologist, Montreal, Quebec

2017

doi: 10.4095/299664

This publication is available for free download through GEOSCAN (http ://geoscan.nrcan.gc.ca/).

Recommended citation
Séjourné, S., 2017. Caprock integrity of the Carboniferous Frederick Brook Shale analyzed by oil and gas well logs: McCully gas field and Elgin area, New Brunswick; Geological Survey of Canada, Open File 8203, 120 p. doi: 10.4095/299664

Publications in this series have not been edited; they are released as submitted by the author.

Table of content

List of tables

List of figures

List of appendices

Summary

This study allowed to establish the geomechanical properties of the Carboniferous Frederick Brook Member (Albert Formation, Horton Group) and its Carboniferous-Permian cover succession, based on petrophysical log data from available oil and gas wells, both at the scale of individual wells and at the regional level, for the McCully gas field and the adjacent area of Elgin.

The Young's modulus, the Poisson's ratio, two brittleness indexes as well as the intensity of the minimum horizontal principal stress were defined. The representativeness of the results derived from the raw logs has been verified by calculating synthetic parameters for additional wells whose dataset was incomplete, and by the comparison of the log results to independent laboratory data.

At the scale of the individual well the results highlight the presence of net geomechanical contrasts between the Frederick Brook Member and the overlying Hiram Brook Member, as well as within the cover succession above these two units. In a context of hydraulic fracturing these mechanical contrasts translate into the existence of barriers that would limit the propagation of hydraulic fractures outside the Frederick Brook Member.

At the regional scale it was noted that the same geomechanical contrasts than those recognized at the well scale are present and confirmed the homogeneity of the mechanical properties within the McCully gas field as well as between this field and the Elgin area. The latter area geologically stands out however, by the absence of evaporite deposits in the Windsor Group.

Further work is recommended in order to better understand the role played by natural fractures – if present – in the possible migration paths through the caprock of the Frederick Brook Member shale. As such it would be relevant to examine the natural fracturing patterns using available geological data and to implement one or more observation wells out of the drilling pads, following the subsurface trajectory of the deviated wells that have been hydraulically fractured, in order to highlight the migration or the absence of migration of fluids in the geological medium at distance from the surface casing of the wells.

List of abbreviations

Abbreviations in the text

BRIT :	Acoustic brittleness index (0 to 100)
E :	Young's modulus (expressed in GPa)
G :	Shear modulus (expressed in GPa)
g :	Gravitational force or g-force (9.806 x 10^{-3} kPa/m)
GPa :	Gigapascals
Grad_* :	Gradient of the parameter identified by the asterisk (expressed in [units of the parameter]/m)
GSC :	Geological Survey of Canada
KB :	Kelly bushing (rotary table of the drill rig)
kPa :	Kilopascals
MD :	Measured depth
MW :	Density of the drilling mud (expressed in kg/m^3)
Pp :	Pore pressure (expressed in kPa)
Shmin :	Minimum horizontal principal stress (expressed in kPa or in GPa)
Sv :	Lithostatic pressure (expressed in kPa)
UWI :	Unique Well Identifier
VD :	Vertical depth
α :	Biot's poroelastic constant (dimensionless)
υ (nu) :	Poisson's ratio (dimensionless)
ρ (rho) :	Bulk density of the rock (expressed in kg/m^3)
*_SYNTH :	Parameter identified by the asterisk, calculated from the synthetic data

Abbreviations in the logs

BRIT_MINERAL (0 to 100) :	Mineralogic brittleness index
BRIT_SONIC (0 to 100) :	Acoustic brittleness index
BRIT_SYNTH (0 to 100) :	Synthetic acoustic brittleness index derived from DTS_SYNTH
CALI (mm) :	Caliper
CALX (mm) :	Caliper
CTR :	Indicates that the curve is centered in the column
DTP (µsec/m) :	P wave slowness derived from the raw data
DTS (µsec/m) :	S wave slowness derived from the raw data
GR (GAPI) :	Gamma ray
HCAL (mm) :	Caliper
NPOR (V/V) :	Neutron porosity, limestone matrix
PEF (b/e) :	Photoelectrique factor
PR (0 à 0,5) :	Poisson's ratio derived from the raw data
RD (ohm/m) :	Deep resistivity
RHOB (kg/m^3) :	Bulk density
SH_MIN (GPa) :	Minimun horizontal principal stress Shmin
VCAL (0 à 1) :	Proportion of calcite
VCARB (0 à 1) :	Proportion of carbonates (calcite and dolomite)
VCLA (0 à 1) :	Proportion of clay
VDOL (0 à 1) :	Proportion of dolomite
VPYR (0 à 1) :	Proportion of pyrite
VQUA (0 à 1) :	Proportion of quartz
YM (GPa) :	Young's modulus derived from the raw data
*_RAW :	Parameter identified by the asterisk, calculated from the raw data
*_GRAD :	Gradient of the parameter identified by the asterisk (SH_MIN_GRAD is expressed in kPa/m, DTS_SYNTH is expressed in µsec/m)
*_SYNTH :	Parameter identified by the asterisk, calculated from the synthetic data

1. Introduction

1.1 Context of the study

This work was undertaken at the request of the Geological Survey of Canada, Quebec division (GSC-Quebec), and is part of the wider study on the vulnerability of aquifers to industrial activities in a gas field located in the region of Sussex, southern New Brunswick.

More specifically, this project aims to estimate and analyze the geomechanical properties of the Carboniferous Frederick Brook Member (Albert Formation, Horton Group) and its Carboniferous-Permian cover succession from oil and gas well data available in the McCully gas field and the nearby area of Elgin (figure 1). The results of the study will support ongoing studies undertaken by the GSC-Quebec in the area (figure 2).

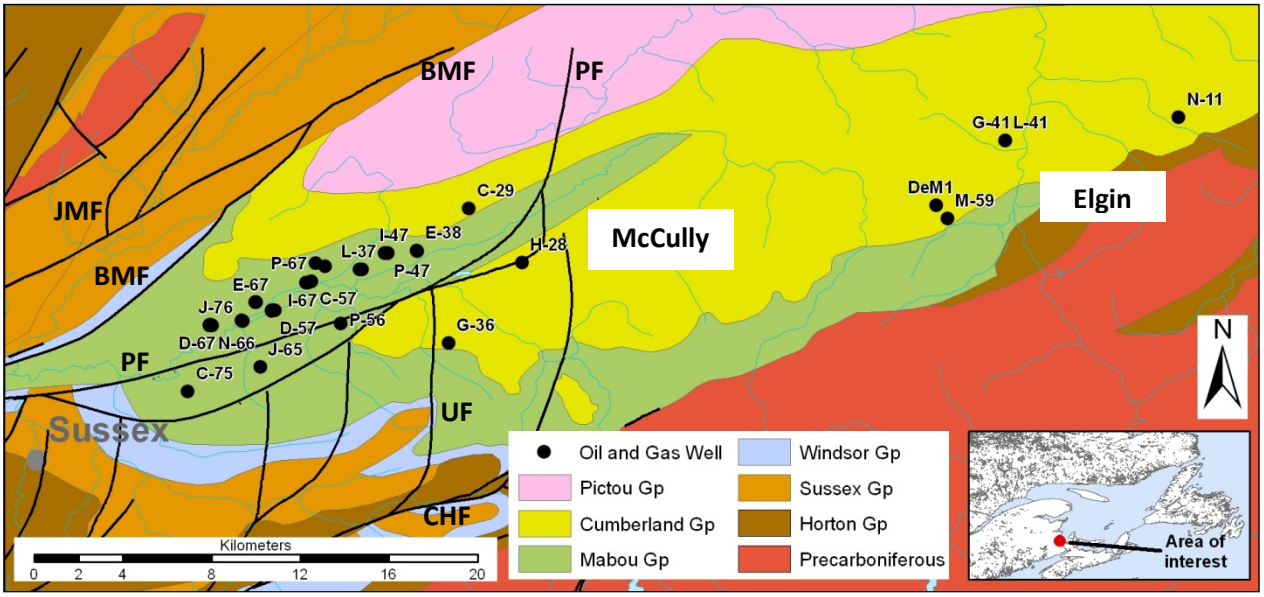

Figure 1 : Simplified geological map of the region of interest with location of the wells studied in the McCully gas field and the sector of Elgin. JMF : Jordan Mountain fault; BMF : Berry Mills fault; PF : Penobsquis fault; UF : Urney fault; CHF : Clover Hill fault. See figure 2 for details of the location of the wells in the McCully field. Adapted from : New Brunswick Department of Natural Resources (2008).

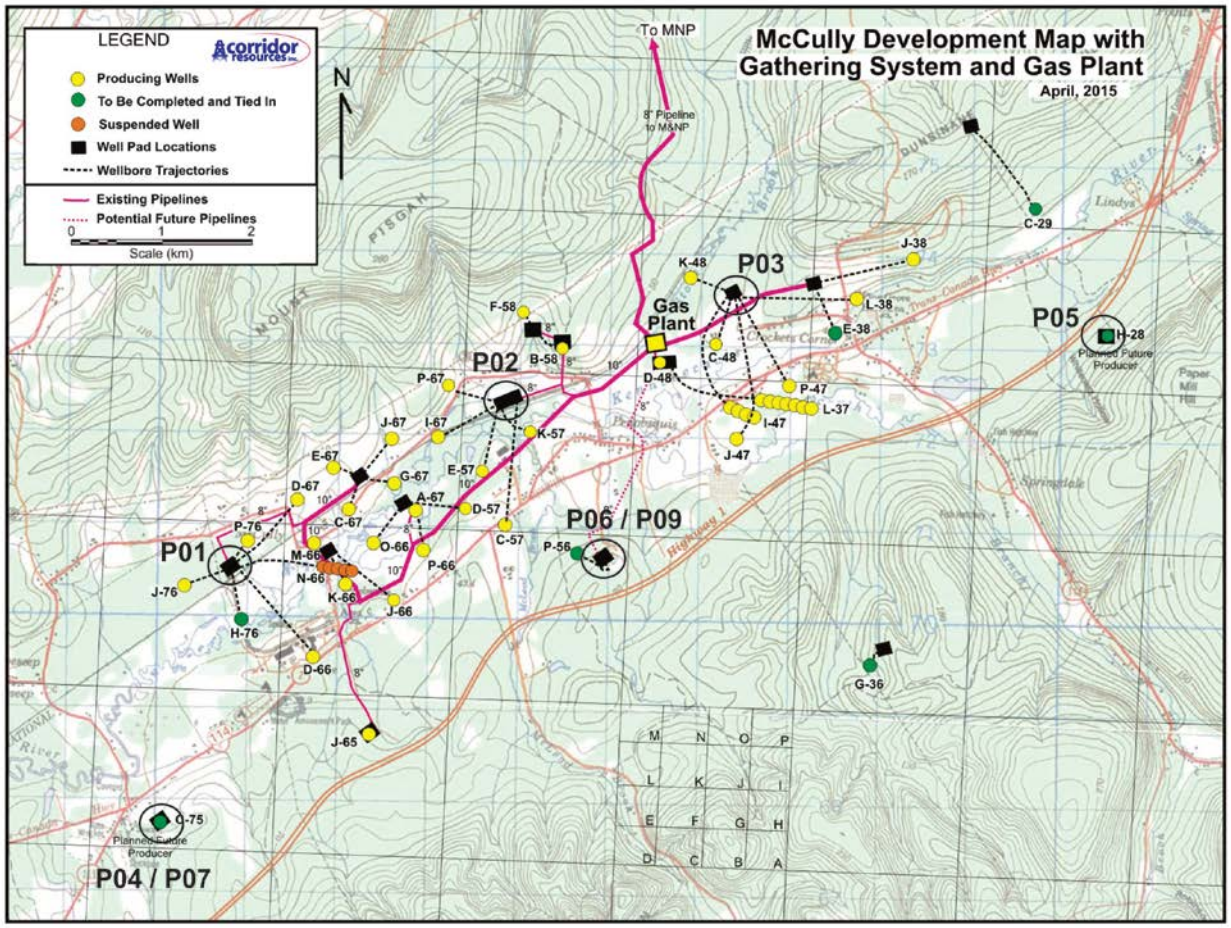

Figure 2 : Surface location of the wells in the McCully field with their projected subsurface trajectories. The black circles identify the drill pads selected by the GSC-Quebec for the drilling of observation wells in the scope of the project on the vulnerability of aquifers to industrial activities in the McCully gas field. Pxx are GSC observation wells drilled in 2015-2016. Adapted from : Corridor Resources (2016).

1.2 Project objectives

The overall aim of this study is to estimate the geomechanical properties of the shale-dominated Frederick Brook Member (Albert Formation, Horton Group) and its cover succession at the scale of a gas field of approximately 60 km^2, based on the available petrophysical logs.

To this end, the acoustic logs (P and S waves) are used to derive the elastic moduli (Young's modulus, Poisson's ratio). A brittleness index is also derived from these properties so as to depict more clearly the subtle qualitative variations observed in the mechanical stratigraphy of the Frederick Brook Member and its cover succession. Pressure data available for some of the studied wells are also analyzed to highlight the variations of the minimum horizontal principal stress and to identify, if appropriate, possible barriers to the propagation of hydraulic fractures.

1.3 Scope and limitations of the study

In a context of hydraulic fracturing the pressure exerted by the fracturing fluid is designed to initiate and propagate fractures in a medium initially devoid of natural fractures, as well as to reopen pre-existing fractures. The elastic moduli estimated in this study allow to evaluate the behavior of the rock in the first case, i.e. considering the rock as a homogeneous and isotropic medium. This is a necessary simplification insofar as the available data do not allow, for the moment, to characterize precisely the heterogeneity and the degree of anisotropy of the Frederick Brook Member and its cover succession. The minimum horizontal principal stress gives an idea of the ease with which certain fractures will be opened or reactivated. In the case of induced hydraulic fractures or in the case of natural fractures that are not cemented the relationship is simple. In the case of cemented natural fractures (veins) knowing the value of the minimum horizontal principal stress is not sufficient to appreciate the ease with which the veins will be reactivated and additional parameters must be taken into account, namely the cohesive strength and the coefficient of internal friction of the rock and of the cement that seals the veins. These parameters can only be estimated from laboratory data, which are not available in this study.

Finally it should be noted that the results presented here are qualitative and relative in nature and cannot be used for purposes of planning a campaign of hydraulic fracturing in the field.

1.4 Geological setting

1.4.1 Stratigraphy

The study area is located in the southwestern part of the Moncton sub-basin. This northeast-southwest oriented sub-basin extends over 200 km between Sussex and Moncton in southern New Brunswick and is part of the larger Carboniferous-Permian Magdalen Basin in eastern Canada (figure 3).

The internal stratigraphy of the Moncton sub-basin (and other Carboniferous-Permian sub-basins) is complex as the result of dominant continental, lacustrine and fluvial deposits with significant and rapid facies changes. The following lithostratigraphic description (figure 4) should be seen as a summary of a complete succession, in many cases the internal stratigraphy (at the formation and intraformation scales) can vary.

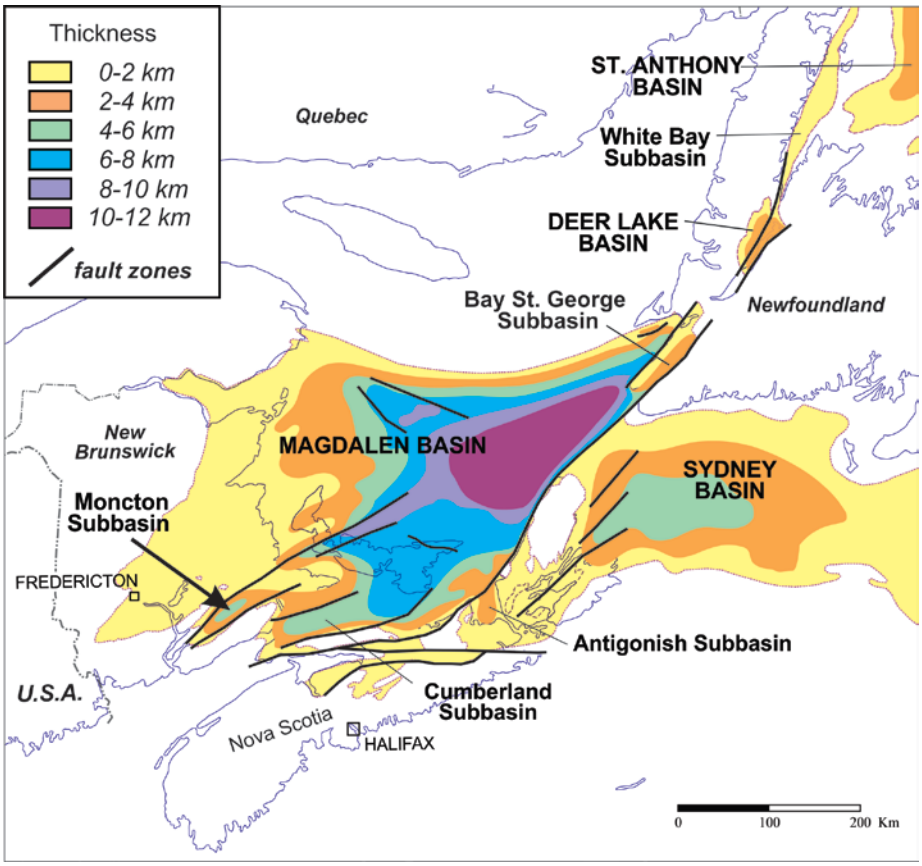

Figure 3 : Regional isopach map of the Devonian-Permian successions of the western part of the Magdalen Basin. The Moncton sub-basin is at the western reach of the Magdalen Basin. Modified from Lavoie et al. (2009).

The basal part the sub-basin is underlined by a series of conglomeratic red beds, the Memramcook Formation (Upper Devonian) of the Horton Group. Within the Horton Group, these conglomerates are overlain by an assemblage of sandstones, siltstones and shales of the Dawson Settlement and of the McQuade Brook members who are laterally equivalent at the base of the Lower Carboniferous (Tournaisian) Albert Formation. The overlying Frederick Brook Member (Albert Formation) is dominated by shales, although a more dolomite-rich shale unit is also recognised at its base. The overlying Hiram Brook Member (Albert Formation) is characterized by an assemblage of sandstones and shales. The deposition of the Horton Group ends with a series of red beds attributed to the Bloomfield Formation. The Lower Carboniferous (Tournaisian) Sussex Group unconformably overlies the Horton Group. It consists mainly of conglomeratic red beds, shales and sandstones. The depositional environments of the Horton and Sussex groups are proximal continental to lacustrine (Martel, 2013; Keighley and Noftall, 2014; Keighley and St. Peter, 2015). The Sussex Group is unconformably overlain by the Lower Carboniferous (Visean) Windsor Group. The carbonates of the Gays River and Macumber formations at the base of the Windsor Group correspond to an important and unique marine transgression in the entire Magdalen Basin, which is followed by the filling of the sub-basin by evaporite deposits at the top of the Windsor Group. The overlying Lower to Upper Carboniferous (Visean to Namurian) Mabou Group also shows a continental affinity and is dominated by red bed sandstones. Finally the Upper

Carboniferous (Namurian to Westphalian) Cumberland (sandstones and mudstones) and Pictou (sandstones, mudstones and coal beds) groups consist of a fluviatile-dominated succession and each of these groups has a basal unconformity. Each unconformity observed in the Moncton sub-basin corresponds to a tectonic pulse accompanied by an interruption in the sedimentation.

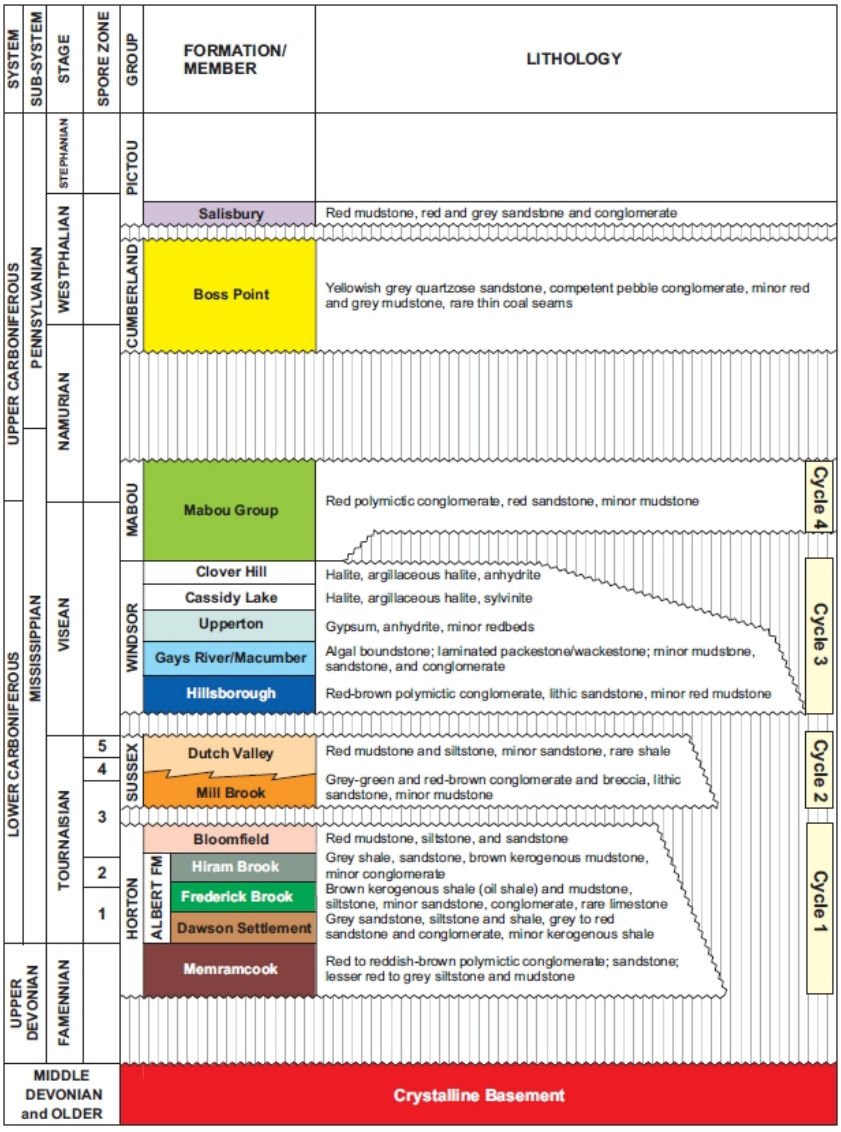

Figure 4 : Simplified stratigraphy of the study area. Source : Hinds and St. Peter (2006).

1.4.2 Structure

A simplified geological cross-section across the McCully gas field illustrates the structural architecture of the study area (figure 5). This architecture is dominated by the decoupling between a thrust-dominated tectonic style expressed near the surface and another, mostly extensional with local inversions at greater depths. The transition from one structural style to the other is marked by the regional Penobsquis fault at the base of the Windsor Group (Hinds and St. Peter, 2016).

North of the gas field the structural architecture is dominated by a system of imbricated faults whose structural front, marked by the Penobsquis fault, propagates to the south above the gas field. The age of this fold and thrust belt postdates the sedimentation of the Sussex Group rocks and the deformation evolved later (after the end of the Lower Carboniferous and the sedimentation of the Mabou Group) in a series of right-lateral strike-slip faults oriented along an east-north-east axis (figure 1).

In the center and to the south, Carboniferous and older strata are crosscut by a series of steeply-dipping faults interpreted as normal faults that were possibly inverted during the Tournaisian after the sedimentation of the Horton and the Sussex groups rocks (Wilson, 2003). In the central area (McCully field), these faults are responsible for a significant increase in the thickness of the Horton Group and for the individualization of open folds. The gas field itself is an anticline oriented east-north-east (Durling and Martel, 2001).

South of the McCully field, the orientation of the faults becomes strongly influenced by the geometry of the basement as showed by the deflections of the Clover Hill and the Urney faults (figure 1) against an interpreted basement high (Hinds and St. Peter, 2016).

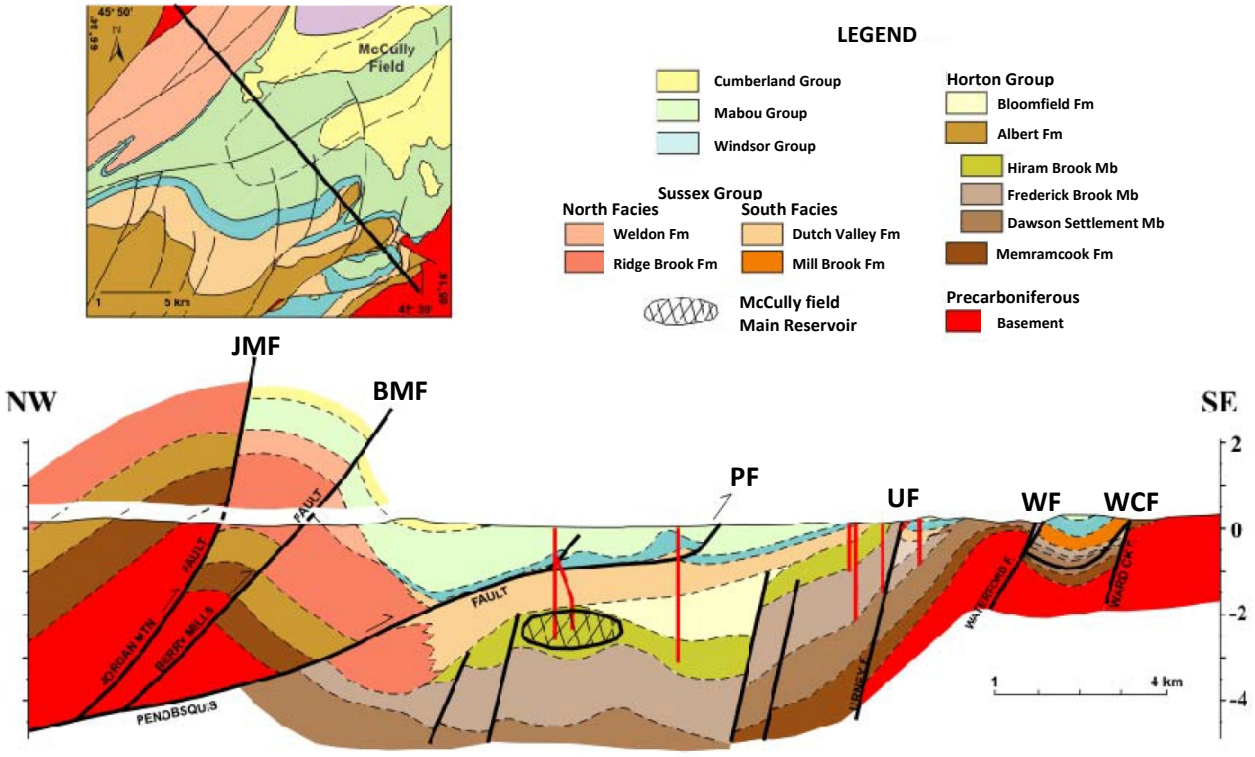

Figure 5 : Simplified geological cross-section the study area showing the location of the McCully gas field. Source : Adapted from Hinds and St. Peter (2016). Fm : Formation; Mb : Member; JMF : Jordan Mountain fault; BMF : Berry Mills fault; PF : Penobsquis fault; UF : Urney fault; WF : Waterford fault; WCF : Ward Creek Fault.

1.4.3 Reservoirs

The main conventional reservoir identified in the study area corresponds to the Hiram Brook Member in the McCully gas field (figures 1 and 5). This field spans over about 15 km long and 5 km wide and was discovered in 2000 (Hinds and St. Peter, 2016). Before this date the region had already been the subject of several exploration campaigns, but these programs primarily targeted the potash resources of the Windsor Group and exploration wells prior to 2000 had not penetrated the Hiram Brook Member. This member consists of dark to gray and locally bituminous shales and tight sandstones. The exploitable gas resource is concentrated in a series of metre- to plurimeter-thick sandstone intervals (designed by the operators as levels A to G). The main source rock corresponds to the interbedded organic-rich shales within the Hiram Brook Member itself and a secondary source is present immediately below with the shales of the Frederick Brook Member (figures 4 and 5). Some end of drilling reports also mention trace amounts of liquid hydrocarbons. In addition to the tight nature of the sandstones (average porosity of 8% and very low permeability), the trap is formed by the anticline geometry of the structure, by the presence of shaly intervals, intra-formational faults, and stratigraphic pinch-outs, and by an extensive unconformity at the base of the overlying Sussex Group (Durling and Martel, 2001; Keighley and St. Peter, 2015) (figure 5). There are currently 30 wells in production in the McCully field, drilled directionally from a dozen surface sites (figures 2 and 6). Low volume hydraulic fracturing seems to be the best method to produce gas from these tight sandstones. Five other drilling pads exist on the periphery of the field, each containing at least one well awaiting completion (figure 2).

A second conventional reservoir could also exist below the Frederick Brook Member, in the sandstones of the Dawson Settlement Formation (Hinds and St. Peter, 2016), but the wells that have penetrated this unit to date have failed to confirm this potential.

Finally, in Nova Scotia, the Lower Carboniferous Gays River Formation locally consists of porous reefs of sizeable diameter (>100 m) (Lavoie et al., 2009). However, these reefs are currently not recognized in southern New Brunswick.

In addition to conventional reservoirs, the McCully and Elgin areas also include an unconventional reservoir of importance, the shale gas of the Frederick Brook Member. To date this unit has been drilled by only a small number of wells, but these wells have delivered promising results with respect to shale gas potential production. In particular, four wells drilled in the McCully gas field have begun to produce in 2015 while two other wells drilled in the Elgin area have produced gas to surface after a period of test (Corridor Resources, 2015). The successful completion method for this type of play consists in massive hydraulic fracturing, either propane-based or slickwater-based. Most of these wells are vertical or oblique, only one has been drilled horizontally to date. A siliceous shale unit at the top and a more dolomitic shale unit at the base are distinguished within the Frederick Brook Member. On the basis of available production test results, the latter unit appears to be more productive than the overlying siliceous shale (Martel, 2013).

A project of delineation of the resource, in the form of a series of vertical wells located between the McCully gas field and the Elgin area, has been contemplated by the operator until the province declared a moratorium on massive hydraulic fracturing in 2016.

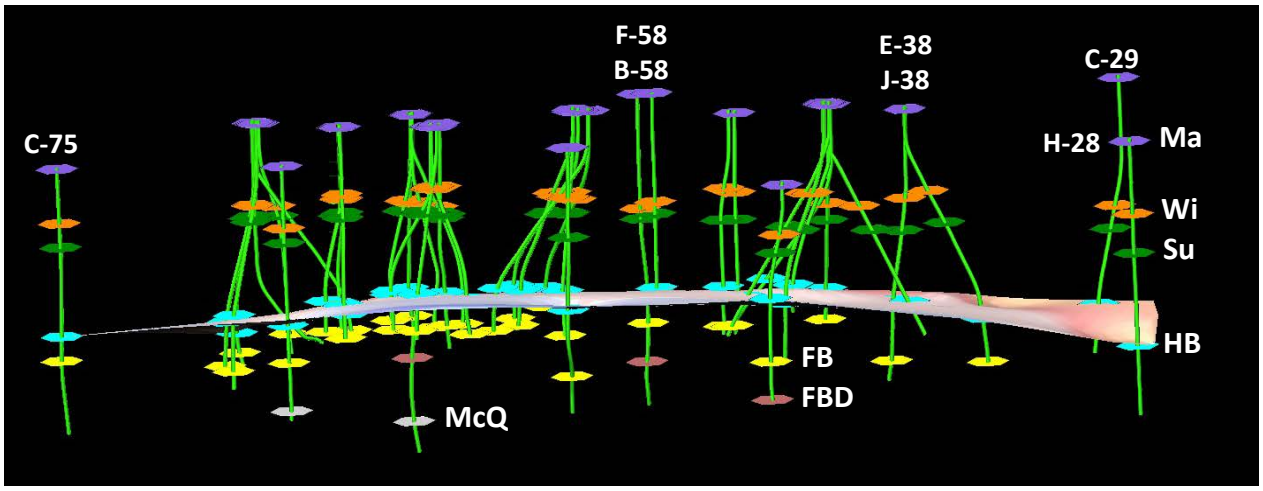

Figure 6 : Three dimensional view to the North of the wells trajectories in the McCully field. A contour map of the top of the Hiram Brook Member is represented, as well as the top of the stratigraphic units considered in this study (Ma : Mabou Group; Wi : Windsor Group; Su : Sussex Group; HB : Hiram Brook Member; FB : Frederick Brook Member; FBD : dolomitic Frederick Brook Member; McQ : McQuade Brook Formation). Some wells are indicated for orientation purpose, all wells are located on figure 2.

2. Data integration

2.1 Log data

The petrophysical logs of forty-six oil and gas wells have been examined for the McCully gas field (forty-one well) and for the Elgin area (five wells). Of these wells, twenty-six were prioritized for the geomechanical analysis because of the quality and completeness of their data sets (table 1). Fifteen other wells were temporarily discarded from the initial study because the data were incomplete (mainly because the S-wave log was missing), but these wells were examined nonetheless so as to get complementary information in a second stage (table 2). Finally, five wells were permanently discarded because of the deficiency of their petrophysical records (table 3). All of the studied wells are located on figure 1. The studied wells are referred to by their unique well identifier number (UWI) and the full name of each well is recorded in Appendix I.

For the purposes of the study, the logs in their LAS digital format have been formatted and integrated. For all wells, the curves considered herein include the gamma ray, the caliper, the porosity density, the neutron porosity, the resistivity curves, the photoelectric factor, the P and S waves, the bulk density and the density correction curve. Other types of logs were also available for some wells, and were also incorporated as appropriate, including the spectral gamma ray, the mineralogy, the total gas count and the drill rate. The abbreviations for the different log curves mentioned in this report are explained in the section "List of abbreviations".

Deviation surveys were also available for all wells, either in digital format or in end of drilling reports. These surveys have been systematically integrated to calculate the vertical depth. Figure 6 illustrates the trajectory of the wells for the McCully gas field.

Table 1 : Wells selected for this study, with compilation of the stratigraphic units for which the geomechanical properties can be estimated from the raw data. Elastic moduli were calculated for each well presented in this table and the result for each well is recorded in appendix II. Statistical summaries have been prepared for eighteen of these wells. Wells excluded from these statistics are those for which the S-wave or the bulk density logs were of poor quality, as mentioned in the last column. Shmin : The minimum horizontal principal stress has also been calculated for these wells. Mb. : Member; Gr. : Group. HB : Hiram Brook Member; FB : Frederick Brook Member. See the list of abbreviations for the identification of log curves.

Well	Curves DTS + DTP + RHOB available :					Shmin	Note
	Frederick Brook Mb.	Hiram Brook Mb.	Sussex Gr.	Windsor Gr.	Mabou Gr.		
B-58		X					
C-29		X	X				DTS mediocre in Sussex+HB
D-57		X	X				
E-38	X	X				X	
E-67	X	X	X			X	
F-58	X						
G-36	X	X	X			X	DTS-RHOB mediocre in HB
G-41	X	X	X			X	
G-67		X	X			X	
H-28			X	X	X	X	
J-38		X	X			X	DTS-RHOB mediocre in Sussex
J-47	X	X	X			X	DTS mediocre in HB+FB
J-65	X	X					DTS-RHOB mediocre in HB+top FB
J-66		X					
J-67		X					
K-48		X	X				
K-57		X				X	
K-66		X					
L-38		X	X				DTS mediocre in HB
M-66		X					
McC1		X	X	X	X		
N-11					X		
O-66		X					
P-47		X	X				DTS mediocre in Sussex+HB
P-56		X					DTS-RHOB mediocre in HB+FB
P-66		X	X	X	X	X	

Table 2 : Wells excluded from the geomechanical study conducted from the raw data, due to the absence of an S-wave in the logs record. Synth. : A synthetic S-wave curve was calculated for these wells. Mb. : Member; Gr. : Group. See the list of abbreviations for the identification of log curves.

Well	Curve DTS missing but DTP + RHOB available :					Synth.	Note
	Frederick Brook Mb.	Hiram Brook Mb.	Sussex Gr.	Windsor Gr.	Mabou Gr.		
C-48		X	X				
C-57			X				
C-67		X					
C-75	X	X	X	X	X	X	RHOB mediocre
C-82			X	X			RHOB mediocre
D-48			X	X	X		
D-66	X	X	X			X	
D-67	X	X	X				
DeM1	X	X	X	X	X	X	DTP-RHOB mediocre
E-57		X					
H-76		X	X				
I-67		X	X				
J-65			X	X	X	X	
J-76		X					
M-59		X				X	
P-67			X				

Table 3 : Wells permanently discarded because of the lack of log coverage. See the list of abbreviations for the identification of log curves.

Well	Reason for rejection from the study
I-47	DTP and RHOB are the only curves available, over 392 m
L-37	GR is the only curve available
L-41	GR is the only curve available
N-66	DTP and RHOB are the only curves available, over 157 m
P-76	Good coverage but DTS and RHOB missing

2.2 End of drilling reports

The end of drilling reports allow to supplement the data available for the studied wells. These reports include, among other things, the following information :

- The tour sheets,
- the daily drilling reports,
- the description of the cuttings,
- the interpreted top of the stratigraphic units,
- the geological log with the gas shows and the drilling rate,
- the mudweight and
- the deviation surveys.

2.3 Definition of the stratigraphic contacts

The stratigraphic framework of the study area is relatively well established (figure 4), but the geological contacts reported in the end of drilling reports are not always positioned according to homogeneous and repetitive criteria from one well to another. Whenever necessary, the geological contacts that are proposed in the end of drilling reports have been adjusted after reviewing the logs, so that any petrophysical contrasts observed at the contact of two stratigraphic units are consistent from one well to another. The logs also reveal the absence of petrophysical contrasts between some units; in these cases the contact is then defined based on cuttings descriptions. In the latter case and for clarity purpose, stratigraphic units that are contiguous but which could not be distinguished clearly on the logs have been regrouped in this study. The petrophysical units that are retained in this study include :

- Mabou Group (Hopewell Formation)
- Undifferentiated Windsor Group (evaporite deposits of the Clover Hill and Cassidy Lake and Upperton formations, carbonates and clastics of the Gays River and Macumber formations)
- Undifferenciated Sussex Group (including the Hillsborough Formation)
- Hiram Brook Member (Albert Formation, Horton Group)
- Frederick Brook Member (Albert Formation, Horton Group)
- Dolomitic shale unit of the Frederick Brook Member (Albert Formation, Horton Group)
- Dawson Settlement Member (Albert Formation, Horton Group) and McQuade Brook Formation (Horton Group)

For each of the studied wells, the measured depth and the vertical depth of the top of the petrophysical units are indicated in Appendix I.

3. Estimation of the geomechanical properties

3.1 Elastic moduli

Given the very limited available laboratory data (see further), the mechanical properties of the various stratigraphic units documented in the wells are primarily defined through the raw acoustic logs of the P and S waves (DTP and DTS) and the bulk density (RHOB). The first step, representing the pivot of the

various methods available, is to calculate the Poisson's ration (υ) and the Young's modulus (E) from the equations (1) to (3) below.

$$Poisson's\ ratio\ (\upsilon) = \frac{\frac{1}{2}\left(\frac{\mathrm{DTS}}{\mathrm{DTP}}\right)^2 - 1}{\left(\frac{\mathrm{DTS}}{\mathrm{DTP}}\right)^2 - 1} \quad (1)$$

$$Shear\ modulus\ (G) = \frac{\mathrm{RHOB} \times 10^3}{\mathrm{DTS}^2} \quad (2)$$

$$Young's\ modulus\ (E) = 2\ \mathrm{G}\ (1 + \upsilon) \quad (3)$$

The Poisson's ratio (υ) is an elastic modulus that corresponds to the relationship between the axial shortening of a material under pressure along this axis, and the lengthening of the material according to the other axes. This ratio expresses the propensity of the rock to expand in a direction perpendicular to that where the stress is applied (Zoback, 2007). The Poisson's ratio is dimensionless and varies usually between 0 and 0.5. A value close to 0.5 characterizes a more ductile rock which tends to expand in a direction perpendicular to the axis along which it is compressed. In laboratory dynamic tests and in log evaluations, the Poisson's ratio is estimated from the slowness of the P and S waves (equation 1).

The Young's modulus (E) is an elastic modulus that corresponds to the relationship between the strain along an axis, and the deformation incurred along the same axis. This modulus expresses the stiffness of a material subjected to an unconfined uniaxial stress (Zoback, 2007). The Young's modulus is expressed here in Giga Pascals (GPa). A high value characterizes a more rigid rock that tends to deform in a brittle way under the effect of a stress. The shear modulus (G) can be defined in the same way as the Young's modulus, but it expresses the rigidity of rock subjected to a shear stress. In laboratory dynamic tests and in log evaluations, the Young's modulus is derived from the shear modulus and the Poisson's ratio (equation 3) and thus it depends on the slowness of the P and S waves as well as on the bulk density (equations 1 and 2).

Once the dynamic values of the Poisson's ratio and Young' modulus are obtained from raw or synthetic acoustic logs, cross-plot diagrams can be prepared for each stratigraphic unit to illustrate the relationship between the two elastic moduli (figures 7 to 13). It is this type of diagram that is most commonly used for a quick geomechanical assessment. The lower right part (higher υ and lower E values) of the diagram corresponds to more ductile lithologies and the upper left part (lower υ and higher E values) to more brittle lithologies. When the parameters used are dynamic, i.e. when they are not calibrated by static geomechanical tests carried out in the laboratory on core samples, there is no consensual limit between the more ductile and more brittle areas from such cross-plots. All of the results obtained for this study are compiled in table 4. The synthesis results shown in figures 7 to 13 as well as in table 4 are compiled from eighteen out of the twenty six wells investigated in the geomechanical study (table 1). The eight wells that were discarded for the statistical computations (identified in table 1 as having a mediocre DTS or RHOB curve) have been excluded because their logs S wave and/or their bulk

density curve was considered of too poor quality to establish representative elastic moduli. An example of elastic moduli derived from poor quality logs (well J-47) is presented in figure 14.

The elastic moduli are also represented as synthetic curves to illustrate their variations with depth and with the various stratigraphic units. An example is shown in figure 15 for the well P-66 and all of the results for each well are reported in Appendix II.

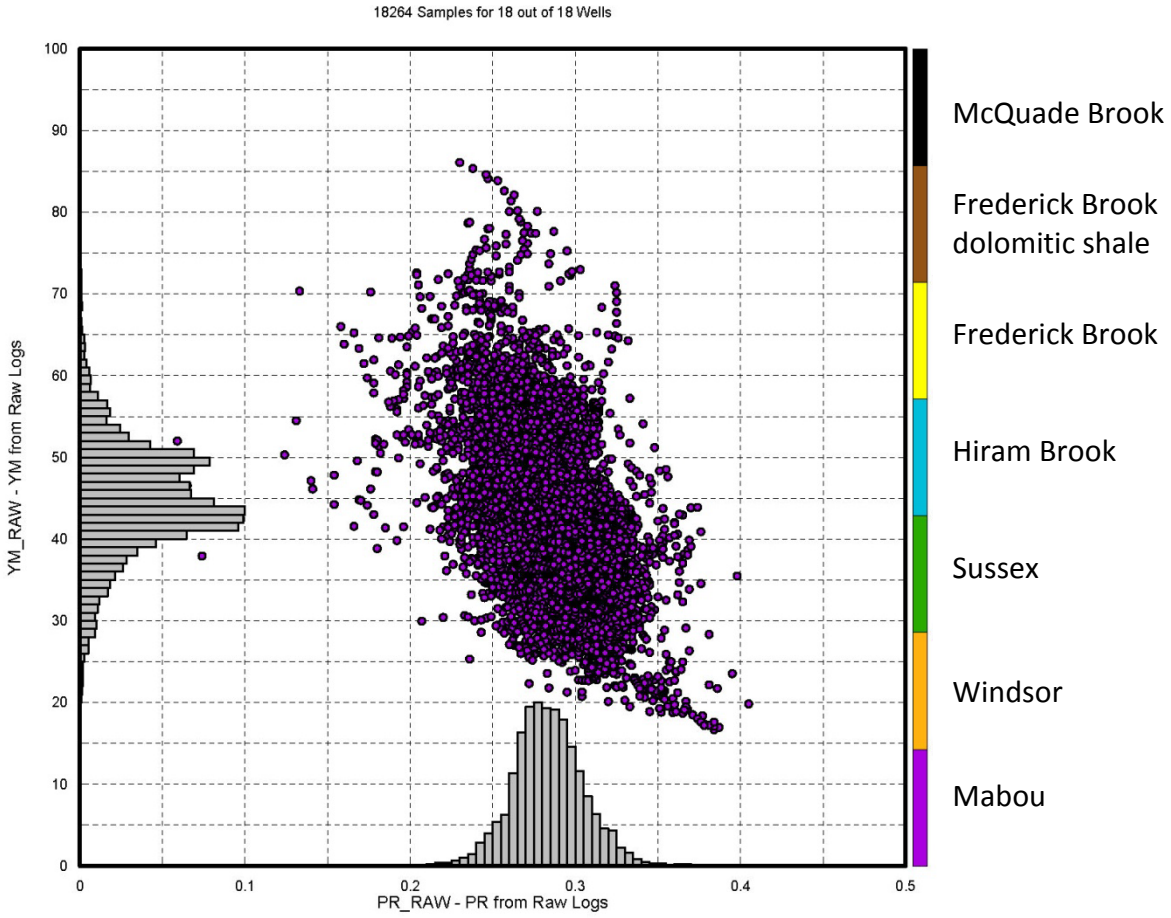

Figure 7 : Cross-plot diagram of the dynamic values of E and υ estimated from acoustic and bulk density logs for the Mabou Group. YM_RAW : Young's modulus (E), expressed in GPa. PR_RAW : Poisson's ratio (υ), dimensionless. The histograms show the relative distribution and spread of the data points.

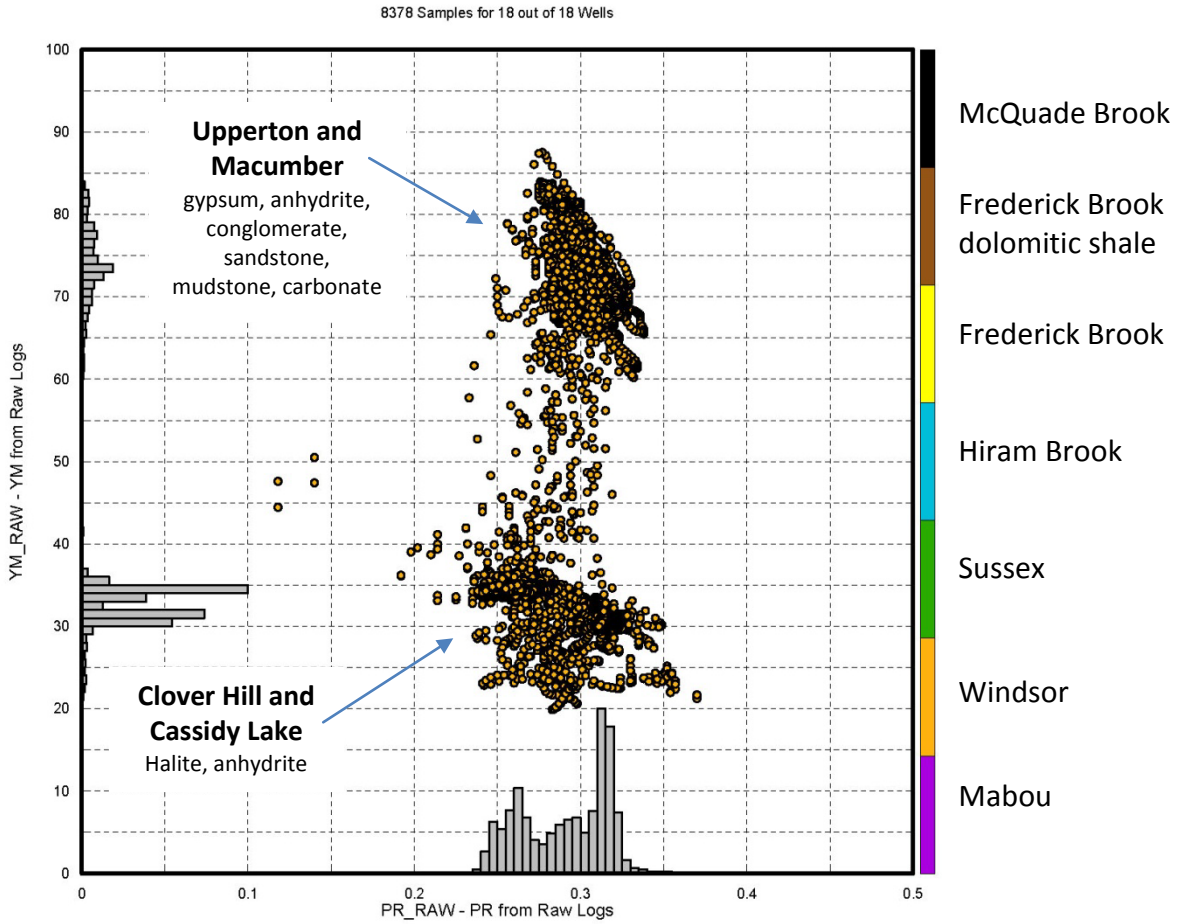

Figure 8 : Cross-plot diagram of the dynamic values of E and υ estimated from acoustic and bulk density logs for the Windsor Group. Two subsets are distinguished by their values of E, according to their lithology (presence of halite, absence of clastics). YM_RAW : Young's modulus (E), expressed in GPa; PR_RAW : Poisson's ratio (υ), dimensionless. The histograms show the relative distribution and spread of the data points.

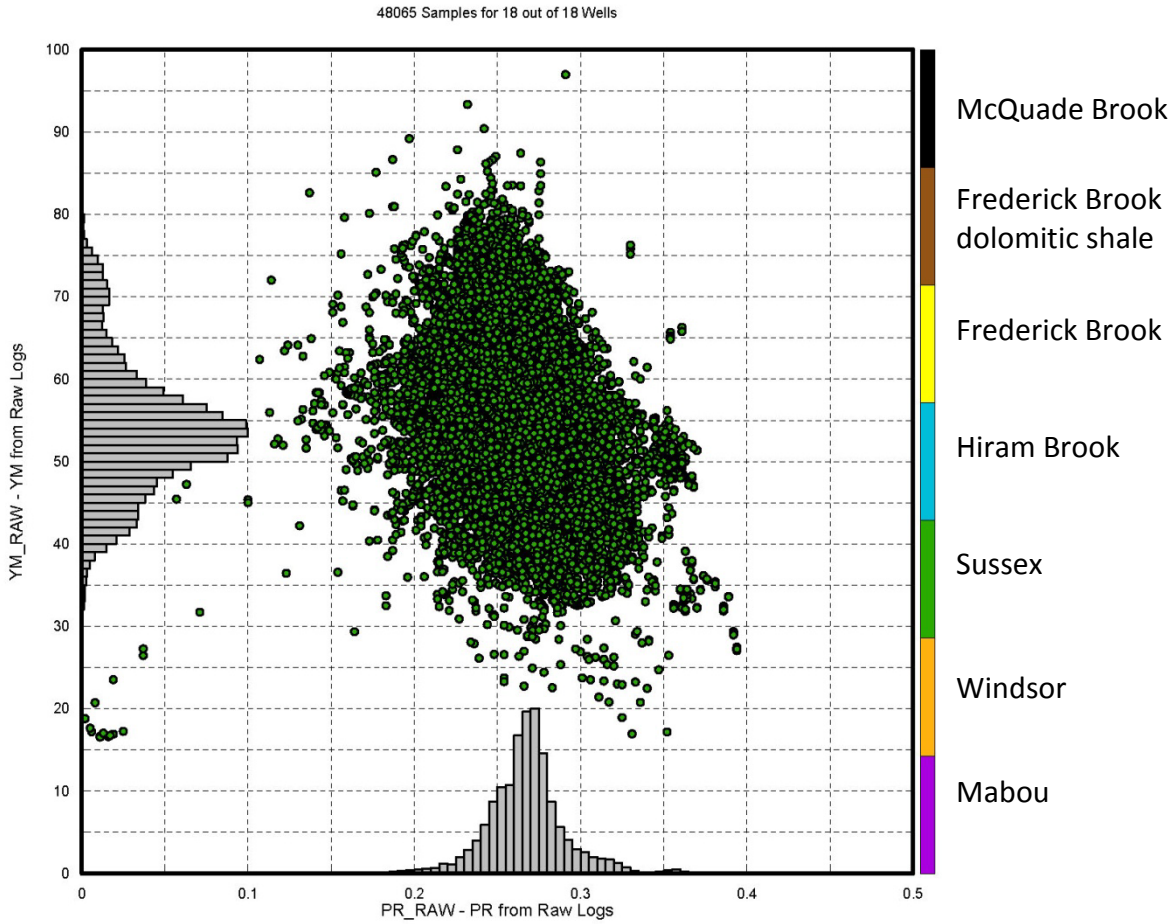

Figure 9 : Cross-plot diagram of the dynamic values of E and υ estimated from acoustic and bulk density logs for the Sussex Group. YM_RAW : Young's modulus (E), expressed in GPa. PR_RAW : Poisson's ratio (υ), dimensionless. The histograms show the relative distribution and spread of the data points.

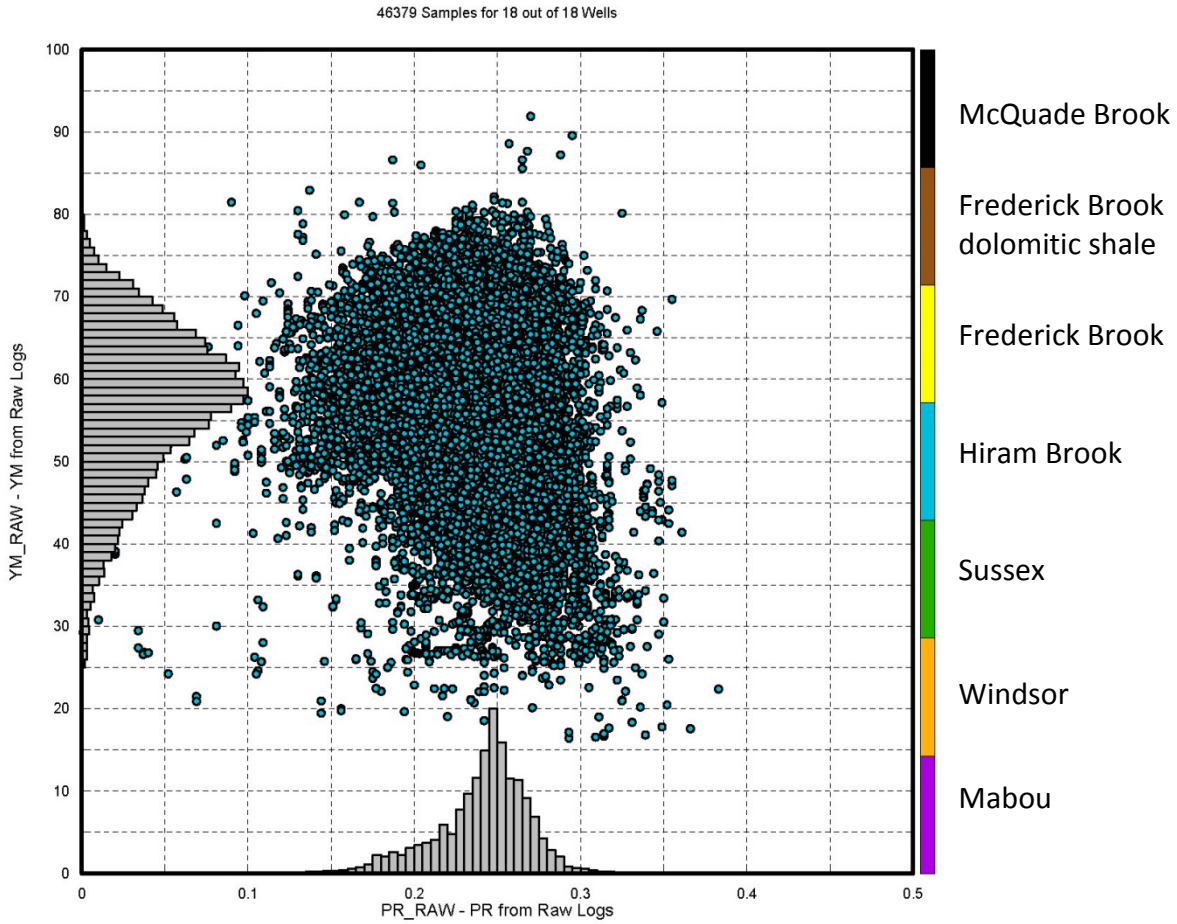

Figure 10 : Cross-plot diagram of the dynamic values of E and υ estimated from acoustic and bulk density logs for the Hiram Brook Member. YM_RAW : Young's modulus (E), expressed in GPa. PR_RAW : Poisson's ratio (υ), dimensionless. The histograms show the relative distribution and spread of the data points.

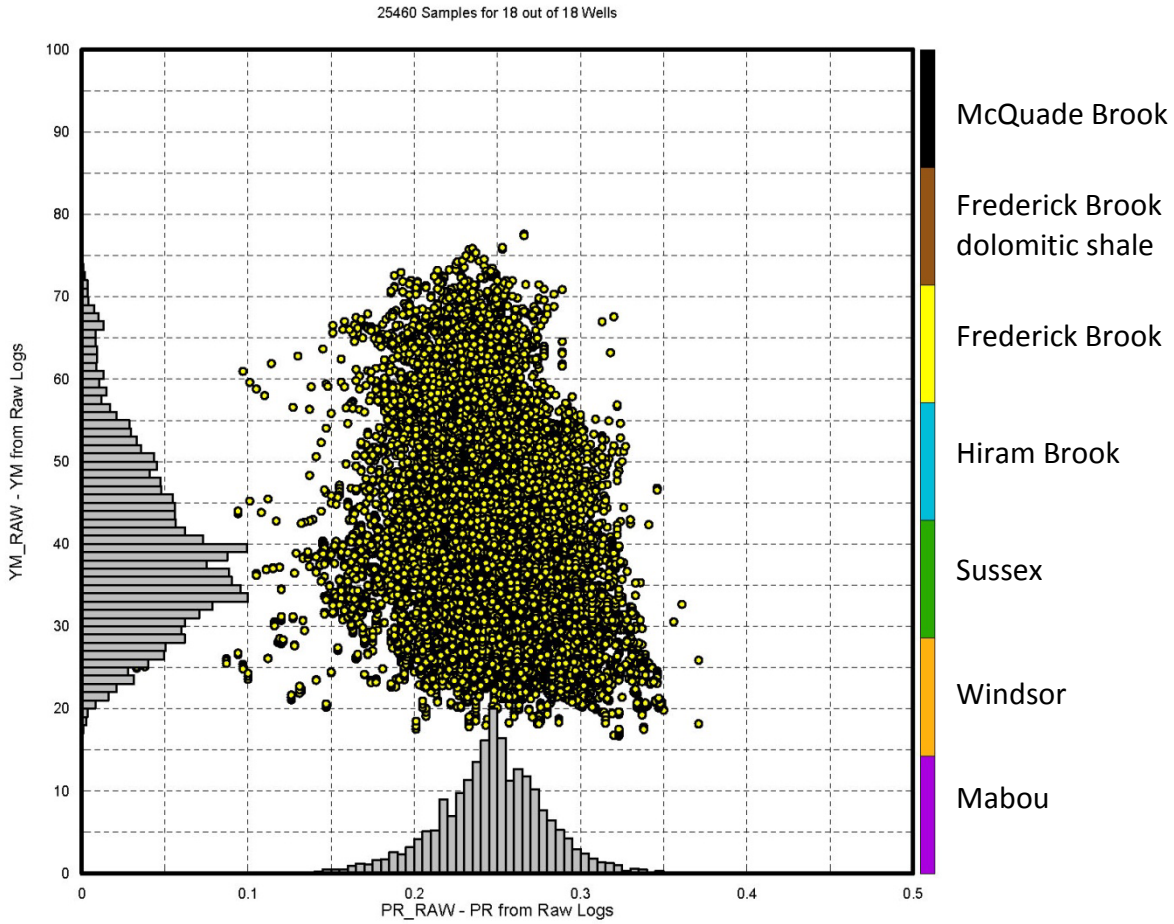

Figure 11 : Cross-plot diagram of the dynamic values of E and υ estimated from acoustic and bulk density logs for the non-dolomitic shale in the upper part of the Frederick Brook Member. YM_RAW : Young's modulus (E), expressed in GPa. PR_RAW : Poisson's ratio (υ), dimensionless. The histograms show the relative distribution and spread of the data points.

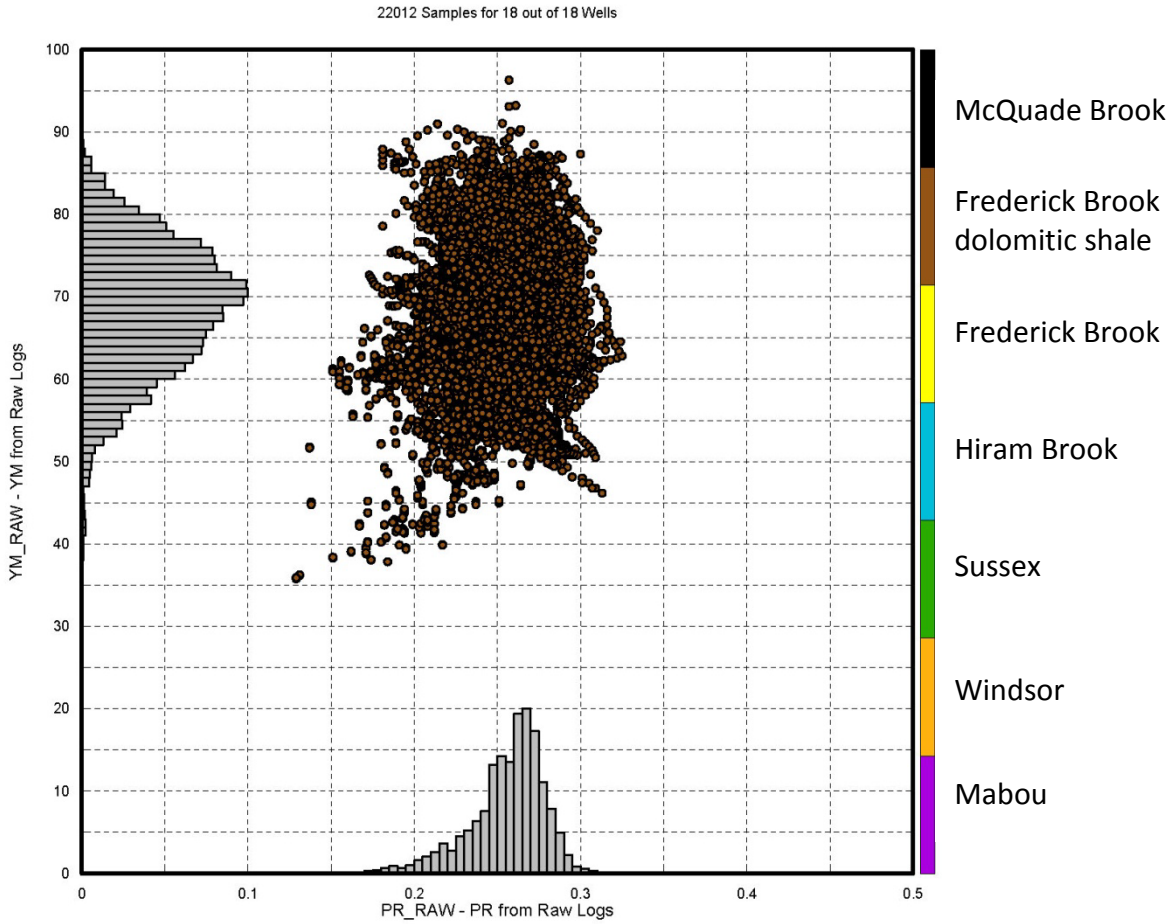

Figure 12 : Cross-plot diagram of the dynamic values of E and υ estimated from acoustic and bulk density logs for the dolomitic shale in the lower part of the Frederick Brook Member. YM_RAW : Young's modulus (E), expressed in GPa. PR_RAW : Poisson's ratio (υ), dimensionless. The histograms show the relative distribution and spread of the data points.

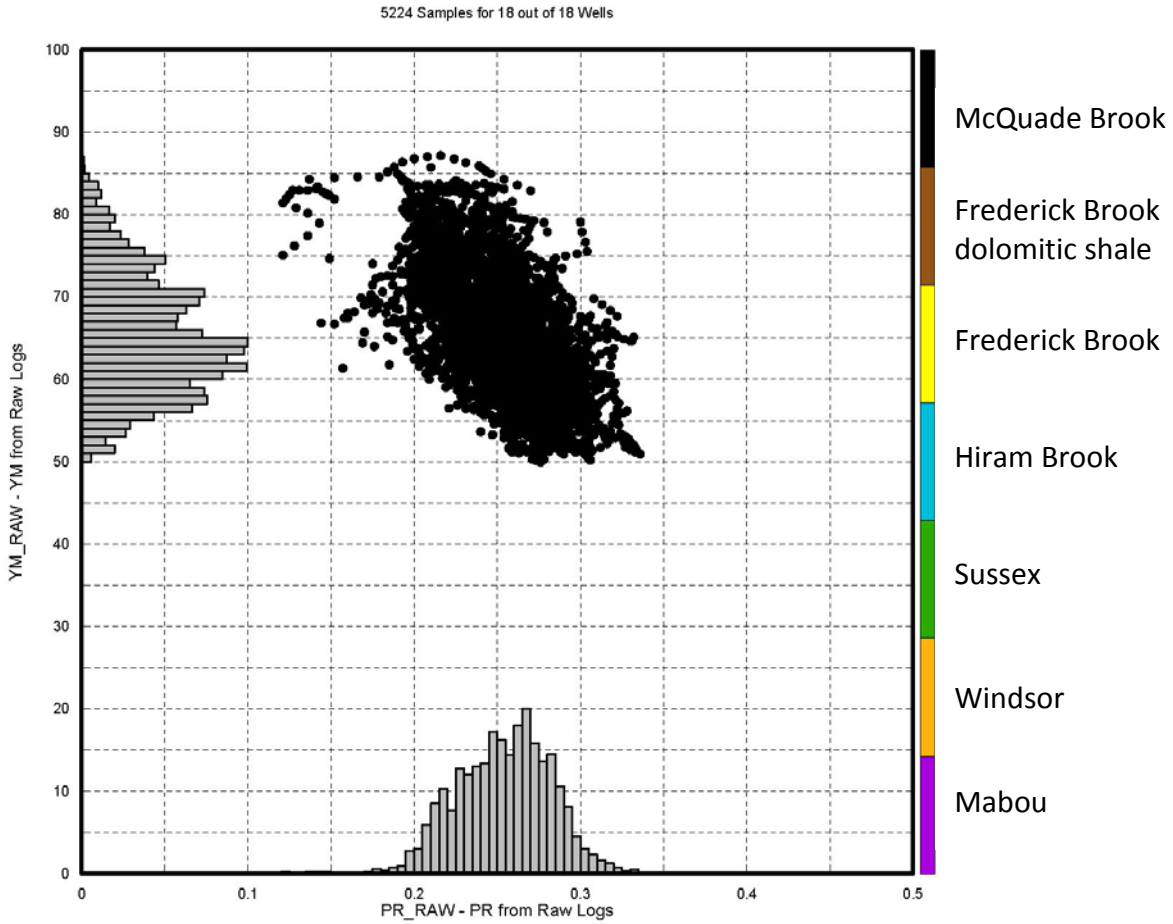

Figure 13 : Cross-plot diagram of the dynamic values of E and υ estimated from acoustic and bulk density logs for the McQuade Brook Formation. YM_RAW : Young's modulus (E), expressed in GPa. PR_RAW : Poisson's ratio (υ), dimensionless. The histograms show the relative distribution and spread of the data points.

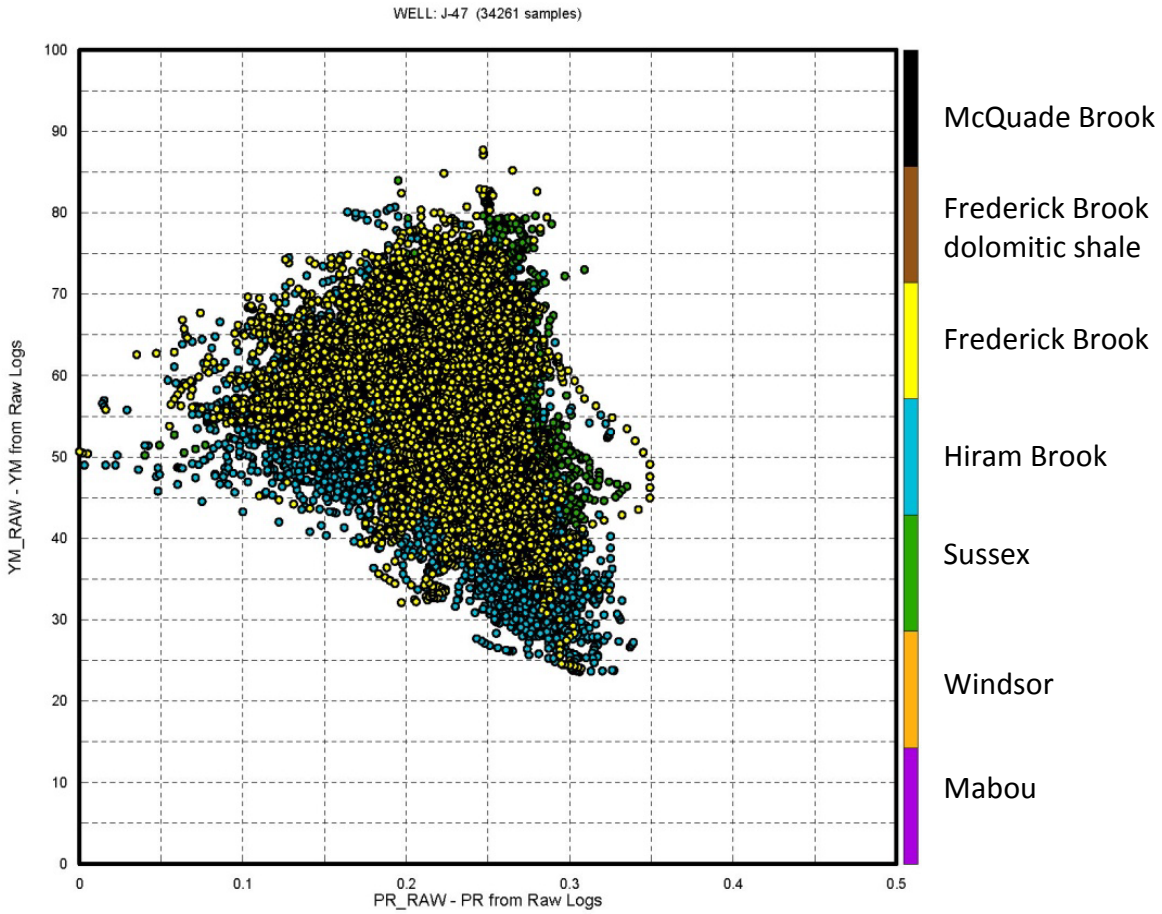

Figure 14 : Cross-plot diagram of the dynamic values of E and υ estimated from acoustic and bulk density logs for the well J-47. In this well the S wave curve is very irregular (noisy), which affects the values of υ (deflection to 0) and the values of E (erratic). YM_RAW : Young's modulus (E), expressed in GPa; PR_RAW : Poisson's ratio (υ), dimensionless. No histogram is presented for this well because several stratigraphic units are superposed.

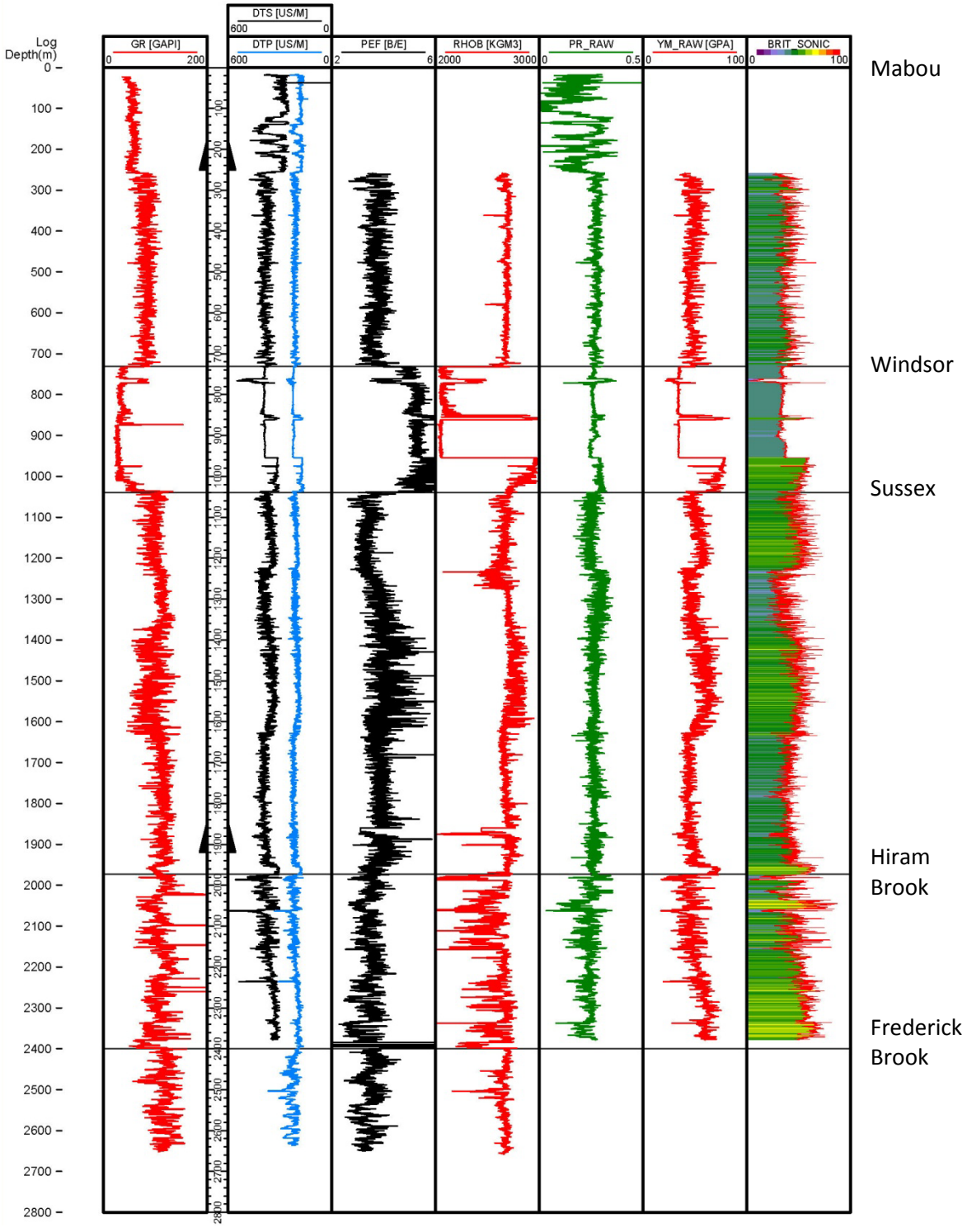

Figure 15 : Variation of the elastic moduli with the depth for the well P-66, between the Mabou Group and the base of the Hiram Brook Member. YM_RAW : Young's modulus (E), expressed in GPa. PR_RAW : Poisson's ratio (υ), dimensionless; BRIT_SONIC : Acoustic brittleness index, expressed in percentage.

Table 4 : Synthesis of the values of the elastic moduli and the acoustic brittleness index estimated for 18 wells. Gr. : Group; Fm. : Formation; Mb. : Member. Min. : Minimum; Avg. : Average; Med. : Median; Max. : Maximum; Dev. : Standard deviation; N : Number of wells.

Mechanical Property		Mabou Gr.	Windsor Gr. (evapo-rites)	Windsor Gr. (carbo-nates / clastics)	Sussex Gr.	Hiram Brook Mb.	Frederick Brook Mb.	Frederick Brook Mb. (dolo-mitic)	McQuade Brook Fm.
Young's Modulus (GPa)	Min.	18.4	19.9	35.0	18.6	18.3	18.1	35.8	47.5
	Avg.	44.8	32.5	72.5	54.3	57.5	39.7	68.5	64.5
	Med.	44.4	32.9	73.4	53.6	58.6	38.3	69.2	63.5
	Max.	86.1	50.5	87.5	87.8	87.7	77.6	87.9	87.2
	Dev.	7.3	2.7	7.6	8.3	9.3	10.5	8.0	7.6
	N	4	3	3	14	15	9	3	1
Poisson's Ratio (0-0.5)	Min.	0.14	0.14	0.18	0.14	0.14	0.14	0.15	0.14
	Avg.	0.28	0.28	0.30	0.27	0.24	0.25	0.26	0.25
	Med.	0.28	0.27	0.30	0.27	0.25	0.25	0.26	0.26
	Max.	0.36	0.36	0.34	0.36	0.36	0.36	0.33	0.34
	Dev.	0.04	0.03	0.02	0.03	0.03	0.03	0.02	0.03
	N	7	6	5	16	16	9	3	1
Acoustic Brittleness Index (0-100)	Min.	0.3	0.3	29.2	0.5	2.3	3.4	30.7	28.9
	Avg.	36.6	25.0	51.8	47.0	53.8	41.3	59.8	57.4
	Med.	36.7	21.1	50.9	46.3	54.1	40.9	59.5	56.3
	Max.	92.6	76.1	68.9	97.4	97.8	90.4	90.6	99.6
	Dev.	9.0	7.4	6.5	10.3	10.0	11.5	6.7	10.6
	N	4	3	3	15	14	9	3	1

3.2 Comparison with the laboratory data

A laboratory geomechanical study independent from the present study is available for the well G-67 (Core Lab, 2005). These tests were conducted on five sandstone and three shale core samples from the Hiram Brook Member. Static analyses performed on these samples have allowed to establish the bulk density and the static υ and E values for each sample. Two series of dynamic analyses at different containment pressures were also conducted on these samples to measure DTP and DTS, in order to derive dynamics values for υ and E. A log of the P and S waves is also available for the well G-67, which allows to calculate dynamics values for υ and E according to the method described in the previous section 3.1 and to compare these values to the static and dynamic results obtained in the laboratory.

Static geomechanical analyses are direct and destructive tests consisting of compression tests conducted on rock samples in the laboratory. Dynamic geomechanical tests are indirect and non-destructive tests aimed at measuring the slowness of the P and S waves through the studied material.

In static tests performed in the laboratory, υ is determined directly by measuring the axial shortening of the material and its stretch along the other axes (e.g., radial deformation) (ASTM, 2015a). In dynamic tests performed in the laboratory and in wireline log evaluations, υ is estimated from the slowness of the P and S waves according to equation (1) presented in section 3.1 (see also ASTM, 2015b). The difference between the static and dynamic values of υ that are obtained in the laboratory is generally low, in the order of a few percents (Barree et al., 2009). A more pronounced difference is sometimes observed between the dynamic values of υ obtained in laboratory and those derived from the logs, especially when the gas saturation of the sample tested in the laboratory is different from that of the *in-situ* rock during the recording of the wireline logs (lower gas saturations correspond to higher apparent υ values and vice versa, Barree et al., 2009).

In the laboratory static tests, E is estimated based on the slope of the axial stress with the axial deformation (ASTM, 2015a). In laboratory dynamic tests and in the wireline log evaluations, E is derived from G and υ according to equation (3) presented in section 3.1 (see also ASTM, 2015b) and depends on the P and S wave velocities, as well as on the bulk density RHOB. In practice, several methods exist to estimate the slope of the axial stress (ASTM, 2015a) and the selection of the method may influence the final results in the case of non-elastic materials, so that a significant difference can exist between the static and dynamic values of E estimated in the laboratory. A marked difference may also exist between the values of E estimated in the laboratory and those estimated from the logs, particularly because of microfractures which can form following the unloading and relaxation of the cores from the moment they are cut and brought to surface, through their transportation, to their final handling the laboratory. This loss of integrity results in a decrease of the static and dynamic values of E measured in the laboratory. The phenomenon of unloading and relaxation can be particularly severe in the case of shale gas due to the laminated fabric and the low permeability of the shale (see the discussion in Séjourné, 2016).

In the case of the laboratory tests undertaken for the well G-67, the sandstone and shale samples of the Hiram Brook Member were saturated with a of 3% KCl solution prior to analysis. Dynamic tests were performed under a minimum and a maximum axial stress and were followed by the static tests. The properties measured and calculated during the dynamic tests are presented in table 5 and the properties measured in the static tests are presented in table 6.

Table 5 : Dynamic geomechanical properties measured and calculated during the laboratory tests on the Hiram Brook Member samples in the well G-67. MD : Measured depth; VD : Vertical depth. Source : Core Lab (2005).

Sample			Dynamic measured					Dynamic calculated			
Sample	MD (m)	VD (m)	Confining pressure (kPa)	Axial pressure (kPa)	Bulk density (kg/m^3)	DTP (µs/m)	DTS (µs/m)	Bulk modulus (GPa)	Young's modulus (GPa)	Shear modulus (GPa)	Poisson's ratio
V1 sand	2416.2	2366.7	7239.5	7239	2540	194.6	326.0	35.2	58.5	23.9	0.22
			7239.5	137895	2540	186.8	315.2	38.7	62.9	25.8	0.23
V2 shale	2417.1	2367.6	13513.7	13514	2680	208.7	385.2	37.5	46.7	18.1	0.29
			13513.7	82737	2680	198.6	373.8	42.5	50.1	19.2	0.30
V3 sand	2418.9	2369.4	7239.5	7239	2540	194.3	323.3	34.9	59.2	24.3	0.22
			7239.5	137895	2540	187.2	316.3	38.7	62.5	25.4	0.23
V4 sand	2420.9	2371.4	7239.5	7239	2510	203.0	351.9	33.9	50.7	20.3	0.25
			7239.5	137895	2510	194.3	329.7	35.7	57.0	23.1	0.23
V5 shale	2424.0	2374.4	13513.7	13514	2770	205.6	378.8	39.8	49.8	19.3	0.29
			13513.7	82737	2770	199.1	370.2	42.9	52.4	20.2	0.30
V6 sand	2429.3	2379.8	7239.5	7239	2540	192.8	328.1	36.8	58.3	23.6	0.24
			7239.5	137895	2540	185.1	317.7	40.5	62.5	25.2	0.24
V7 sand	2430.8	2381.2	7239.5	7239	2520	203.0	340.6	32.3	53.3	21.8	0.22
			7239.5	137895	2520	193.1	329.8	36.7	57.5	23.2	0.24
V8 shale	2432.1	2382.5	13513.7	13514	2760	209.4	386.9	38.3	47.6	18.4	0.29
			13513.7	82737	2760	201.5	374.5	41.7	51.0	19.7	0.30
Avg. sand			7239.5	72567	2530	193.4	327.9	36.4	58.3	23.6	0.23
Avg. shale			13513.7	48125	2737	203.8	378.2	40.4	49.6	19.1	0.30

Table 6 : Static geomechanical properties measured during laboratory tests on the Hiram Brook Member samples in the well G-67. MD : Measured depth; VD : Vertical depth. Source : Core Lab (2005).

Sample	MD (m)	VD (m)	Static measured				
			Confining pressure (kPa)	Bulk density (kg/m^3)	Compressive strength (kPa)	Young's modulus (GPa)	Poisson's ratio
V1 sand	2416.2	2366.7	7239.5	2540	255381.8	49.0	0.22
V2 shale	2417.1	2367.6	13513.7	2680	89287.1	23.0	0.32
V3 sand	2418.9	2369.4	7239.5	2540	230284.9	45.4	0.19
V4 sand	2420.9	2371.4	7239.5	2510	213323.8	42.5	0.23
V5 shale	2424.0	2374.4	13513.7	2770	161406.3	20.9	0.30
V6 sand	2429.3	2379.8	7239.5	2540	209807.5	45.4	0.22
V7 sand	2430.8	2381.2	7239.5	2520	206222.2	42.4	0.22
V8 shale	2432.1	2382.5	13513.7	2760	170507.3	20.1	0.30
Avg. sand			7239.5	2530	223004.0	45.0	0.22
Avg. shale			13513.7	2737	140400.2	21.3	0.31

The comparison between the dynamic and static values of E and υ obtained in the laboratory for the well G-67 shows that these values coincide with the fields of the dynamic and static values compiled in Barree et al. (2009). The dynamic values of υ are very close to the static values as expected (± 6% on average, figure 16). The dynamic E values are higher than the static values as expected too, but with a marked difference according to the lithology (+ 25% for the sandstone and + 125% for the shale, figure 17).

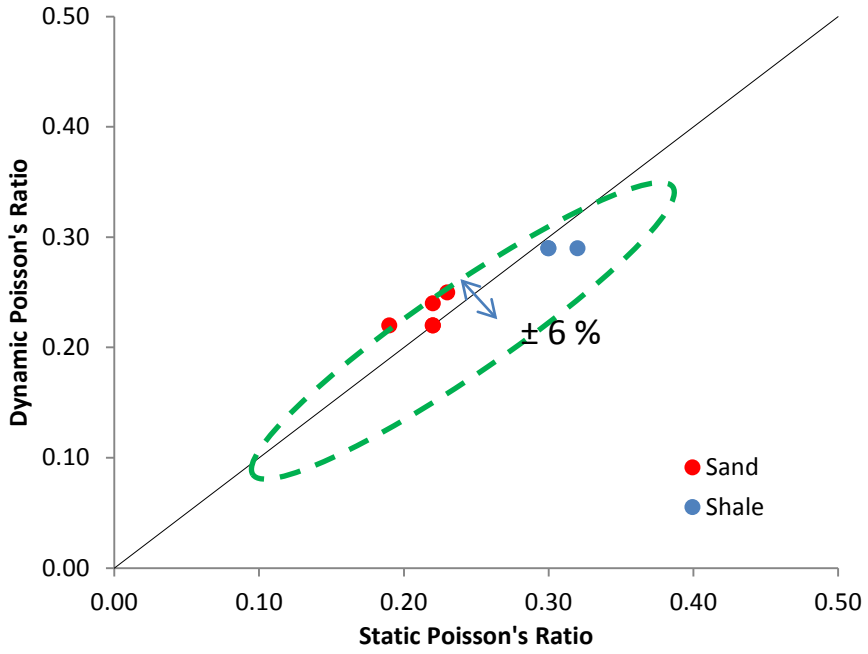

Figure 16 : Comparison between the dynamic and static values of υ obtained in the laboratory for the well G-67. The field delimited by green dashes corresponds to the values of reference compiled in Barree et al. (2009) for tight gas and shale gas core samples.

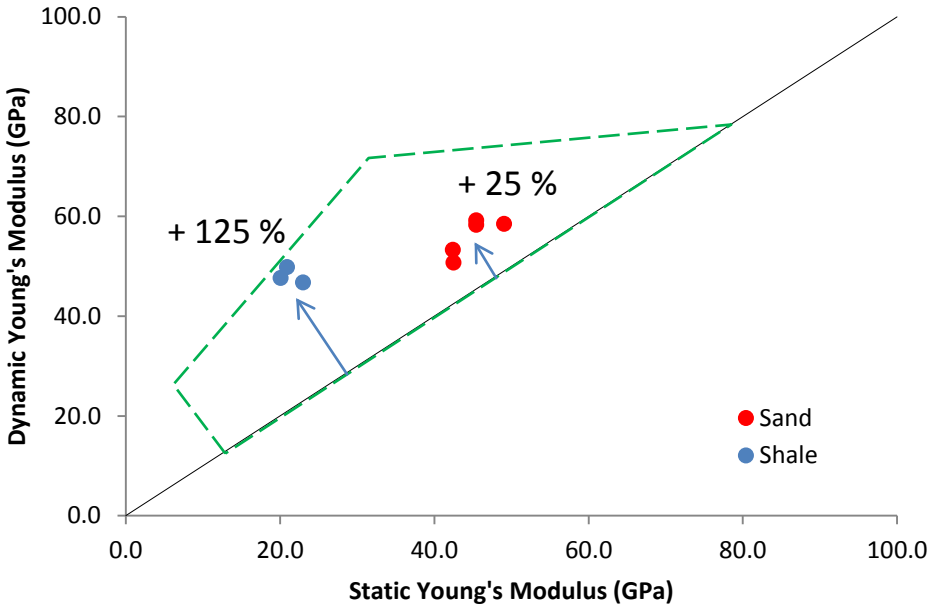

Figure 17 : Comparison between the dynamic and static values of E obtained in the laboratory for the well G-67. The field delimited by green dashes corresponds to the values of reference compiled in Barree et al. (2009) for tight gas and shale gas core samples.

The DTP and DTS values measured in the laboratory at low and high axial pressures also show a good correlation with each other (figure 18), so that the laboratory dynamic values of E and υ are little affected by the choice of the axial pressure applied. The laboratory dynamic values of E and υ obtained by applying the maximum axial pressure are retained hereafter for comparisons with the log-derived E and υ values.

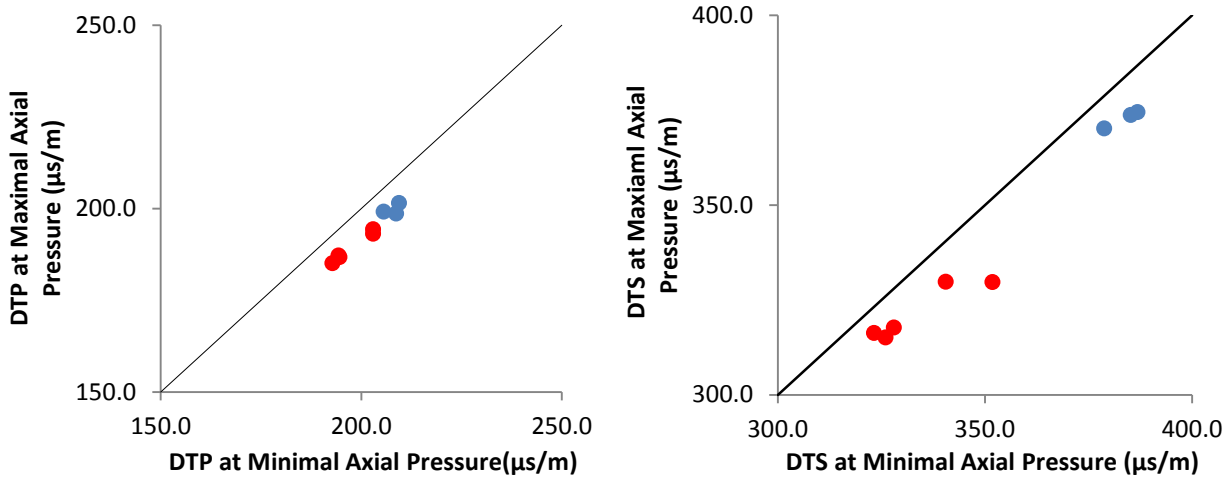

Figure 18 : Comparison between DTP or DTS values measured in the laboratory at maximum and minimum axial pressure for the G-67 well. Red : Sand; Blue : Shale.

The laboratory dynamic values of E and υ show no clear correlation with the log-derived values, although the relationship between the two sets of data is close to 1. In the case of υ, the log-derived values are 20% lower on average (n = 8) compared to the laboratory dynamic values (figure 19). In the case of E, the log-derived values are 8% higher on average (n = 8) compared to the laboratory dynamic values (figure 20).

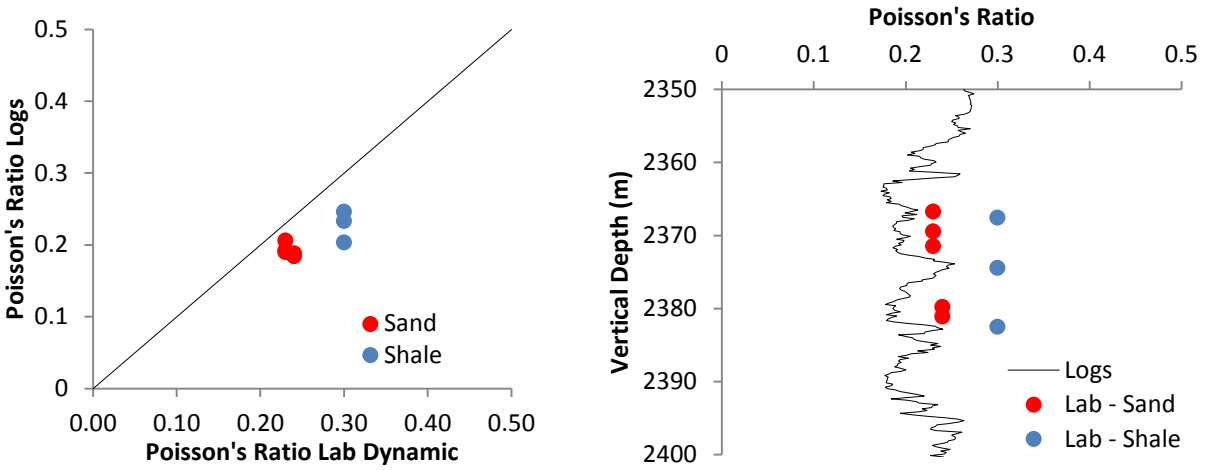

Figure 19 : Comparison between the laboratory dynamic values of υ and the log-derived values of υ for the well G-67.

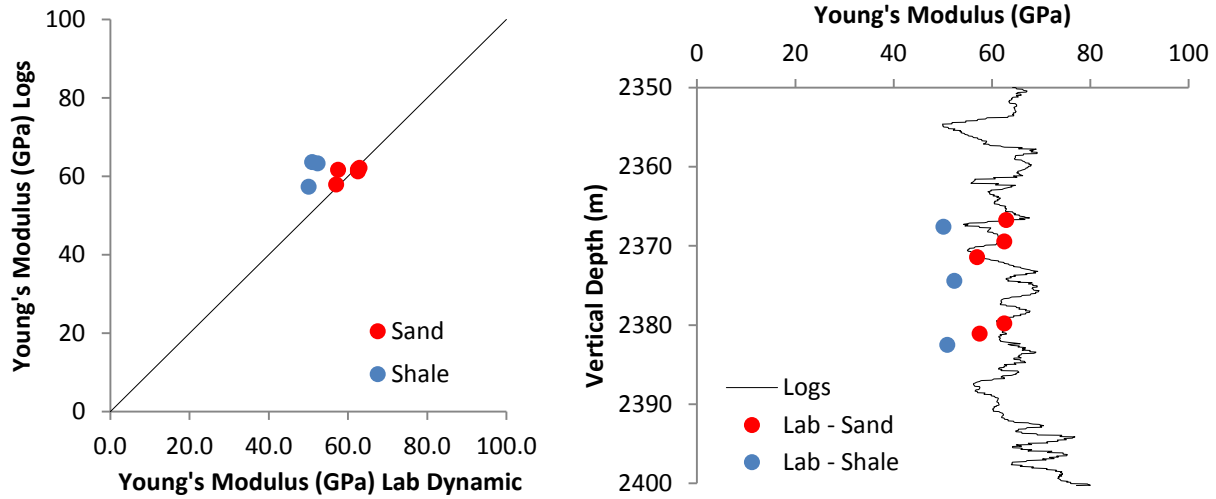

Figure 20 : Comparison between the laboratory dynamic values of E and the log-derived values of E for the well G-67.

These results confirm the closeness observed between the values measured in the laboratory and those recorded by the logs for the P and S waves and the bulk density. In the case of the P and S waves, the values measured in the laboratory do not coincide exactly with the logs for the corresponding intervals but are close, with the exception of the shale samples in the case of the S wave, that stand out significantly from the corresponding DTS curve (figure 21). In the case of the bulk density the coincidence between the log and laboratory data is also good and confirms that the shale intervals have been identified adequately (figure 22). The gap between the S wave slowness measured in the laboratory and the corresponding peaks in the intervals of shale on the wireline log (figure 21) can be explained in a simple way by the resolution of the log (19.5 cm), which is higher than the standard length of the laboratory samples (5 to 7.5 cm). However, alternative explanations can be proposed, including the

possibility that the laboratory dynamic tests do not fully account for the anisotropy of the samples. There is however no samples description to appreciate this anisotropy (presence of fractures, lamination, etc.).

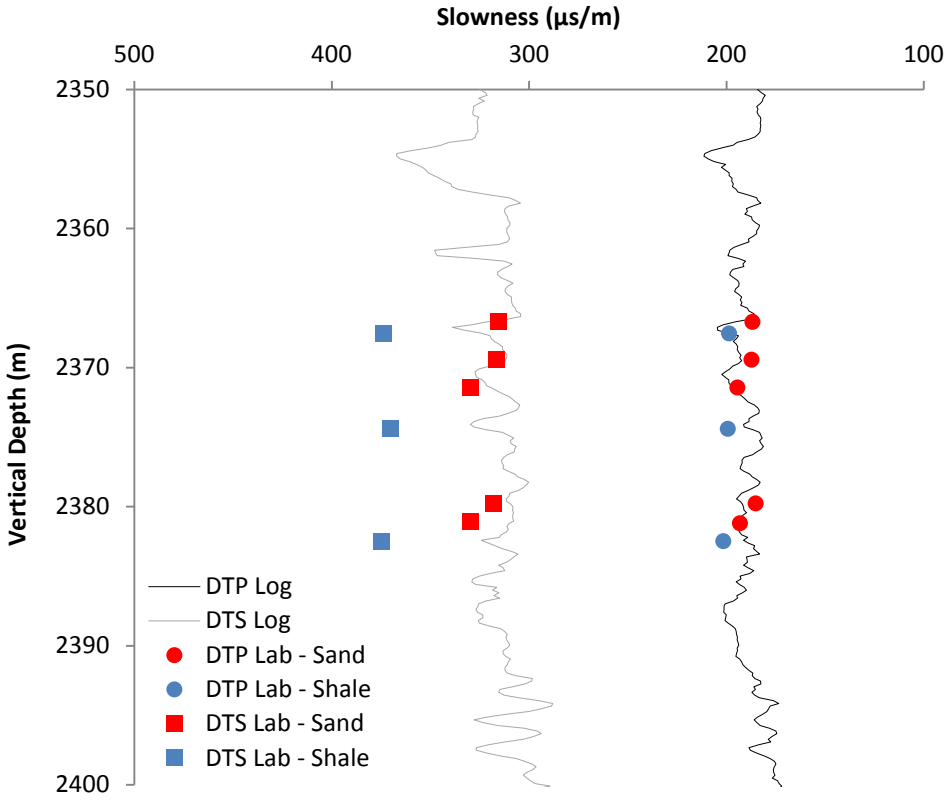

Figure 21 : Comparison between the P and S waves slowness measured in laboratory and that recorded by the wireline logs for the well G-67. DTP DTS : Slowness of the P and S waves from wireline logs or from laboratory tests.

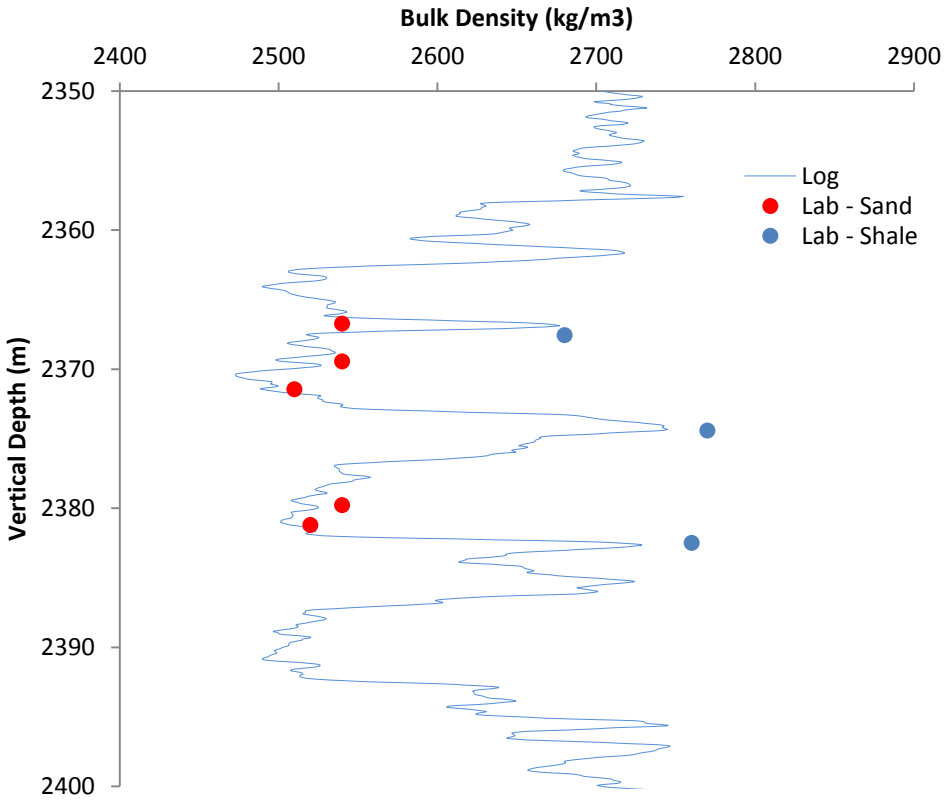

Figure 22 : Comparison between the bulk density measured in the laboratory and that recorded by wireline logging for the well G-67.

The coincidence of the ranges of values between laboratory dynamic data and wireline log data for the studied parameters indicates that it is possible to use the lab results to calibrate the log-derived values of E and υ in the case of the sandstones but the shales results are too different for a sound calibration, at least in the case of the Hiram Brook Member in the well G-67.

Therefore, a calibration integrating both the sandstones and the shales intervals based on average values would have only a semi-quantitative meaning in that it would introduce errors in the absolute static values of E and υ derived from the logs at the scale of the bed, but would also preserve the major geomechanical contrasts observed between main stratigraphic units. In the same way and with the same limitations, it will be possible to use the laboratory results to derive Shmin values and to compare them with the values estimated from the logs and from the mud density (section 3.4.4).

3.3 Brittleness indexes

To graphically illustrate the geomechanical properties of the rock, it is also possible to normalize the Poisson's ratio and the Young's modulus on a scale from 0 to 100 (υ being dimensionless, and E being expressed in GPa) in order to combine them into a single parameter called acoustic brittleness index. For this index the highest values correspond to a more brittle rock (fragile), the lowest values correspond to a rock that is more ductile and less able to develop or maintain open natural or induced fractures (figures

24 and 25, examples from the wells J-38 and G-41). Equation (4) adopted here is the one proposed by Grieser and Bray (2007) :

$$BRIT\_SONIC = \frac{1}{2}(\upsilon_{\text{brit}} + \text{E}_{\text{brit}}) \quad (4)$$

With $$\upsilon_{brit} = 100\ \frac{\upsilon - \upsilon_{\text{max}}}{\upsilon_{\text{min}} - \upsilon_{\text{max}}} \quad (5)$$

$$E_{brit} = 100\ \frac{E - E_{\text{min}}}{E_{max} - E_{min}} \quad (6)$$

υ_{min} = 0.14; υ_{max} = 0.36; E_{min} = 18.13 GPa and E_{max} = 88.04 GPa

The maximum and minimum values of E and υ were obtained by combining in a cross-plot diagram all stratigraphic units for the eighteen selected wells (figure 23). The results are compiled for each stratigraphic unit in table 4 above and an example is illustrated graphically for the well P-66 on figure 15. All of the graphical results for each well are also reported in Appendix II.

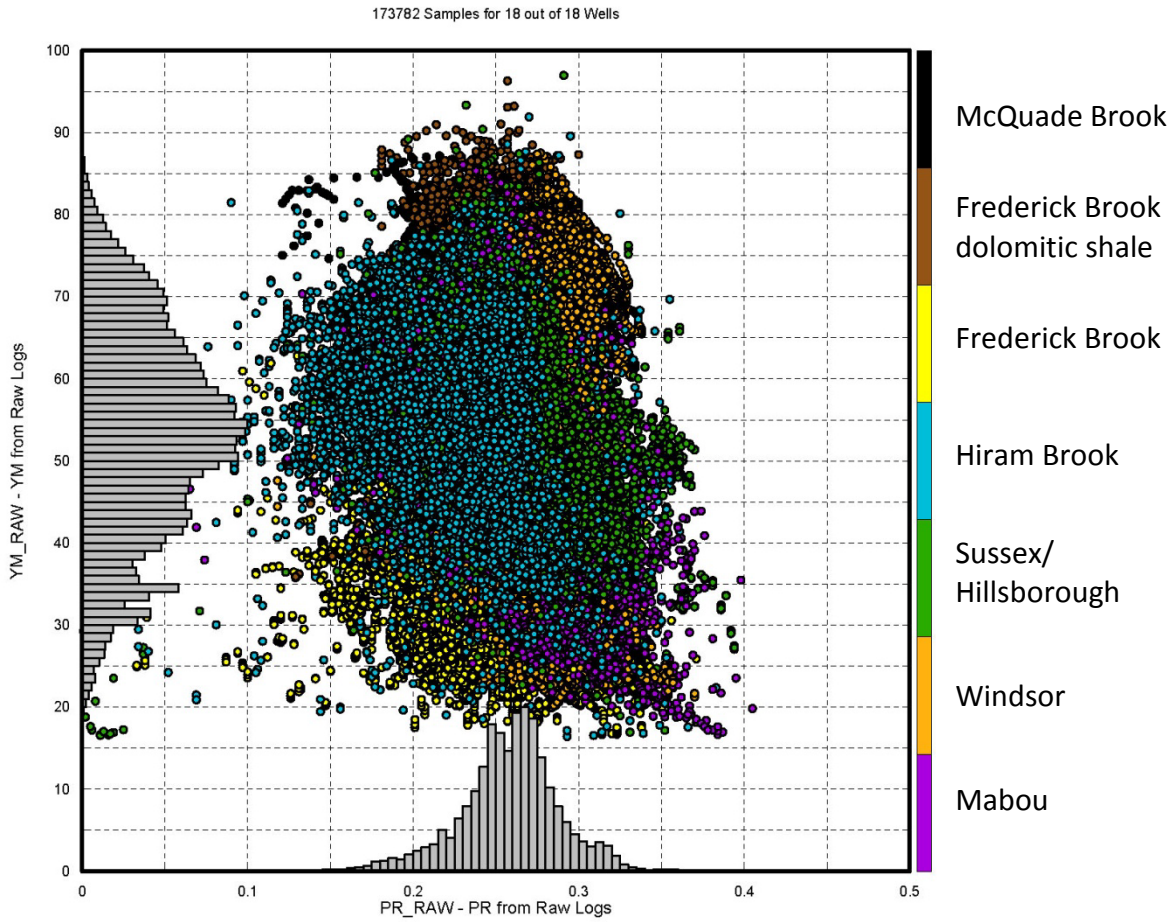

Figure 23 : Cross-plot diagram of the dynamic values of E and Y estimated from acoustic and bulk density logs for eighteen wells, all stratigraphic units combined. YM_RAW : Young's modulus (E), expressed in GPa. PR_RAW : Poisson's ratio (υ), dimensionless.

A second brittleness index, referred to as the mineralogical brittleness index, was also calculated for the wells J-38 and G-41 from their elemental capture spectroscopy logs using equation (7) adapted from Glorioso and Rattia (2012) :

$$BRIT\_MINERAL = \frac{\text{Quartz+Dolomite+Calcite}}{\text{Quartz+Dolomite+Calcite+Clay}} \quad (7)$$

This dataset for the well J-38 covers an interval of 836 m from the Hiram Brook Member up to the base of the Sussex Group. For the well G-41 the data cover an interval of 1406 m from the basal dolomitic shale interval of the Frederick Brook Member up to the Sussex Group. The comparison between the acoustic and mineralogical brittleness indexes calculated for each of these wells (figures 24 and 25) highlights the locally significant differences between the absolute values of the two indexes for a given stratigraphic interval, differences that are explained by the fact that different parameters are taken into account for the standardization of these indexes (see equations (4) and (7)). This comparison highlights also the overall convergence of the values calculated for the two brittleness indexes, which mark independently the same geomechanical contrasts at the contact between two stratigraphic units or within the same unit.

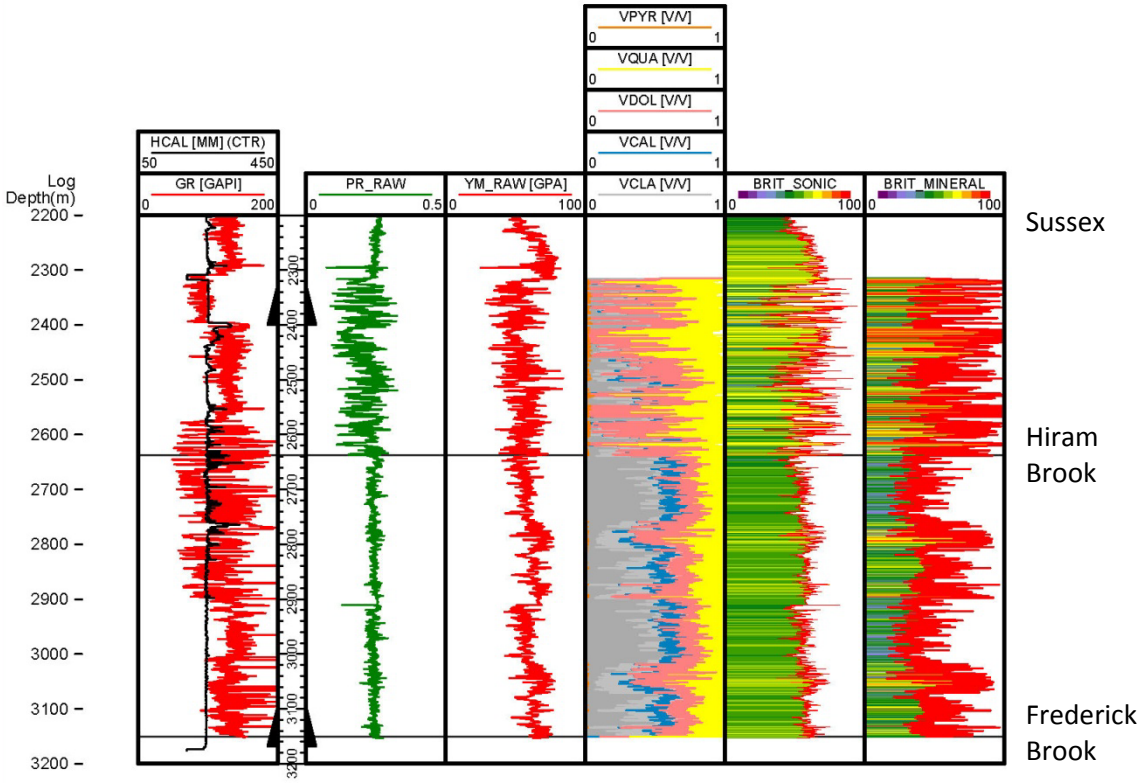

Figure 24 : Detail of the variation with depth of the elastic moduli for the well J-38. YM_RAW : Young's modulus (E), expressed in GPa. PR_RAW : Poisson's ratio (υ), dimensionless; VPYR, VDOL, VCAL, VQUA and VCLA : The proportion expressed as a fraction of pyrite, dolomite, calcite, quartz, and clay, respectively; BRIT_SONIC and BRIT_MINERAL : Respectively the acoustic and the mineralogical brittleness indexes, expressed as percentages.

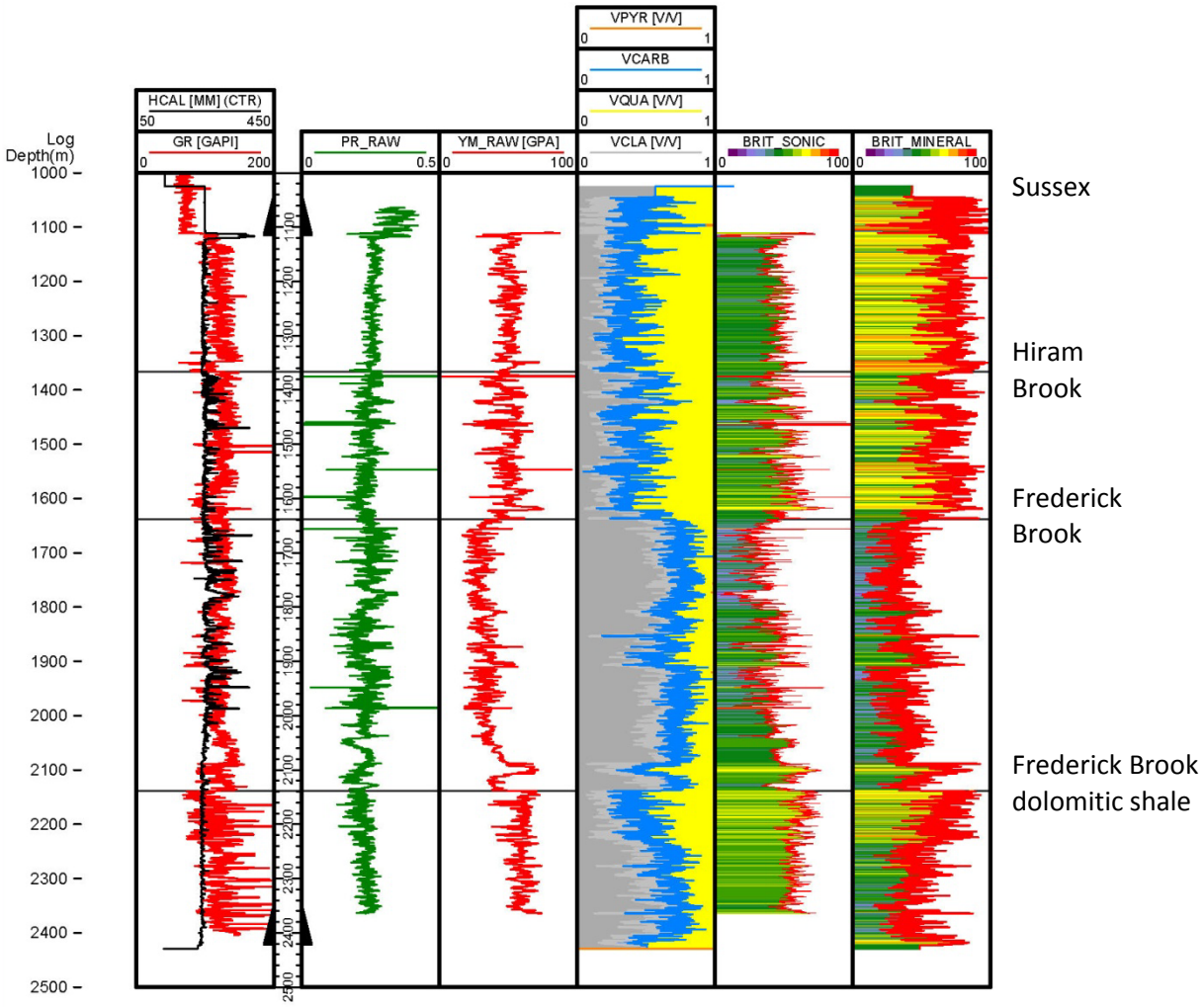

Figure 25 : Detail of the variation with depth of the elastic moduli for the well G-41. YM_RAW : Young's modulus (E), expressed in GPa. PR_RAW : Poisson's ratio (υ), dimensionless; VPYR, VDOL, VCAL, VQUA and VCLA : The proportion expressed as a fraction of, respectively, pyrite, dolomite, calcite, quartz, and clay; BRIT_SONIC and BRIT_MINERAL : Respectively the acoustic and the mineralogical brittleness indexes, expressed as percentages.

3.4 Minimum horizontal principal stress

The minimum horizontal principal stress (Shmin) represents the stress that the fracturing fluid must overcome before an induced fracture can be maintained open after its creation. In this context, Shmin is equated with the closure pressure of the fracture. Variation of the Shmin gradient with depth informs in particular on the existence or the absence of barriers to the propagation of induced fractures across two stratigraphic units.

Shmin is dependent on both lithostatic and pore pressures : these two parameters are reviewed below before calculating the minimum horizontal principal stress gradient. A total of ten wells have been studied in this section (wells E-38, E-67, G-41, G-36, G-67, H-28, J-38, J-47, K-57 and P-66, located in

figure 26). The intermediate and final results are illustrated here only for the wells E-67, G-41 and P-66. All of the final results are compiled in Appendix II.

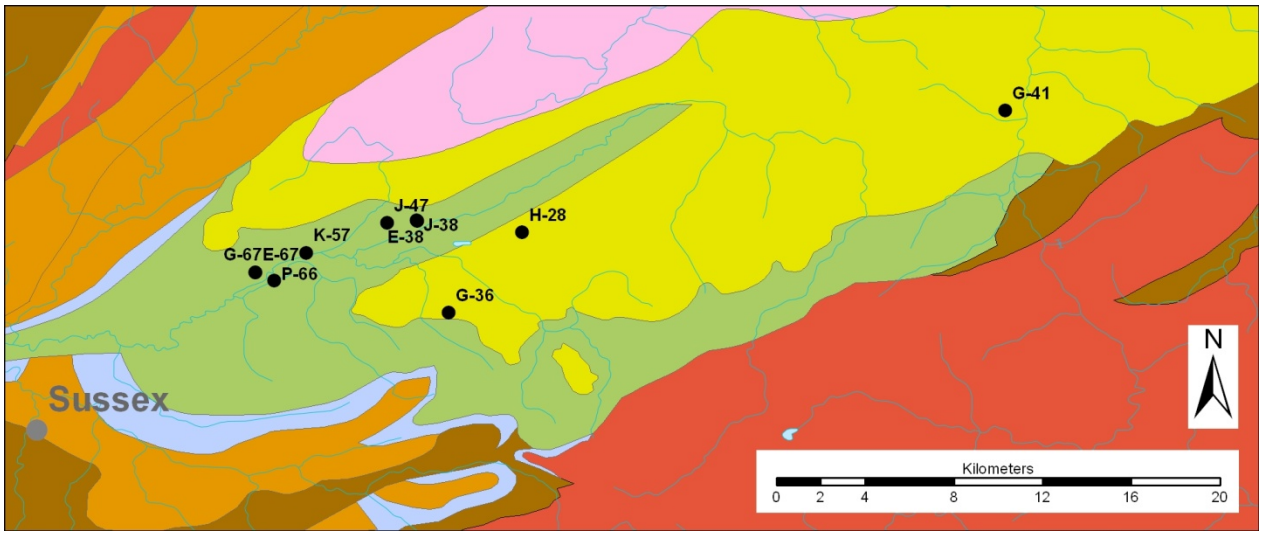

Figure 26 : Location map of the ten wells selected for the minimum horizontal principal stress Shmin study. See figure 1 for the geological legend. Map adapted from New Brunswick Department of Natural Resources (2008).

3.4.1 Estimation of the lithostatic pressure

The lithostatic pressure (Sv) is considered here to be equivalent to the principal vertical stress. Sv has been estimated from the bulk density log (RHOB) by integrating the sum of variations in the bulk density along the profile of a well according to equation (8) below.

$$Sv = \int_0^z \rho(z)\, g\, dz \qquad (8)$$

With : Sv = Lithostatic pressure expressed in kPa/m

$\rho(z) =$ Bulk density (RHOB) as a function of the vertical depth

$g =$ gravitational force or g-force (9.806×10^{-3} kPa/m)

The missing data in the shallow part of the well are approached by extrapolating the bulk density curve up to surface. For some wells RHOB is not recorded above the Sussex Group and a constant replacement density has to be used for each of the missing stratigraphic units. Replacement density values were derived from nearby wells for which an RHOB log was available. In the case of the McCully field, the replacement density values are set at 2694 kg/m^3 for the clastics of the Mabou Group, 2053 kg/m^3 for the evaporites of the Windsor Group, 2825 kg/m^3 for the carbonates of the Windsor Group and 2731 kg/m^3 for the clastics of the Sussex Group (or extrapolated from the base of the unit whenever possible). In the case of the Elgin area a single replacement density of 2608 kg/m^3 was set for the Mabou, Windsor (devoid of halite) and Sussex groups.

3.4.2 Estimation of the pore pressure

The pore pressure (Pp), or internal pressure of fluid, is an important intermediate parameter in the calculation of the minimum horizontal principal stress. Three independent sets of data are available to estimate this pore pressure, i.e downhole pressure gauge records (or pressure logs), pressure build-ups after a production test or a hydraulic fracturing event, and the density of the drilling mud.

Pore pressures estimated from pressure logs or test build-ups are available essentially for the Hiram Brook Member (thirteen wells, fifty-five data points in total). A single data point is also available for the Frederick Brook Member and another, of questionable quality, for the underlying Dawson Settlement Member. Absolute pore pressures and their gradients are compiled in table 7. From this data set the mean and median values of the pore pressure gradient in the Hiram Brook Member are estimated respectively to 12.07 kPa/m and 11.88 kPa/m. The pore pressure gradient (Grad_Pp) in the Hiram Brook Member is arbitrarily set to 12.00 kPa/m in this study.

The pore pressure can also be estimated with a simple relationship from the density of the drilling mud and the gravitational force according to the relationship expressed by equation (9) :

$$Pp = MW \times g \times VD \qquad (9)$$

With : Pp = Pore pressure expressed in kPa

MW = Density of the drilling mud expressed in kg/m^3

g = Gravitational force or g-force (9.806×10^{-3} kPa/m)

VD = Vertical depth expressed in meters

This relationship is considered here as a reasonable first approximation on the condition that it is consistent with, and confirmed by, other sets of data including pressure logs and pressure build-ups records, the occasional water and gas show documented during drilling, as well as the possible losses of circulation. This validation was verified individually for each of the wells for which Shmin was calculated. Examples are presented below for the wells E-67, G-41 and P-66. These three wells were selected for the quality of the available data and for the representativeness of the documented cases (figures 26 to 28).

Table 7 : Synthesis of pore pressure data compiled from the pressure logs and the build-up pressure measurements for the McCully gas field.

Well	Measured Depth (m)	Vertical Depth (m)	Pore Pressure (kPa)	Pore Pressure Gradient (kPa/m)	Stratigraphic Unit	Type of test
D-66	3060.98	2604.64	30357.36	11.66	A Sand	Volumetric limited draw-down
	2466.71	2025.38	24851.02	12.27	F Sand	Volumetric limited draw-down
	2975.51	2520.71	29185.25	11.58	B Sand	Volumetric limited draw-down
	2991.7	2536.62	29903.1	11.79	B Sand	Volumetric limited draw-down
E-38	2702.47	2702.47	34246.3	12.67	C Sand	Volumetric limited draw-down
	2612.41	2612.41	20933.8	8.01	D Sand	Volumetric limited draw-down
H-76	2850.38	2755.54	33279.41	12.08	A Sand	Volumetric limited draw-down
	2847.02	2752.23	33887.93	12.31	A Sand	Volumetric limited draw-down
	2842.89	2748.14	32848.14	11.95	A Sand	Volumetric limited draw-down
	2839.66	2744.95	31581.61	11.51	A Sand	Volumetric limited draw-down
	2826.74	2732.2	33430.88	12.24	A Sand	Volumetric limited draw-down
	2829.44	2734.86	31429.01	11.49	A Sand	Volumetric limited draw-down
	2710.94	2617.72	31278.25	11.95	B Sand	Volumetric limited draw-down
	2707.47	2614.28	29784.81	11.39	B Sand	Volumetric limited draw-down
J-38	2817.68	2559.55	32037.49	12.52	D Sand	Normal pretest - CMR noise
	2817.68	2559.55	32030.84	12.51	D Sand	Normal pretest
	2816.31	2558.18	31644.41	12.37	D Sand	Normal pretest
	2811.39	2553.28	32322.47	12.66	D Sand	Normal pretest
	2678.78	2421.26	29955.98	12.37	E Sand	Normal pretest
	2676.48	2418.97	27502.87	11.37	E Sand	Normal pretest
	2674.38	2416.88	27493.95	11.38	E Sand	Normal pretest
	2669.23	2411.76	27882.47	11.56	E Sand	Normal pretest
	2673.47	2415.98	27482.44	11.38	E Sand	Normal pretest
	2683.99	2426.45	29732.35	12.25	E Sand	Normal pretest
J-47	2985.1	2433.74	30896.95	12.70	Frederick Brook	Volumetric limited draw-down
	2909.02	2364.83	30956.38	13.09	A Sand	Volumetric limited draw-down
	2588.9	2085.55	26271.96	12.60	D Sand	Volumetric limited draw-down
L-38	2917.54	2496.88	35630.36	14.27	E Sand	Volumetric limited draw-down
	2917.07	2496.42	35628.83	14.27	E Sand	Volumetric limited draw-down
	2917.07	2496.42	35628.05	14.27	E Sand	Volumetric limited draw-down
	2917.07	2496.42	35629.02	14.27	E Sand	Volumetric limited draw-down
P-76	2529.03	2495.55	29650.05	11.88	A Sand	Volumetric limited draw-down
	2525	2491.54	29040.95	11.66	A Sand	Volumetric limited draw-down
	2522.47	2489.02	28955.68	11.63	A Sand	Volumetric limited draw-down
	2517.96	2484.53	28980.54	11.66	A Sand	Volumetric limited draw-down
	2528.97	2495.49	29576.06	11.85	A Sand	Repeat of test at 2529 M
	2424.97	2392	29251.82	12.23	B Sand	Volumetric pretest
	2425.97	2392.99	28919.1	12.08	B Sand	Volumetric limited draw-down
F-58	2698.14	2698.14	31538.66	11.69	A Sand	Volumetric limited draw-down
	2569.04	2569.04	27221.07	10.60	B Sand	Volumetric limited draw-down
	2718.74	2718.74	31718.73	11.67	A Sand	Volumetric limited draw-down
	2718.41	2718.41	31714.45	11.67	A Sand	Volumetric limited draw-down
	2717.53	2717.53	31741.98	11.68	A Sand	Volumetric limited draw-down
	2716.52	2716.52	31842.42	11.72	A Sand	Volumetric limited draw-down
	2715.02	2715.02	32808.36	12.08	A Sand	Volumetric limited draw-down
	2718.71	2718.71	31469.72	11.58	A Sand	Volumetric limited draw-down
	2705.73	2705.73	31731.04	11.73	A Sand	Volumetric limited draw-down
	2699.02	2699.02	31452.89	11.65	A Sand	Volumetric limited draw-down
G-67	2373.3	2324.1	27476	11.6	A-B Sands	Post-frac
J-65	2546	2545.3	27244	11.6	B-C-D-E Sands	Post-frac
C-67	2368.5	2330.2	26987	11.4	A-B Sands	Post-frac
C-75	2942.3	2937.8	27412	9.3	Dawson Settlement	Post-frac
D-48	2454.6	2425.5	29688	12.2	B Sand	Post-frac
	2222.5	2201.8	28644	13	D Sand	Pre-frac
	2334	2311.1	29047	12.6	Shale zone in HB	Pre-frac
	2303	2280.6	28841	12.6	Natural fracture in HB	Pre-frac
	2280	2258.1	29238	12.95	B-D-E Sands	Post-frac

In the case of the well E-67 (figure 27), drilling was started underbalance (the pressure of the drilling mud was lower than the pore pressure) but had to be interrupted due to borehole collapse. A first sidetrack, also drilled underbalance, showed the same integrity flaws, with the same consequence. A second sidetrack drilled with a higher mud density finally reached the target depth of 4133 mKB/MD (4083 mKB/VD). The mud density used successfully for the second sidetrack (1200 to 1260 kg/m^3) corresponds to a pore pressure of 11.8 to 12.4 kPa/m, comparable to the mean pore pressure of 12.00 kPa/m that was independently estimated for the Hiram Brook Member from the logs of pressure build-ups (table 7).

In the case of the well G-41 (figure 28) a total gas curve is also available, that allows to independently verify the pore pressure derived from the mud density. The comparison between the mud density and the gas shows that had to be controlled by increasing the mud density, confirms that the pore pressure gradient inferred from the density of the mud is slightly undervalued but still realistic for this well. The overpressured intervals documented in the Frederick Brook Member seem to coincide with naturally fractured intervals.

In the case of the well P-66 (figure 29) the mudweight is high from the base of the surface casing, but not abnormal for the region. The well was drilled on air in the Sussex Group between 1800 and 1990 mKB/VD. Two attempts to drill on air were also made in the Hiram Brook Member but these were interrupted due to downhole fires and the drilling resumed with a water-based mud. The mud density had to be increased but the pressure was difficult to maintain. Finally the last section of the well could be drilled on air again, from 2169 mKB/VD down. The pore pressure gradient inferred from the mud density above the base of the intermediate casing is possibly slightly overestimated by comparison with other wells. The gradient inferred below the base of the intermediate casing is also overestimated, this time due to operational issues despite an attempt to bring down the density of the mud.

In the end, the comparison of the different datasets for the ten wells considered here indicates that a realistic approach is to distinguish two pore pressure gradients on a stratigraphic basis, one gradient set at 11.35 kPa/m from the Mabou Group to the Sussex Group and one gradient set at 12.00 kPa/m from the Hiram Brook Member down to the total depth.

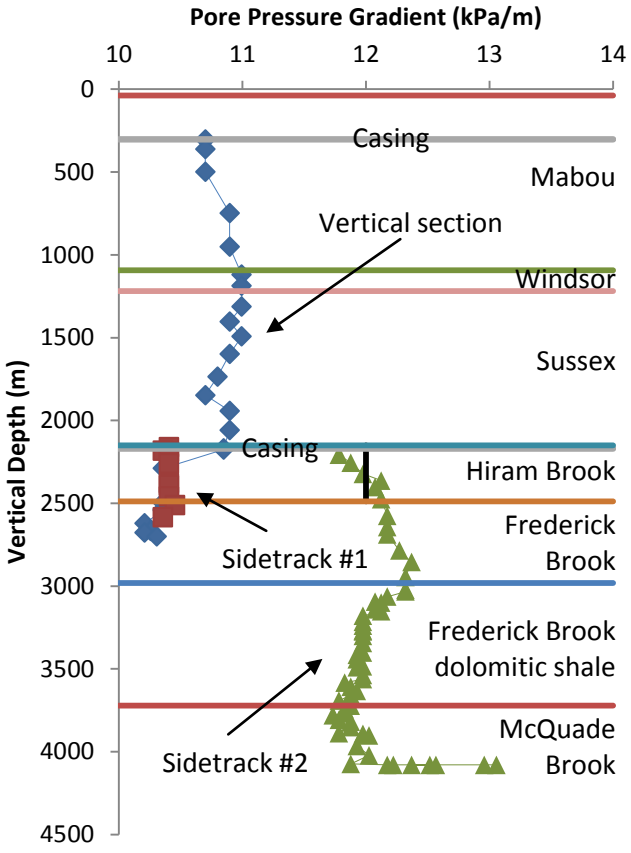

Figure 27 : Variation of the pore pressure gradient with the depth and the stratigraphic assemblages considered for the well E-67. The black vertical line corresponds to the pore pressure gradient established from thirteen wells for the Hiram Brook Member (12.00 kPa/m).

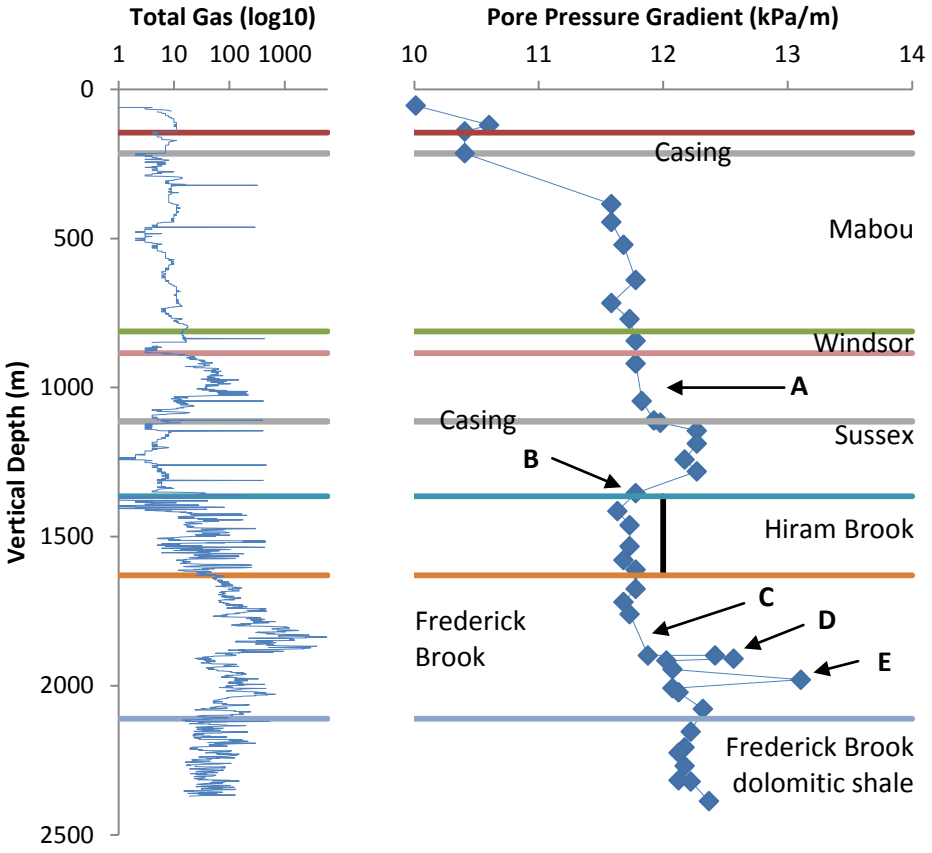

Figure 28 : Variation of the pore pressure gradient with the depth and the stratigraphic assemblages considered for the well G-41. A : Gas show at 1013-1027 mKB/VD; B : Gas show at 1362 mKB/VD; C : Strong gas show at 1842-1856 mKB/VD; D : Strong gas show at 1883-1895 mKB/VD; E : Increase in the mudweight to 1285 kg/m^3 before coring at 1928-1935 mKB/VD, after several hours of flaring at 1200 kg/m^3. The black vertical line corresponds to the pore pressure gradient established from thirteen wells for the Hiram Brook Member (12.00 kPa/m).

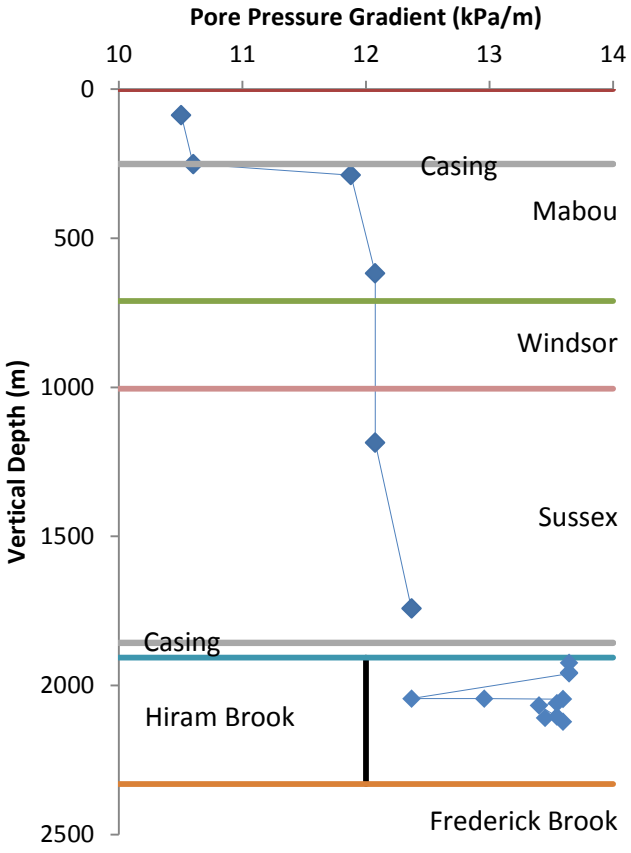

Figure 29 : Variation of the pore pressure gradient with the depth and the stratigraphic assemblages considered for the well P-66. The black vertical line corresponds to the pore pressure gradient established from thirteen wells for the Hiram Brook Member (12.00 kPa/m).

3.4.3 Estimation of the minimum horizontal principal stress

The gradient of the minimum horizontal principal stress (Grad_Shmin) is estimated using the relationship between the Poisson's ratio, the lithostatic pressure and the pore pressure according to equation (10) established by Eaton (1969) :

$$Grad\_Sh_{min} = \frac{1}{VD}\left(\frac{\upsilon}{1-\upsilon} \times (Sv - Pp) + Pp\right) \qquad (10)$$

With : Sh_{min} expressed in kPa/m

υ = Poisson's ratio (dimensionless)

Sv = Lithostatic pressure expressed in kPa

Pp = Pore pressure expressed in kPa

VD = Vertical depth expressed in meters

The gradient of the minimum horizontal principal stress (Grad_Shmin) has been calculated for wells E-38, E-67, G-41, G-36, G-67, H-28, J-38, J-47 K-57 and P-66 (located to figure 26). The results are summarized in table 8 and presented graphically for each well in Appendix II. As an illustration, the variation of Grad_Shmin based on the stratigraphic units (figures 30 to 32) as well as the variation of the principal stresses with depth (figures 33 to 35) are presented below for the wells E-67, G-41, and P-66.

Table 8 : Synthesis of the values estimated for the gradient of the minimum horizontal principal stress (Grad_Shmin). The list of the wells considered here is recorded in table 1. Gr. : Group; Fm. : Formation; Mb. : Member; Min. : Minimum; Avg. : Average; Med. : Median; Max. : Maximum; Dev. : Standard deviation; N : Number of wells.

Grad_Shmin (kPa/m)	Mabou Gr.	Windsor Gr. (evapo-rites)	Windsor Gr. (carbo-nates / clastics)	Sussex Gr.	Hiram Brook Mb.	Frederick Brook Mb.	Frederick Brook Mb. (dolo-mitic)	McQuade Brook Fm.
Min.	14.55	13.30	15.86	6.67	4.93	11.27	14.00	13.96
Avg.	17.17	17.21	17.32	16.24	16.24	16.34	16.83	16.85
Med.	17.09	17.43	17.39	16.32	16.38	16.39	16.97	16.90
Max.	18.83	19.91	18.62	22.17	23.30	19.93	18.84	19.20
Dev.	0.54	0.77	0.38	0.91	1.00	0.86	0.63	0.72
N	2	2	2	10	9	6	3	1

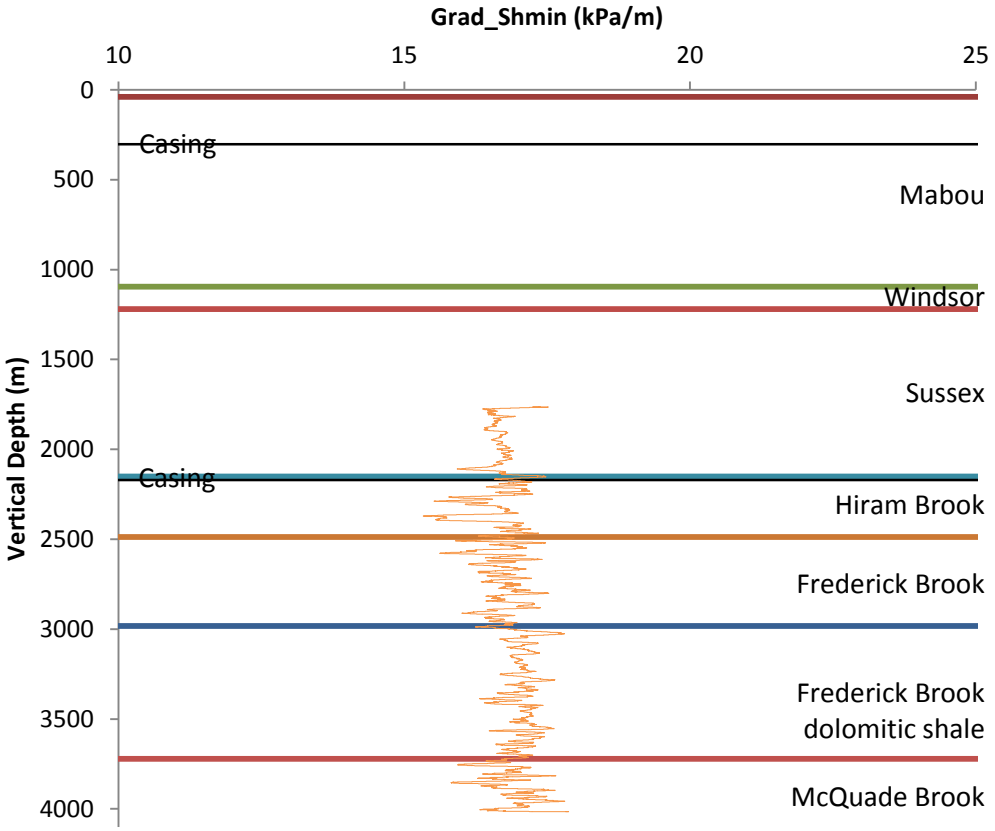

Figure 30 : Variation of the gradient of the minimum horizontal principal stress (Grad_Shmin) based on the vertical depth for the well E-67.

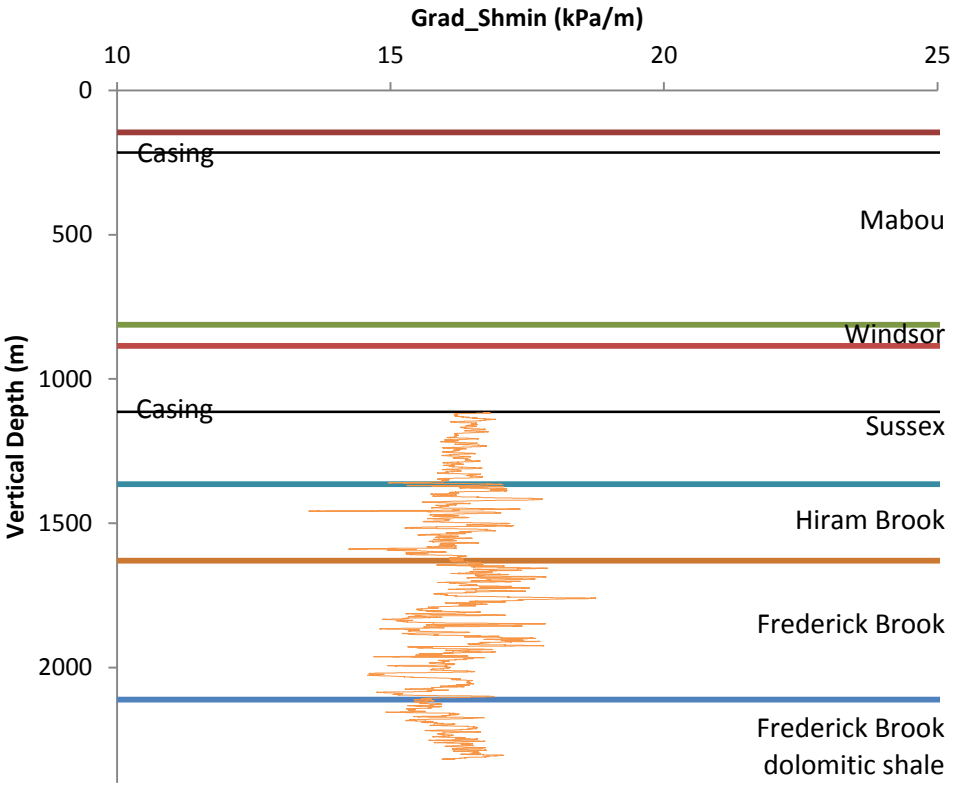

Figure 31 : Variation of the gradient of the minimum horizontal principal stress (Grad_Shmin) based on the vertical depth for the well G-41.

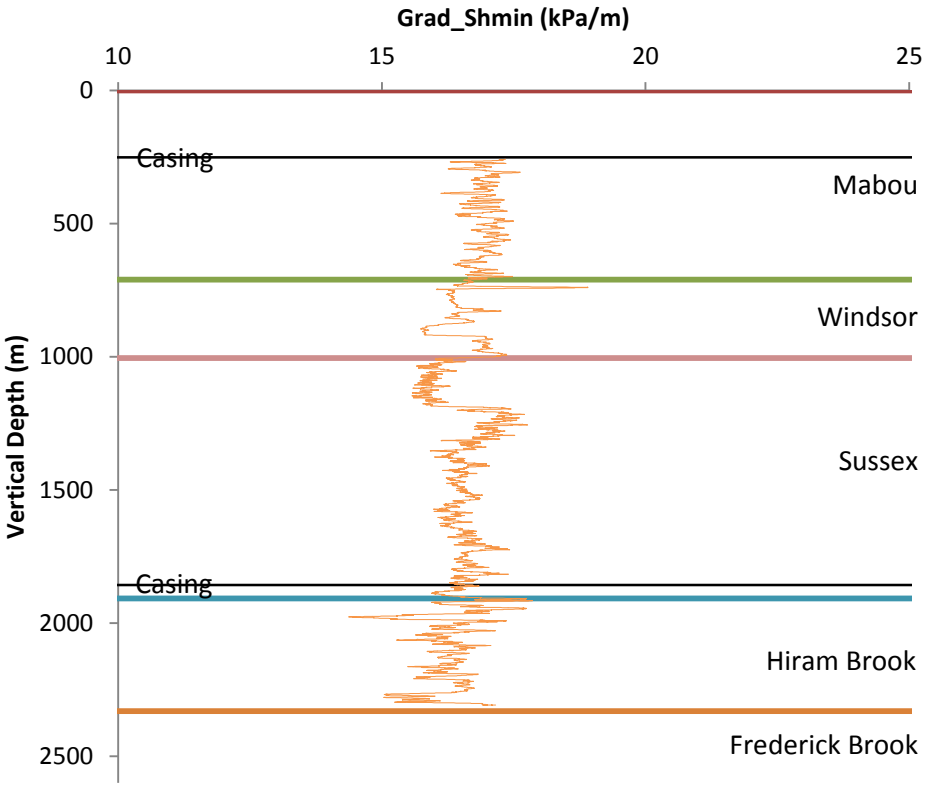

Figure 32 : Variation of the gradient of the minimum horizontal principal stress (Grad_Shmin) based on the vertical depth for the well P-66.

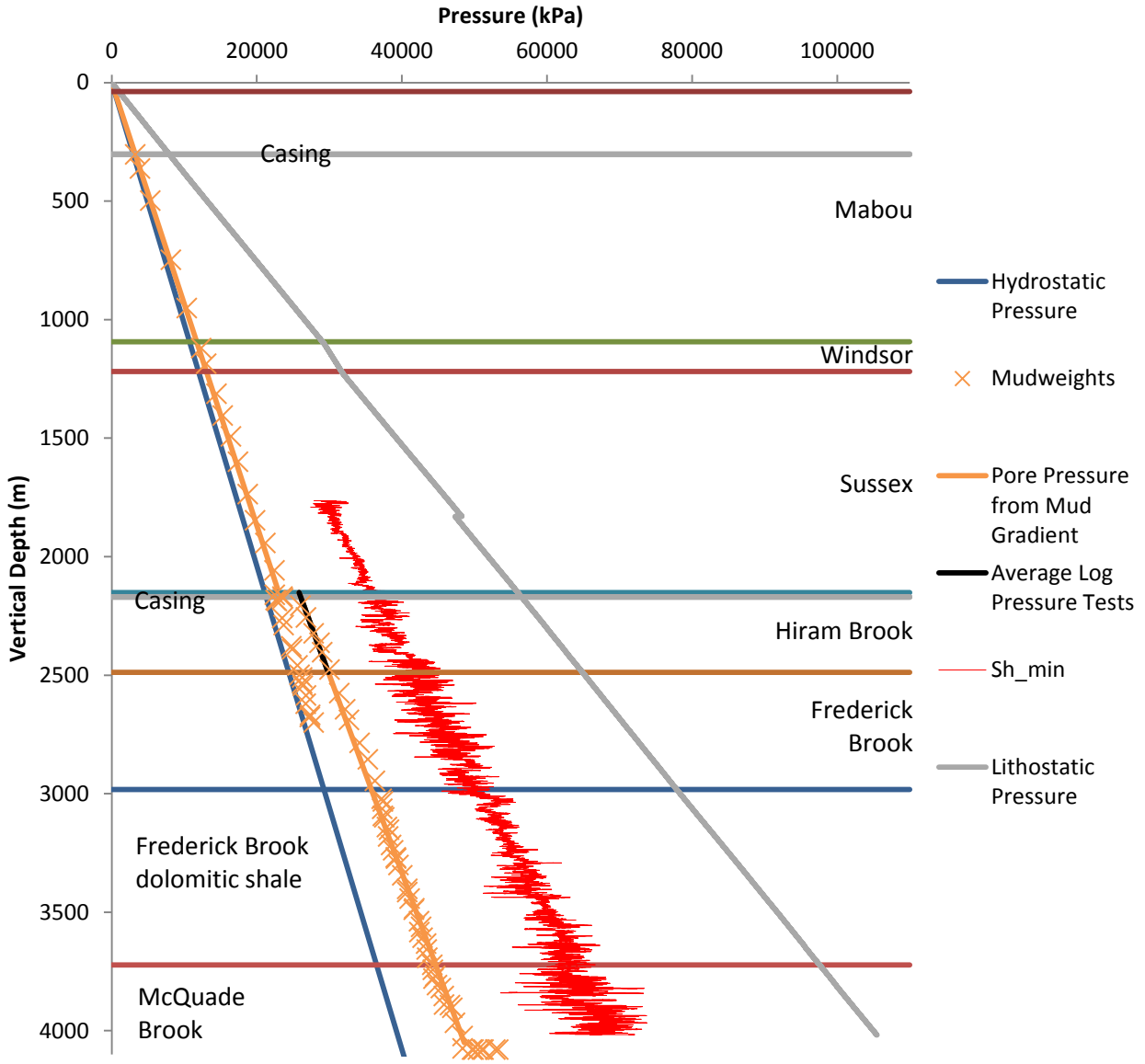

Figure 33 : Pressure profiles as a function of the vertical depth for the well E-67.

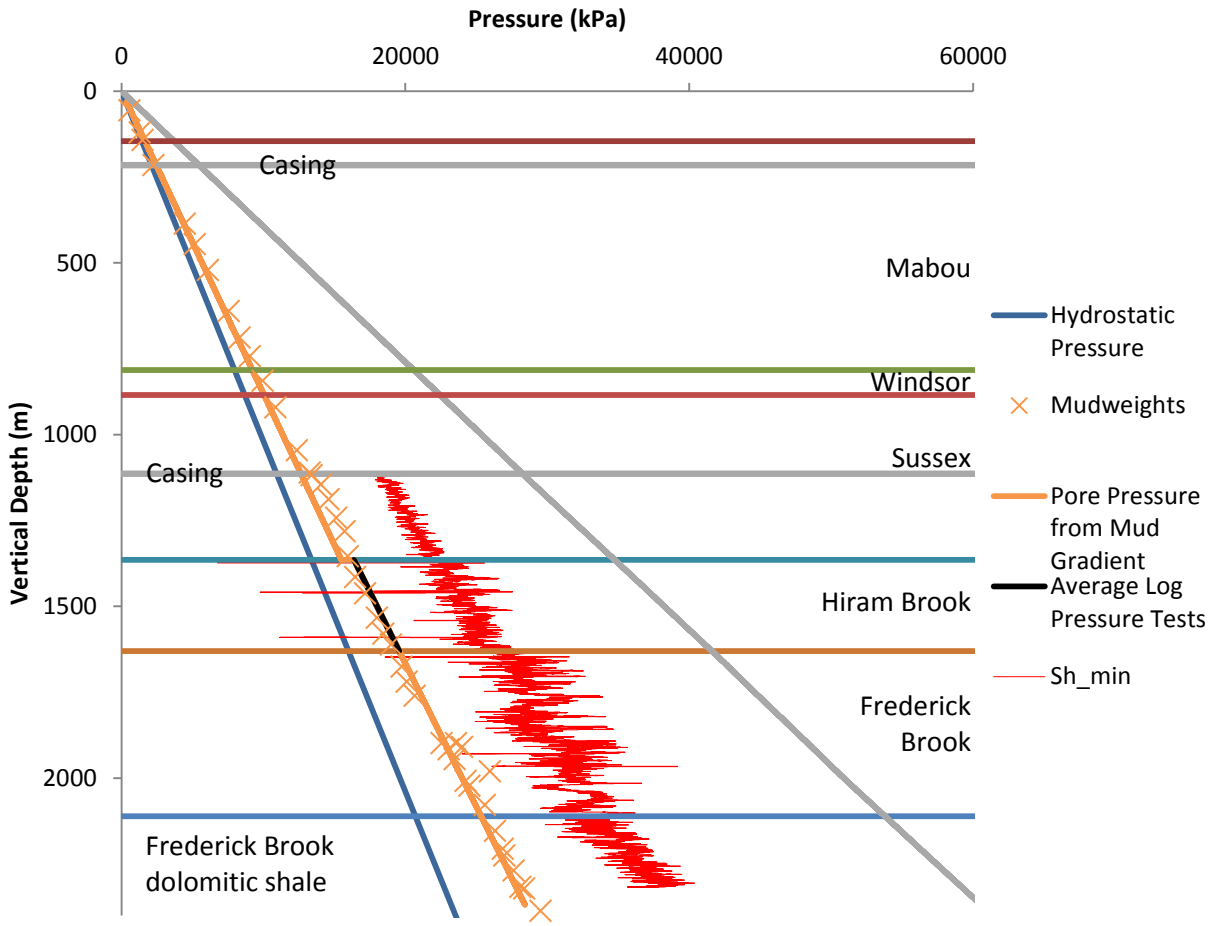

Figure 34 : Pressure profiles as a function of the vertical depth for the well G-41.

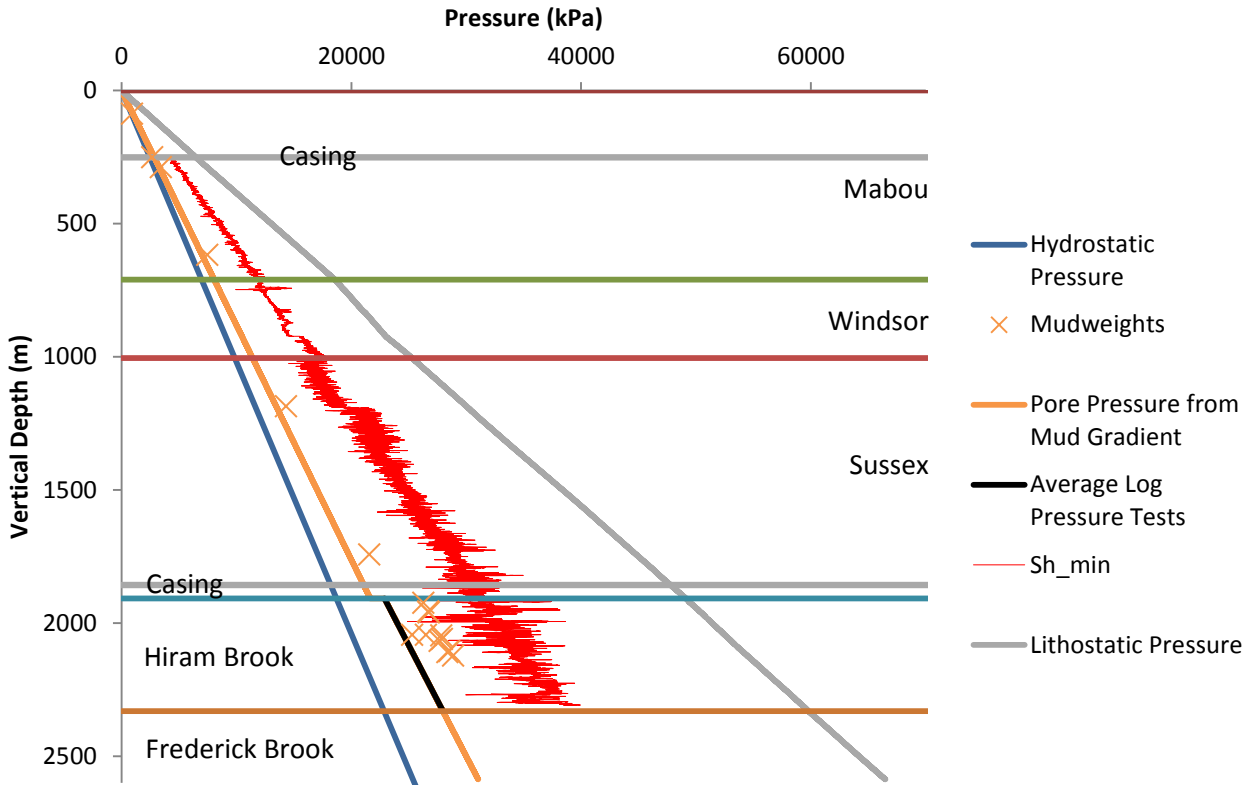

Figure 35 : Pressure profiles as a function of the vertical depth for the well P-66.

3.4.4 Comparison with laboratory data

The laboratory geomechanics tests available for the well G-67 (Core Lab, 2005), already discussed in section 3.2, may be used to estimate Shmin from the static values of υ measured in the laboratory for the Hiram Brook Member in this well (table 6). Figure 36 compares the Shmin values derived from the laboratory data to those estimated independently from the logs. Equation (10) has been used in both cases, with Sv = 22.61 kPa/m and Pp = 12.00 kPa/m. Examination of figure 36 reveals that Shmin derived from laboratory data values evolves within a range comparable to that obtained from the logs, as it was already observed for the values of E and υ (see section 3.2), for both the sandstone and shale samples (one data point stands out for the shales). However, the calibration of Shmin values derived from the logs by the static values of υ measured in the laboratory would only have a semi-quantitative meaning and would introduce errors in the absolute values of Shmin : the values of Shmin derived from laboratory data are therefore used here only to confirm the validity of the assumptions used for calculating Shmin from the logs and the mud density.

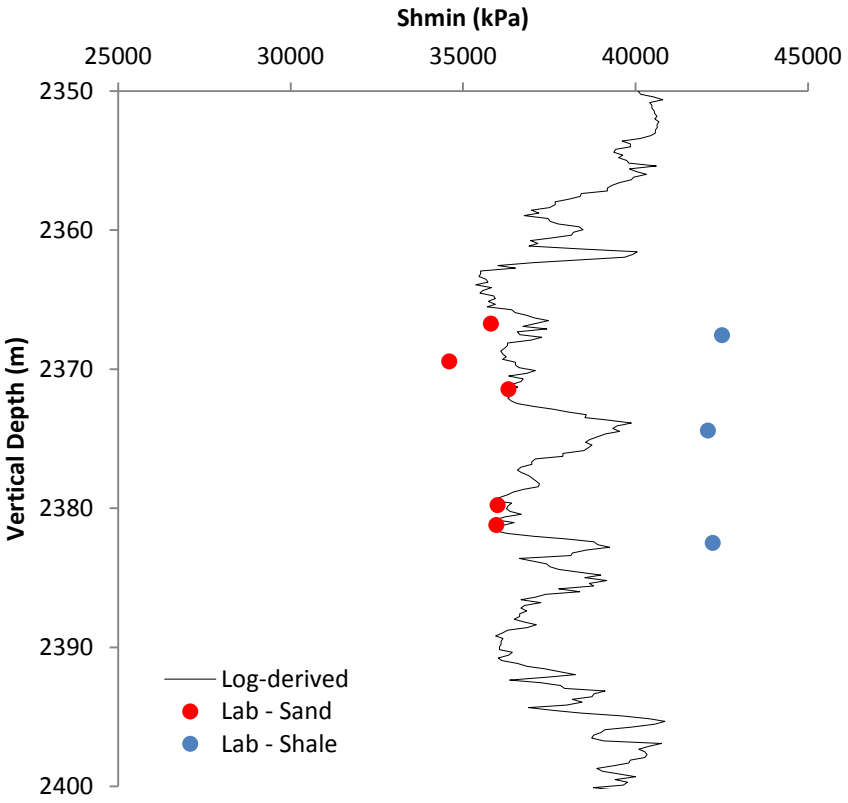

Figure 36 : Minimum horizontal principal stress for the Hiram Brook Member in the well G-67. Comparison between the values derived from the laboratory data (red dots) and the values derived from the logs.

It is worth mentioning that the laboratory data available for the well G-67 include the calculation of Biot's poroelastic constant (α), which contributes to the calculation of Shmin according to equation (11) after Zoback (2007), which is more complex than the equation (10) used for this study. In the case of the well G-67 this constant is calculated in the laboratory for each of the samples. The integration of α to the Shmin equation (equation 11) increases the absolute value calculated for Shmin.

$$Grad\_Sh_{min} = \frac{1}{VD}\left(\frac{\upsilon}{1-\upsilon} \times (Sv - \alpha \times Pp) + Pp\right) \quad (11)$$

With : Sh_{min} expressed in kPa/m

υ = Poisson's ratio (dimensionless)

Sv = Lithostatic pressure expressed in kPa

α = Biot's poroelastic constant (dimensionless)

Pp = Pore pressure expressed in kPa

VD = Vertical depth expressed in meters

In the case of the Hiram Brook Member in the well G-67, α varies between 0.6 and 0.66 (average of 0.64, n = 5) for the sandstone samples and between 0.81 and 0.87 (average of 0.83, n = 3) for the shale samples. The addition of α in the calculation of Shmin increases the latter by 2849 kPa on average in the sandstone intervals and by 2129 kPa on average in the shales, which represents an increase of 8% and 5%, respectively. However, the value of α varies from one sample to another, and it is not possible to extrapolate α to the entire stratigraphic succession, so that this parameter was not included in our previous calculations. Too few data are available yet to allow to extrapolate α to other stratigraphic units in the well G-67, or to other wells in the McCully field. When and if this ever becomes possible, more precise absolute values can be estimated for Shmin.

4. Representativeness of the data and variations at the scale of the gas field

4.1 Extension of the dataset to the western part of McCully and Elgin

In section 3 above it has been possible to estimate geomechanical properties for a representative number of wells in the McCully field and the Elgin area (the latter with incidentally very little data points). However the geographical coverage of these data sets shows an information gap in the western part of each of the two regions. S wave curves are not available in these areas, thus preventing to estimate u, E, BRIT and Shmin for these westernmost areas. To overcome this limitation, a synthetic curve of the S wave has been generated for the wells C-75, D-66 and J-65 in the western part of the McCully field and for the wells DeM1 and M-59 in the western part of the Elgin area (figure 37 and table 2). This synthetic curve allowed to estimate u, E, BRIT and Shmin for these wells and to extend the geographical coverage of the calculated geomechanical parameters across the entire study area.

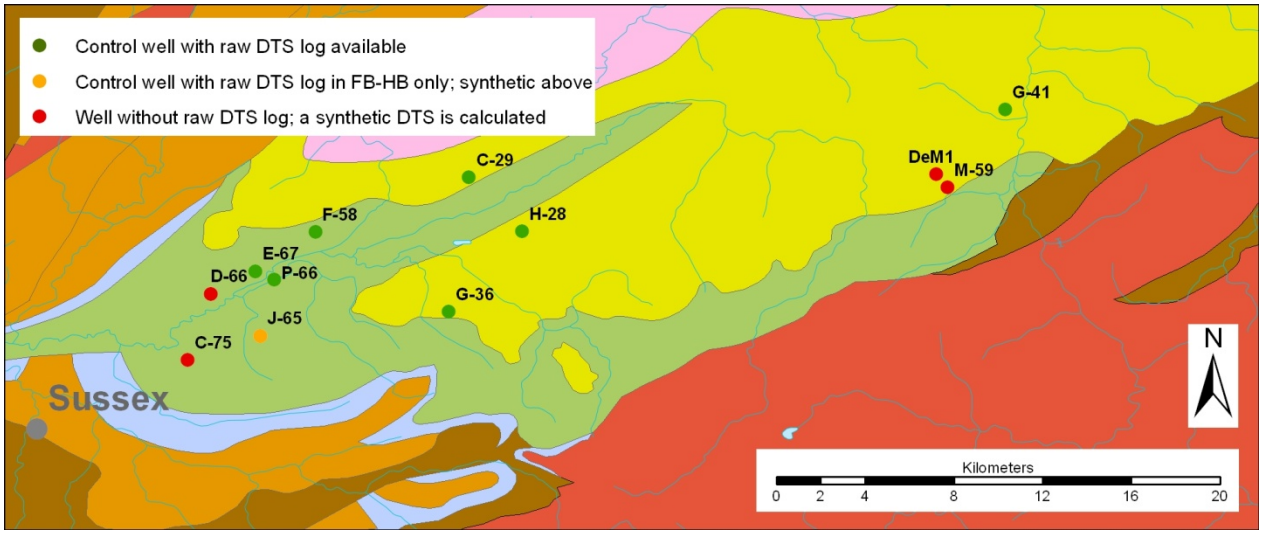

Figure 37 : Location map of the control wells for which an S wave curve was available and location of the wells for which the missing S wave curve has been generated. See figure 1 for the geological legend. Map adapted from New Brunswick Department of Natural Resources (2008).

4.1.1 Generation of a synthetic S wave curve

The technique used to generate synthetic curves for the S wave (DTS_SYNTH) is presented in Séjourné (2015a, 2015b, 2017) and is only summarised here. Based on relationships established specifically for the study area in southern New Brunswick, DTS_SYNTH is derived from the neutron porosity (NPOR), the deep resistivity (RD) and the P wave (DTP) according to equation (12) below. The Windsor Group is an exception here: in the absence of sufficient log data to calculate DTS_SYNTH using equation (12), fixed values have been assigned to this group, respectively 415 µs/m and 325 µs/m for the halite/anhydrite interval (Clover Hill and Cassidy Lake formations) and for the gypsum, anhydrite, conglomerate, sandstone, mudstone, carbonate interval (Upperton and Macumber formations).

$$DTS\_SYNTH = (0.798 \times (554.61721906 \times \mathrm{NPOR} + 263.9771) + 0.4446 \times (563.10465438 - 152.51691860 \times \mathrm{LOG(RD)} + 23.46816576 \times \mathrm{LOG(RD)}^2) + 0.898 \times (1.93821238 \times \mathrm{DTP} - 39.6643)) / (0.798 + 0.44460 + 0.898) \quad (12)$$

A DTS_SYNTH curve was generated for eight control wells for which an S wave curve was available (wells C-29, E-67, F-58, G-36, G-41, H-28, J-65 and P-66) as well as for five wells for which the S wave curve was missing (wells C-75, D-66, DeM1, J-65 and M-59) (figure 37). A particular case, the well J-65, has a raw DTS curve for the Hiram Brook and Frederick Brook members but not for the overlying units. Therefore, this well was used both as a control well (lower part) and as a synthetic well (upper part).

The quality of the correlation obtained between DTS and DTS_SYNTH is evaluated globally for the eight control wells (figure 38) and individually for each of these wells (examples are shown on figure 39 for the well C-29 and on figure 40 for the well G-41).

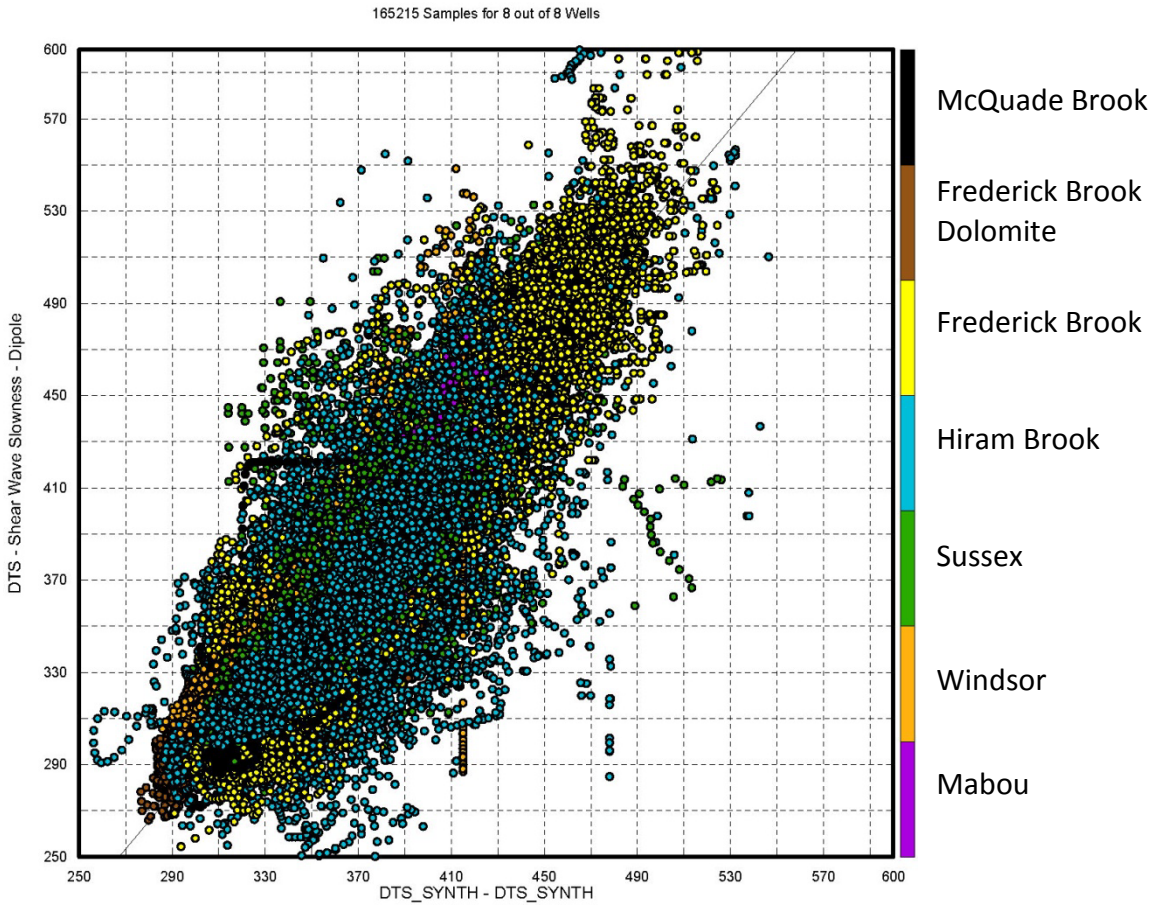

Figure 38 : Correlation obtained between the raw (DTS) and synthetic (DTS_SYNTH) S wave curves for eight control wells. The coefficient of correlation obtained by combining all wells is 0.914. The dispersion of the values in this cross-plot is caused by the aggregation of the results obtained for the eight control wells. In detail this dispersion is reduced when considering each well individually (see figures 39 and 40 for examples).

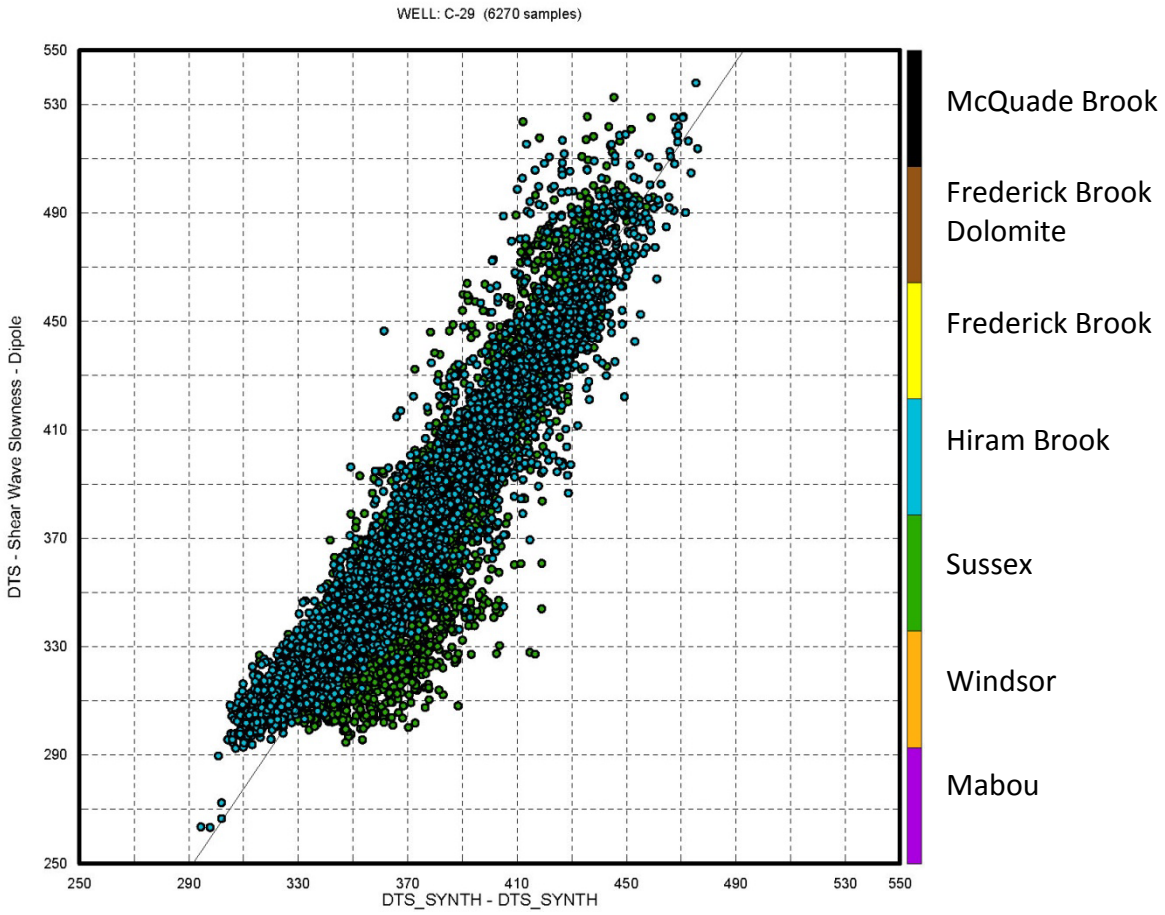

Figure 39 : Comparison between the raw (DTS) and synthetic (DTS_SYNTH) S wave curves for the well C-29 (McCully field). The coefficient of correlation for this well is 0.922.

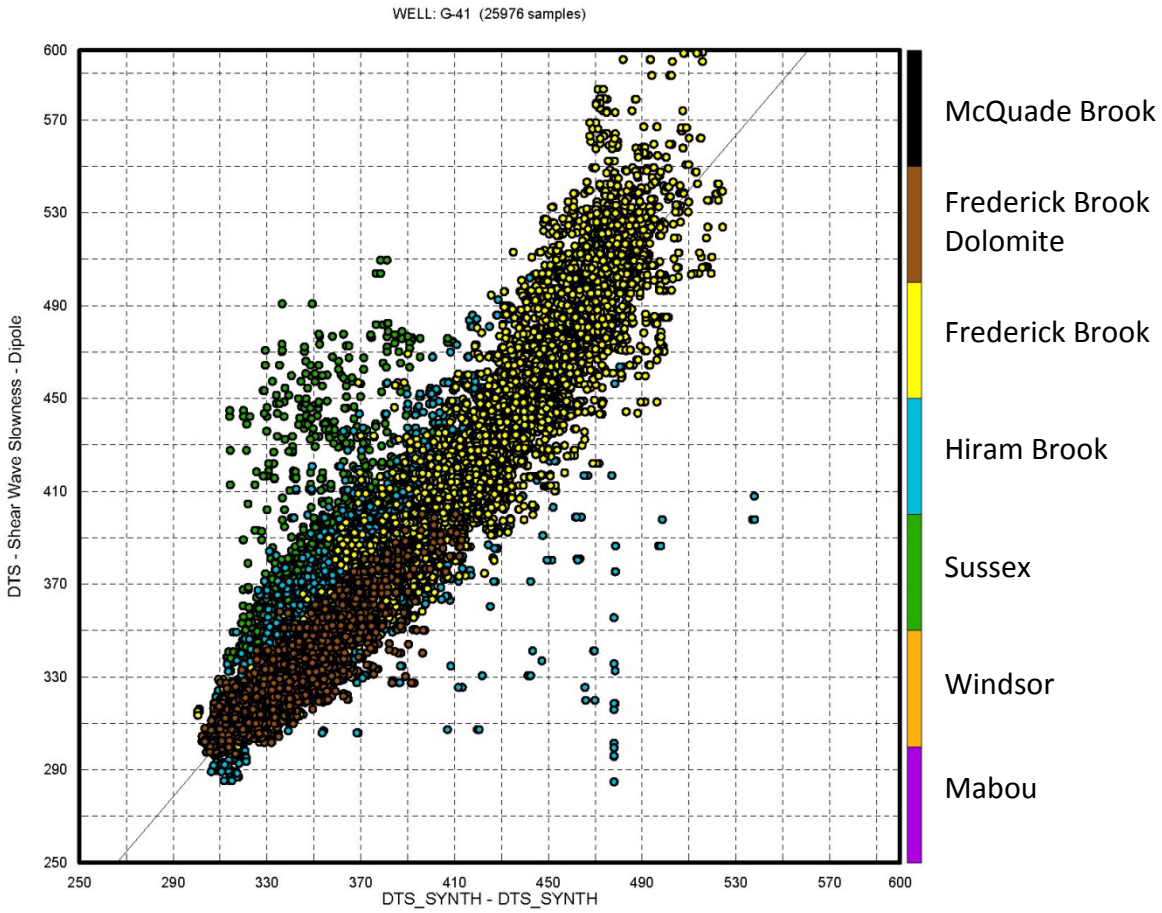

Figure 40 : Comparison between the raw (DTS) and synthetic (DTS_SYNTH) S wave curves for the well G-41 (Elgin area). The coefficient of correlation for this well is 0.925.

4.1.2 Synthetic elastic moduli

For each of the wells considered, synthetic curves for υ, E and BRIT (υ_SYNTH, E_SYNTH and BRIT_SYNTH) were derived from DTS_SYNTH following the method developed in section 3.

In a first step the correlation between the raw and synthetic elastic moduli is verified for each of the control wells. This correlation is illustrated for the McCully gas field (well C-29; figure 41) and for the Elgin area (well G-41; figure 42). The correlation observed for these control wells is not perfect if we consider the absolute values, the synthetic curves being generally smoother than the raw curves. However the general profile of the curves as well as the geomechanical contrasts observed within the same unit and between stratigraphic units are preserved, which confirms that the synthetic elastic moduli and acoustic brittleness indexes generated for the five wells devoid from raw S wave data are representative of the geomechanical properties that would have been calculated if the raw S waves were available.

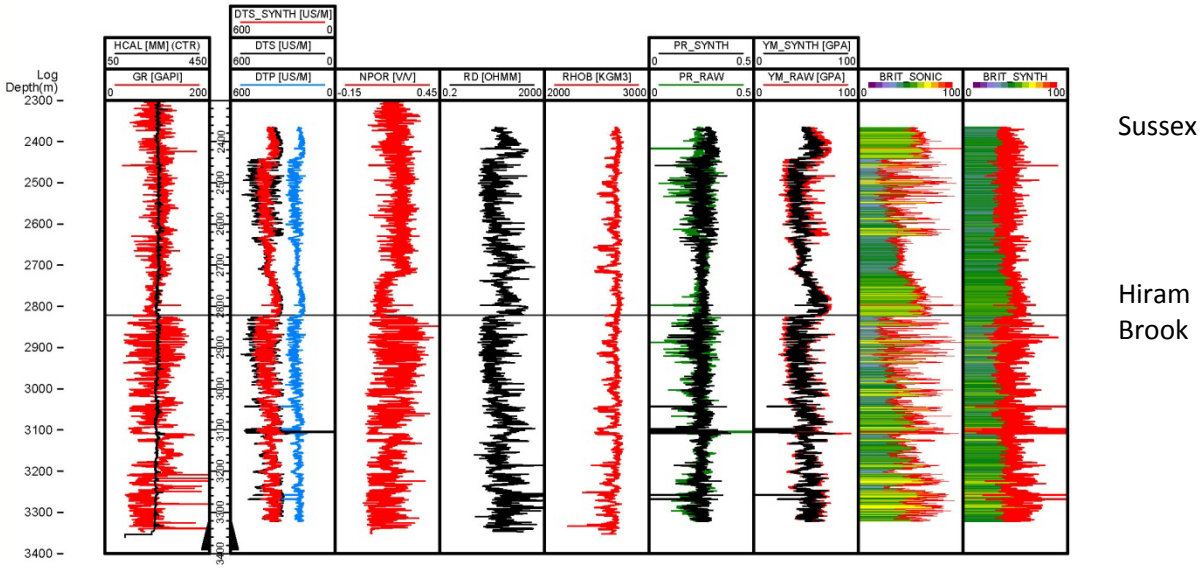

Figure 41 : Comparison between the elastic moduli derived from the raw and synthetic data for the well C-29. YM_RAW : Young's modulus (E), expressed in GPa. PR_RAW : Poisson's ratio (υ), dimensionless; BRIT_SONIC : Acoustic brittleness index, expressed as a percentage; * _SYNTH : Same parameters as above, derived from the synthetic S wave (DTS_SYNTH) instead of the raw curve (DTS).

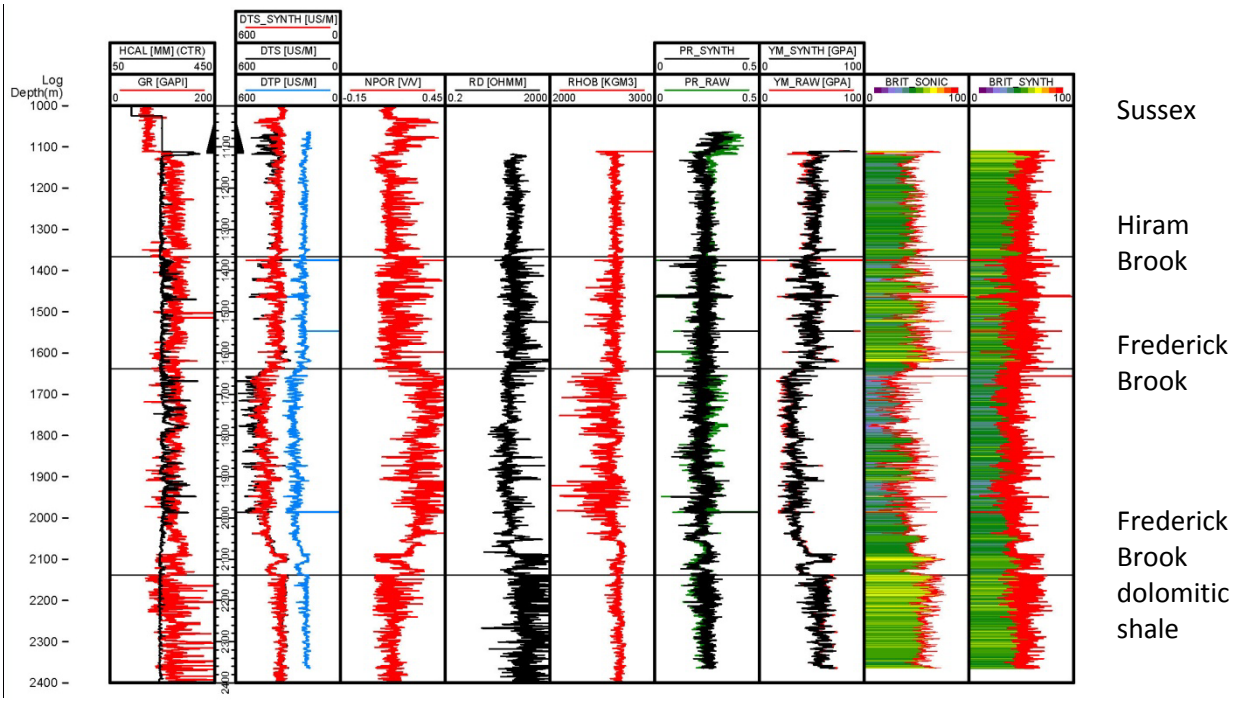

Figure 42 : Comparison between the elastic moduli derived from the raw and synthetic data for the well G-41. YM_RAW : Young's modulus (E), expressed in GPa. PR_RAW : Poisson's ratio (υ), dimensionless; BRIT_SONIC : Acoustic brittleness index, expressed as a percentage; * _SYNTH : Same parameters as above, derived from the synthetic S wave (DTS_SYNTH) instead of the raw curve (DTS).

The synthetic curves established for the wells C-75, J-65, D-66, DeM1 and M-59 are presented in Appendix III. The results for two of these wells are also presented in figure 43 (McCully gas field) and figure 44 (Elgin area) for illustration. All of the results obtained for these five wells are integrated in the analysis of the regional variations of the geomechanical properties that are presented in section 4.2.

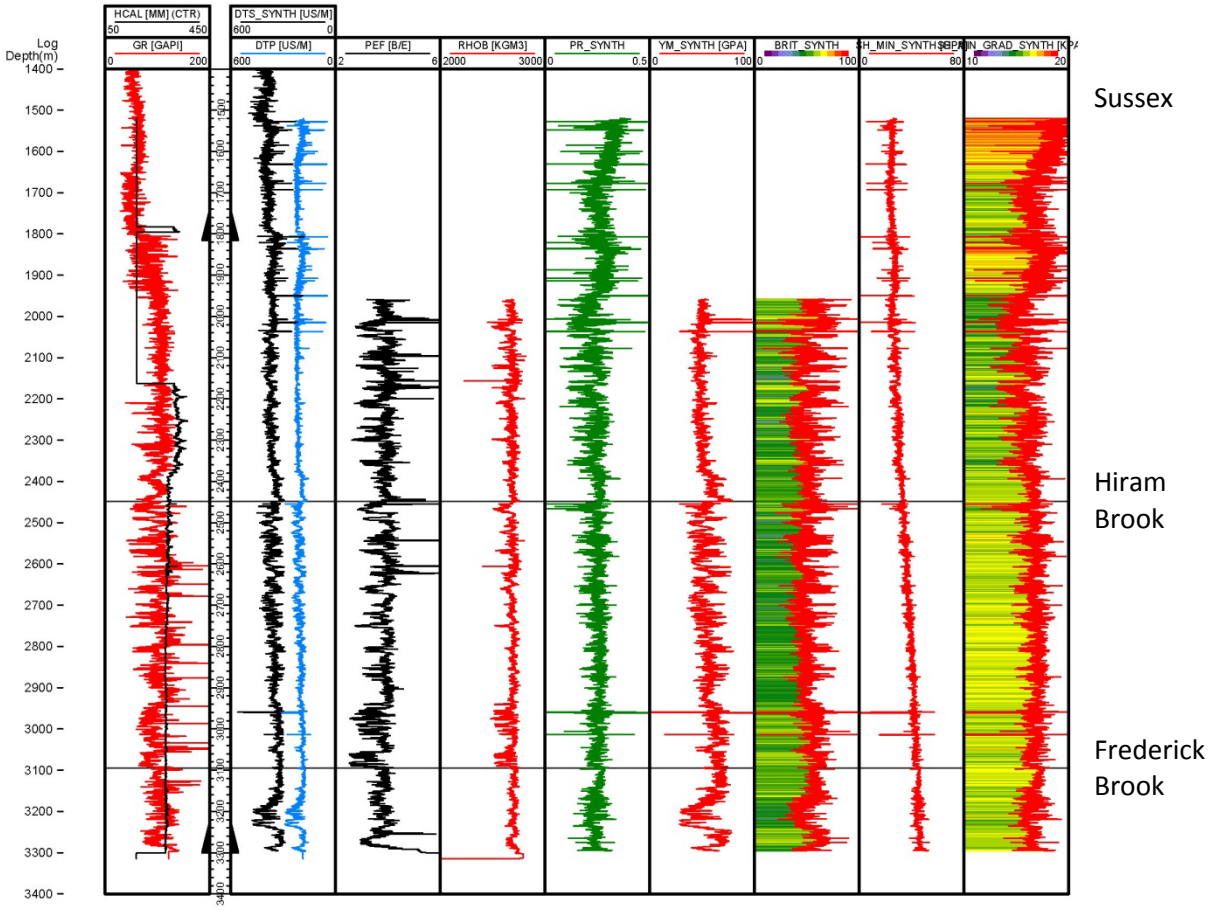

Figure 43 : Illustration of the synthetic geomechanical properties derived from the synthetic data for the well D-66. YM_SYNTH : Young's modulus (E) derived from the synthetic S wave, expressed in GPa. PR_SYNTH : Poisson's ratio (υ) derived from the synthetic S wave, dimensionless; BRIT_SONIC_SYNTH : Acoustic brittleness index derived from the synthetic S wave, expressed as a percentage; SH_MIN_SYNTH : Minimum horizontal principal stress derived from the synthetic S wave, expressed in GPa; SH_MIN_GRAD_SYNTH : Gradient of Shmin derived from the synthetic S wave, expressed in kPa/m. The span of depths for which SH_MIN_SYNTH and SH_MIN_GRAD_SYNTH have been calculated is larger than for the Young's modulus and the acoustic brittleness index because a replacement bulk density curve has been used for the missing interval in the Sussex Group (section 3.4.1)

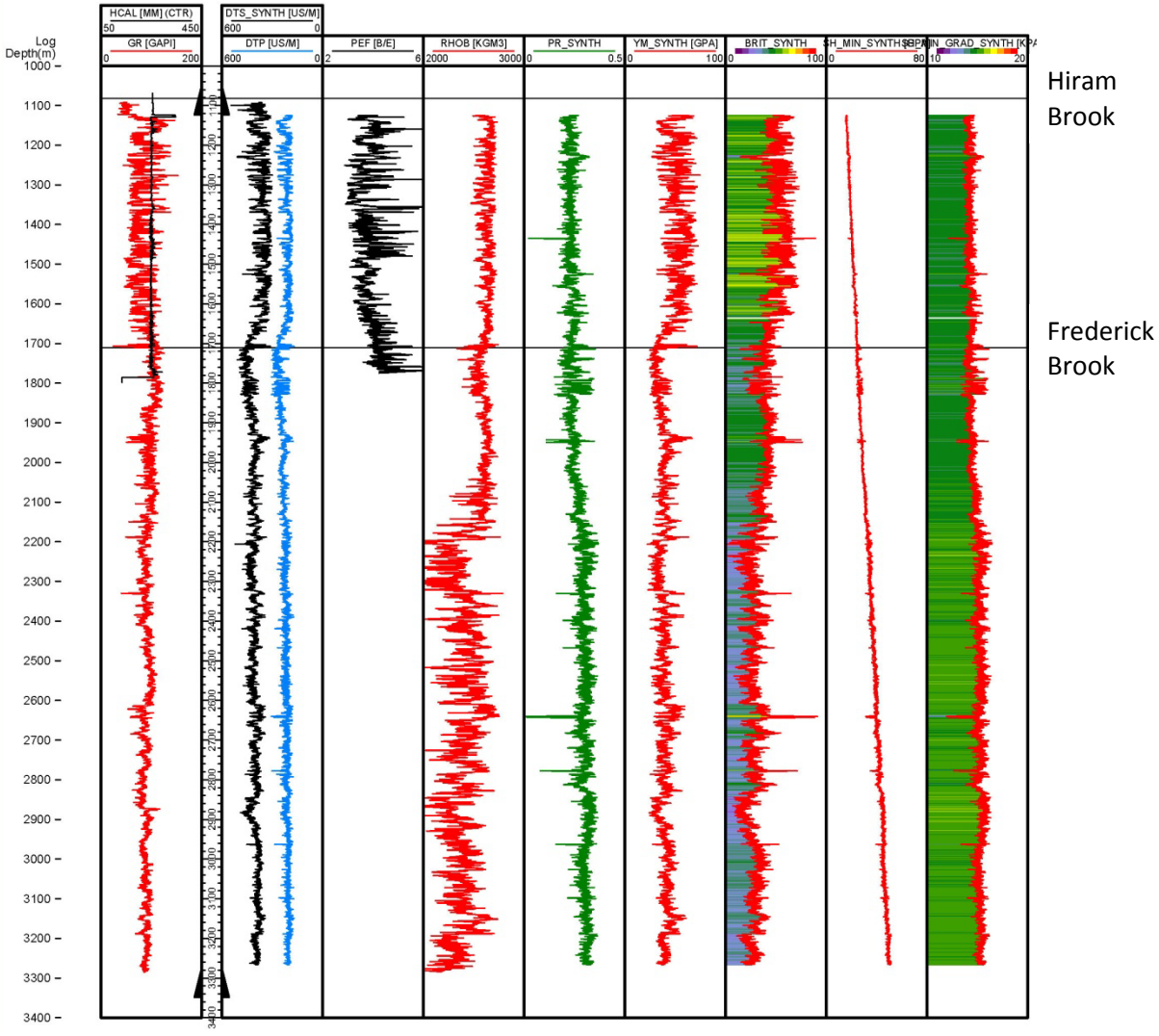

Figure 44 : Illustration of the synthetic geomechanical properties derived from the synthetic data for the well M-59. YM_SYNTH : Young's modulus (E) derived from the synthetic S wave, expressed in GPa. PR_SYNTH : Poisson's ratio (υ) derived from the synthetic S wave, dimensionless; BRIT_SONIC_SYNTH : Acoustic brittleness index derived from the synthetic S wave, expressed as a percentage; SH_MIN_SYNTH : Minimum horizontal principal stress derived from the synthetic S wave, expressed in GPa; SH_MIN_GRAD_SYNTH : Gradient of Shmin derived from the synthetic S wave, expressed in kPa/m.

4.1.3 Synthetic minimum horizontal principal stress

A synthetic Shmin gradient curve (Grad_Shmin_SYNTH) can be calculated from equation (10) by replacing the term υ with the term υ_SYNTH established in section 4.1.2 above. As well as for the elastic moduli, the geographical coverage of the wells for which Shmin values are available was expanded by considering the wells C-75, D-66 and J-65 for the McCully gas field and the wells DeM1 and M-59 for the Elgin area (figure 37).

In the case of the McCully gas field, wells C-75 and J-65 have been discarded because the bulk density curve needed to establish the principal vertical stress that enters the calculation of Shmin was of poor

quality (tables 1 and 2). Well D-66, although closer to the heart of the gas field, is the only well that has been analysed to estimate Shmin_SYNTH and Grad_Shmin_SYNTH. In the case of the Elgin area, the well DeM1 was also discarded for the same reason (table 2) and only the well M-59 was adequate to calculate synthetic Shmin values.

The validity of the results has been verified beforehand by comparing the values of Shmin and Grad_Shmin estimated from the raw and synthetic data from a control well (H-28) for which all of the raw and synthetic datasets were available (figure 45). The superposition of the raw and synthetic values for this well is not perfect if we consider the absolute values, the synthetic curves being generally smoother than the raw curves. The values of the synthetic curves appear also to be slightly underestimated compared to those of the raw curves, particularly in the case of the Mabou Group and to a lesser extent in the Sussex Group. However the general profile of the curves as well as the geomechanical contrasts observed between stratigraphic units and within the same unit are preserved, as was the case for the synthetic elastic moduli (see section 4.1.2), which confirms that Shmin_SYNTH and Grad_Shmin_SYNTH curves generated for the wells devoid from S wave curves are representative of the Shmin values that would have been calculated from the raw data if they would have been available.

The raw and synthetic results for wells D-66 and M-59 are shown respectively in figures 43 and 44. They are also compiled in Appendix III and are integrated in the analysis of the regional variations of the geomechanical properties that is presented in section 4.2

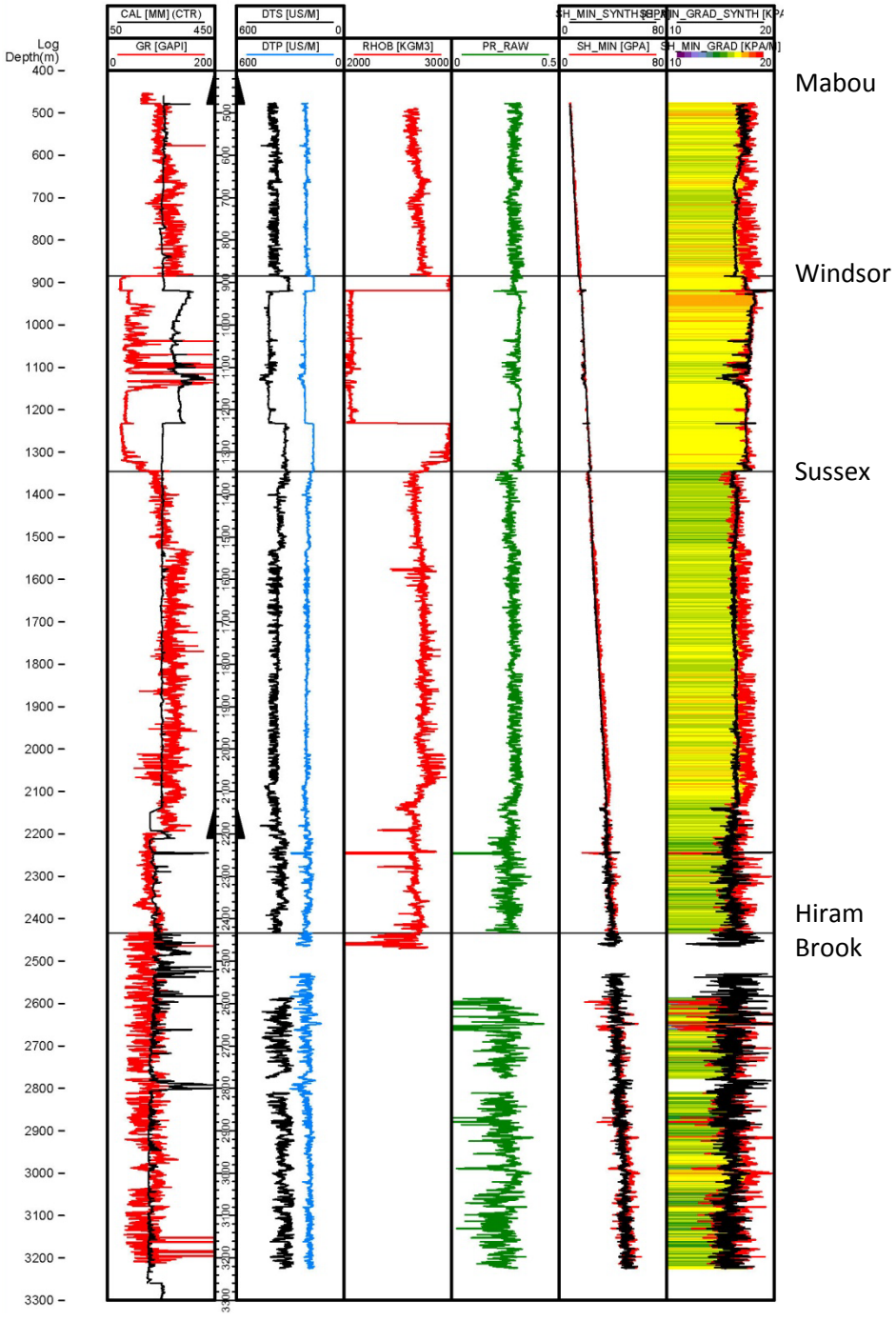

Figure 45 : Comparison of Shmin its gradient derived from the raw and synthetic data for the well H-28. PR_RAW : Poisson's ratio (υ), dimensionless; SH_MIN and SH_MIN_SYNTH : minimum horizontal principal stress Shmin derived from the raw and synthetic data, expressed in GPa. SH_MIN_GRAD and SH_MIN_GRAD_SYNTH : Gradient of Shmin derived from the raw and synthetic data, expressed in kPa/m.

4.2 Variation of the mechanical properties at the scale of the gas field

The variability of the geomechanical properties at the scale of the gas field is examined using the acoustic brittleness index along three cross-sections : a southwest-northeast cross-section in the McCully gas field (figures 46A and 47), a northwest-southeast cross-section in the same field (figures 46B and 48) and a west-east cross-section through the McCully field and the Elgin area (figures 46C and 49). The selection of wells for the construction of these cross-sections is based on the quality of the logs and the representativeness of the petrophysical units for which geomechanical data have been estimated.

A qualitative review of these three cross-sections confirms the low variability of geomechanical properties from one well to another for a given petrophysical unit, and the persistence of the geomechanical contrasts recognized between two petrophysical units from one well to another. A relative homogeneity of the results is thus established within the McCully gas field as well as between this field and the Elgin area, the main geological distinction being the absence of evaporitic units in the Windsor Group in the Elgin area.

Figures 47 to 49 also show that it is possible to establish a complete vertical geomechanical profile of all the petrophysical units by combining data from a small number of type wells, as discussed in section 5 below.

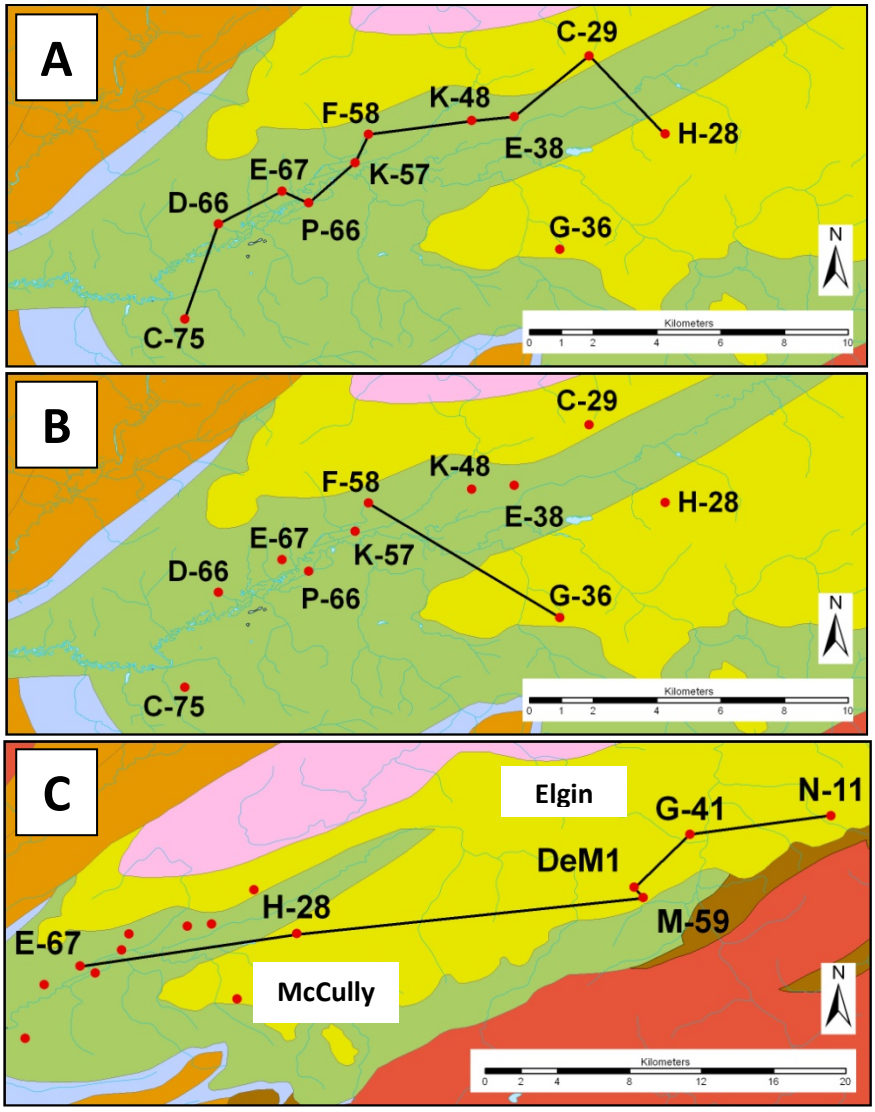

Figure 46 : Location map of the cross-sections prepared to illustrate the regional variability of the geomechanical properties. A : McCully gas field, southwest-northeast cross-section shown in figure 47. B : McCully gas field, northwest-southeast cross-section shown in figure 48; C : McCully gas field and Elgin area, west-east cross-section shown in figure 49. Map adapted from New Brunswick Department of Natural Resources (2008).

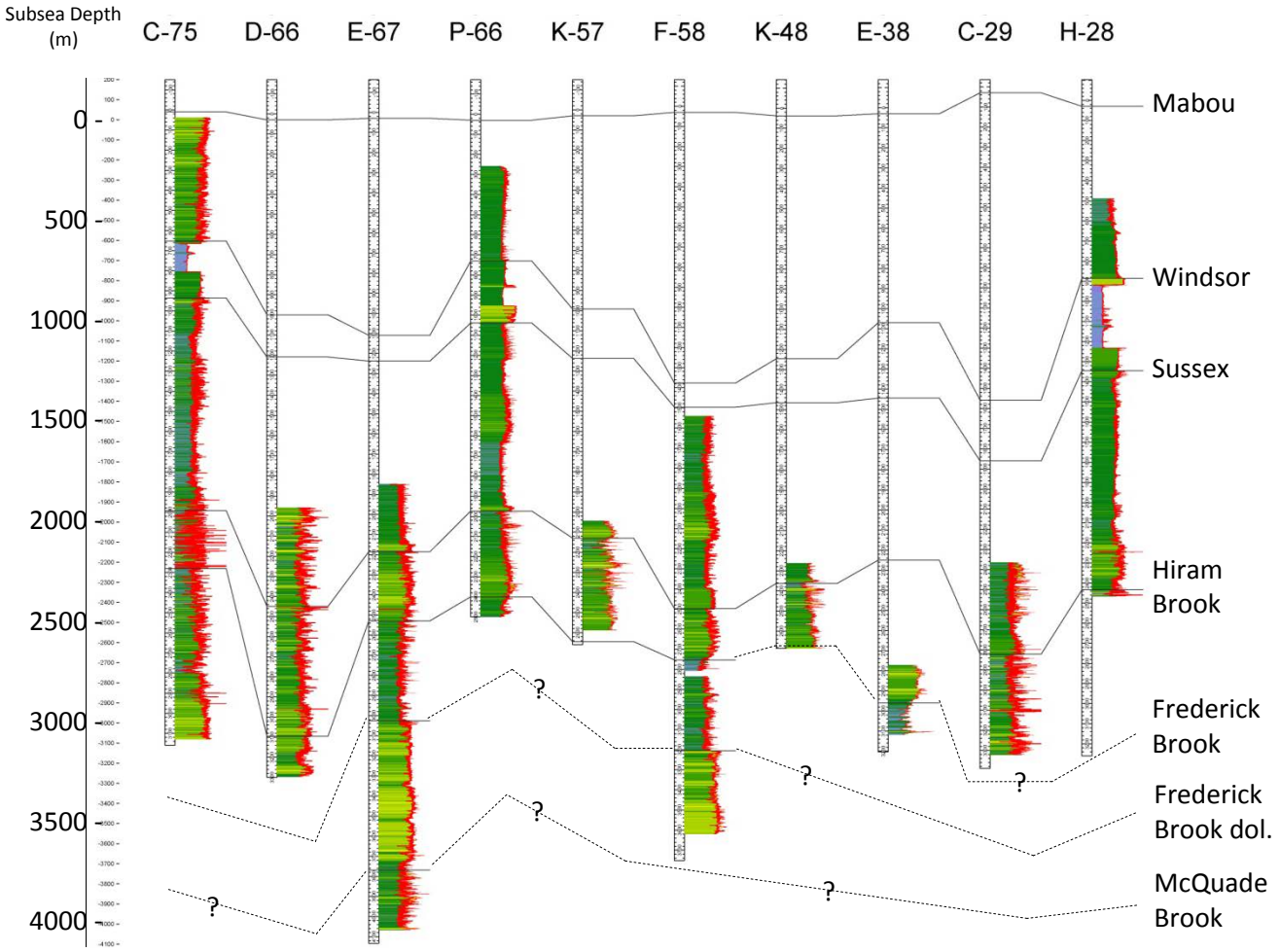

Figure 47 : Variation of the acoustic brittleness index within the McCully gas field along a southwest-northeast cross-section. Datum line for correlation is 200m above sea level. The cross-section is located on figure 46A. Acoustic brittleness indexes calculated for wells C-75 and D-66 are derived from the synthetic S wave.

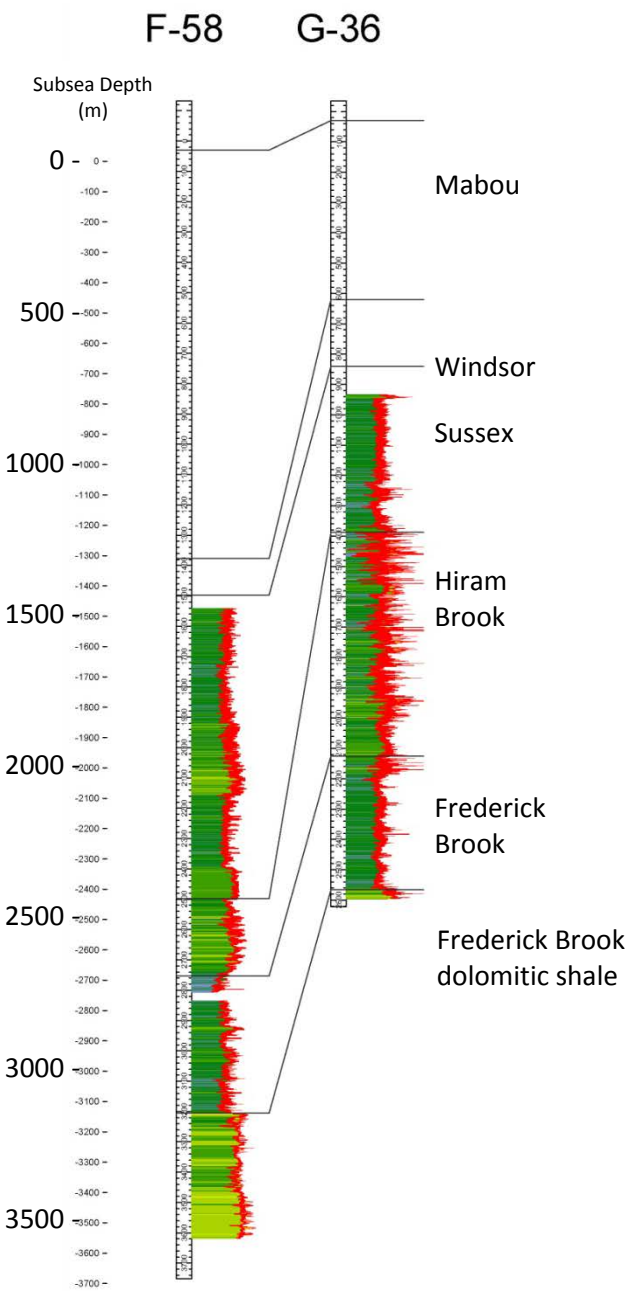

Figure 48 : Variation of the acoustic brittleness index within the McCully gas field along a northwest-southeast cross-section. Datum line for correlation is 200m above sea level. The cross-section is located on figure 46B.

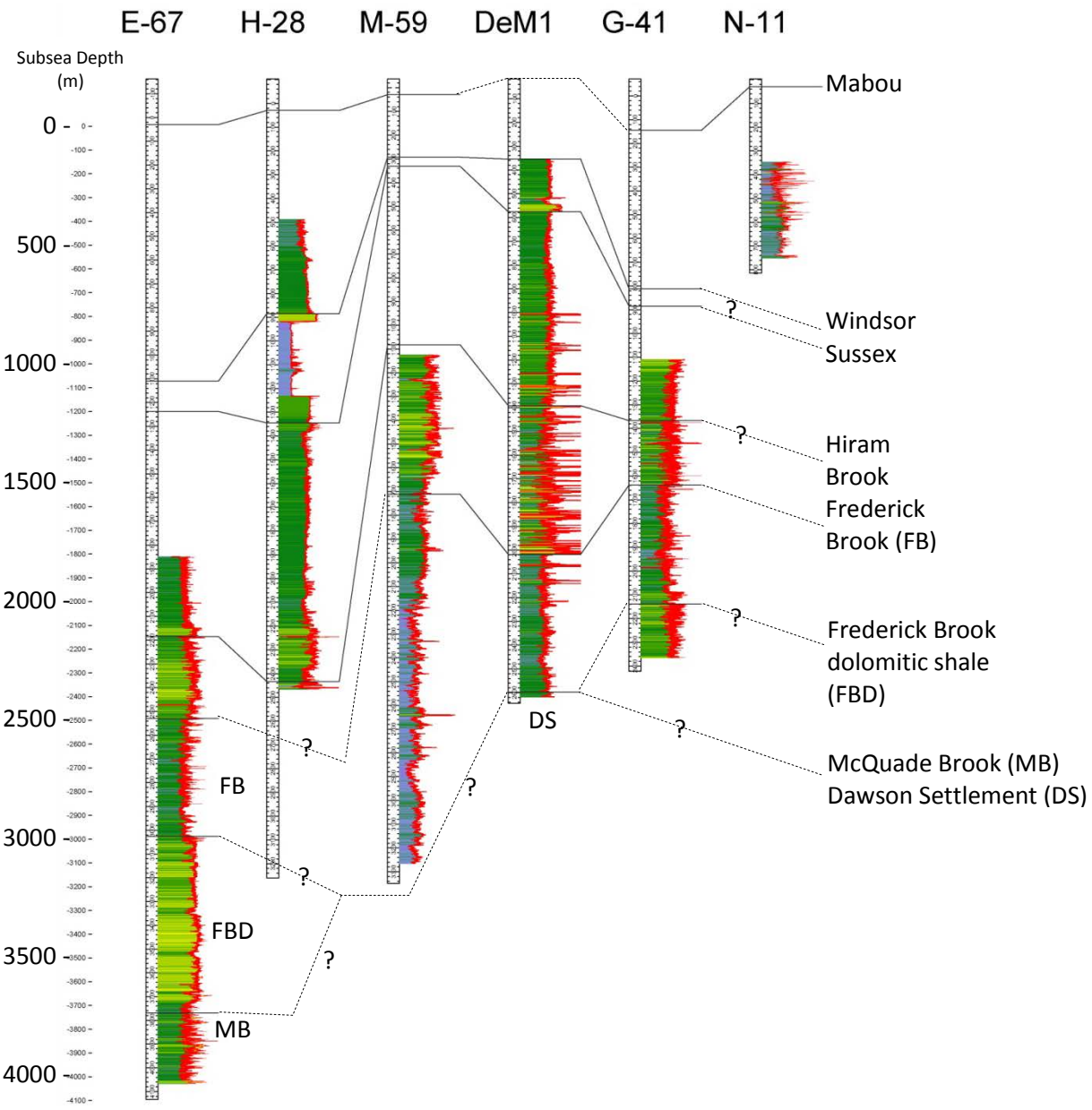

Figure 49 : Variation of the acoustic brittleness index between the McCully gas field and the Elgin area along a west-east cross-section. Datum line for correlation is 200m above sea level. The cross-section is located on figure 46C. Acoustic brittleness indexes calculated for wells DeM1 and M-59 are derived from the synthetic S wave.

5. Interpretation of the geomechanical properties

The Poisson's ratio (v), the Young's modulus (E) and acoustic brittleness index (BRIT) were estimated from the raw data for twenty-six wells (table 4). The minimum horizontal principal stress (Shmin) and its gradient have also been estimated for ten of these wells (table 8). The geographical coverage of these data across the McCully gas field and the Elgin area was then extended by calculating the same parameters for five additional wells from synthetic data (sections 4.1.2 and 4.1.3) so that the regional

homogeneity of the geomechanical properties could be verified using three representative cross-sections (section 4.2). This section examines now the vertical variations in the geomechanical properties from one stratigraphic unit to another and interprets their meanings in the context of hydraulic fracturing and of integrity of the cover succession above the Frederick Brook Member.

Although none of the wells presents a complete suite of petrophysical logs from the basal McQuade Brook Formation to the Mabou Group at surface, the review of table 1 and figures 47 to 49 reveals that it is possible to build a complete vertical geomechanical profile of all stratigraphic units by combining data from a small number of type wells. Figures 50 and 51 illustrate this exercise for the McCully gas field, using respectively the well E-67 (McQuade Brook Formation to Sussex Group) and the well P-66 (Hiram Brook Member to Mabou Group). Figure 52 shows the same results for the Elgin area using well G-41 (dolomitic part of the Frederick Brook Member to Sussex Group). The vertical variation of the geomechanical properties from one stratigraphic unit to another is described and discussed below based on these three representative wells, taking into account the low regional variability highlighted in section 4.2.

The geomechanical contrasts are minimal or not present between the basal portion of the McQuade Brook Formation and the dolomitic shale interval at the base of the overlying Frederick Brook Member, as well as within each of these units. A very conspicuous contrast however, is developed between the dolomitic shale interval at the base of the Frederick Brook Member and the shaly interval at the top of this member, this uppermost interval being more ductile (lower acoustic brittleness index) and locally more resistant (higher Shmin gradient in the well G-41) than the underlying dolomitic interval. The upper shaly interval of the Frederick Brook Member is also characterized by the presence of sandstone intervals interbedded with the shales, which creates strong geomechanical contrasts within this unit.

The shaly upper part of the Frederick Brook Member is also more brittle (higher acoustic brittleness index) and less resistant (lower Shmin gradient) than the overlying Hiram Brook Member. The latter is, as the underlying unit, characterized by the presence of strong internal geomechanical contrasts due to the presence of sandstone intervals interbedded with the shales.

There are minimal geomechanical contrasts between the Hiram Brook Member and the overlying Sussex Group, the latter being slightly more ductile and slightly more resistant than the Hiram Brook Member. In some wells however (E-67 and P-66) a thin (30 to 40m-thick) conglomeratic interval at the base of the Sussex Group, the Millbrook Member, shows a more pronounced geomechanical contrast. Apart from the Millbrook Member, the main characteristic of the Sussex Group that differentiates it from the underlying Hiram Brook Member, is its homogeneity, except near the top of the group (well P-66).

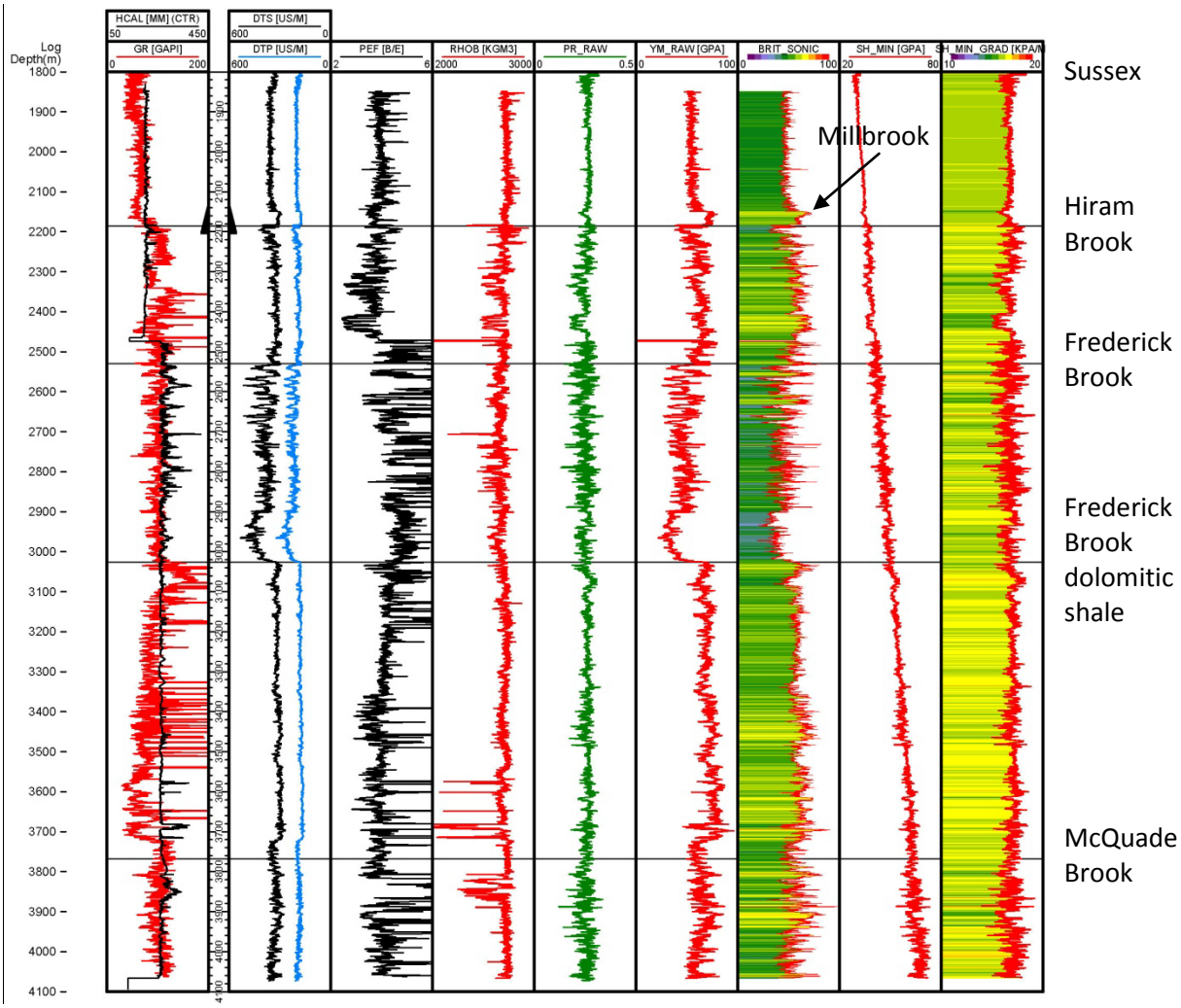

Figure 50 : Synthesis of the geomechanical properties estimated for the well E-67. YM_RAW : Young's modulus (E), expressed in GPa. PR_RAW : Poisson's ratio (υ), dimensionless; BRIT_SONIC : Acoustic brittleness index (0 to 100); SH_MIN : minimum horizontal principal stress, expressed in GPa. SH_MIN_GRAD : Gradient of Shmin, expressed in kPa/m. The Millbrook is a conglomeratic member at the base of the Sussex Group.

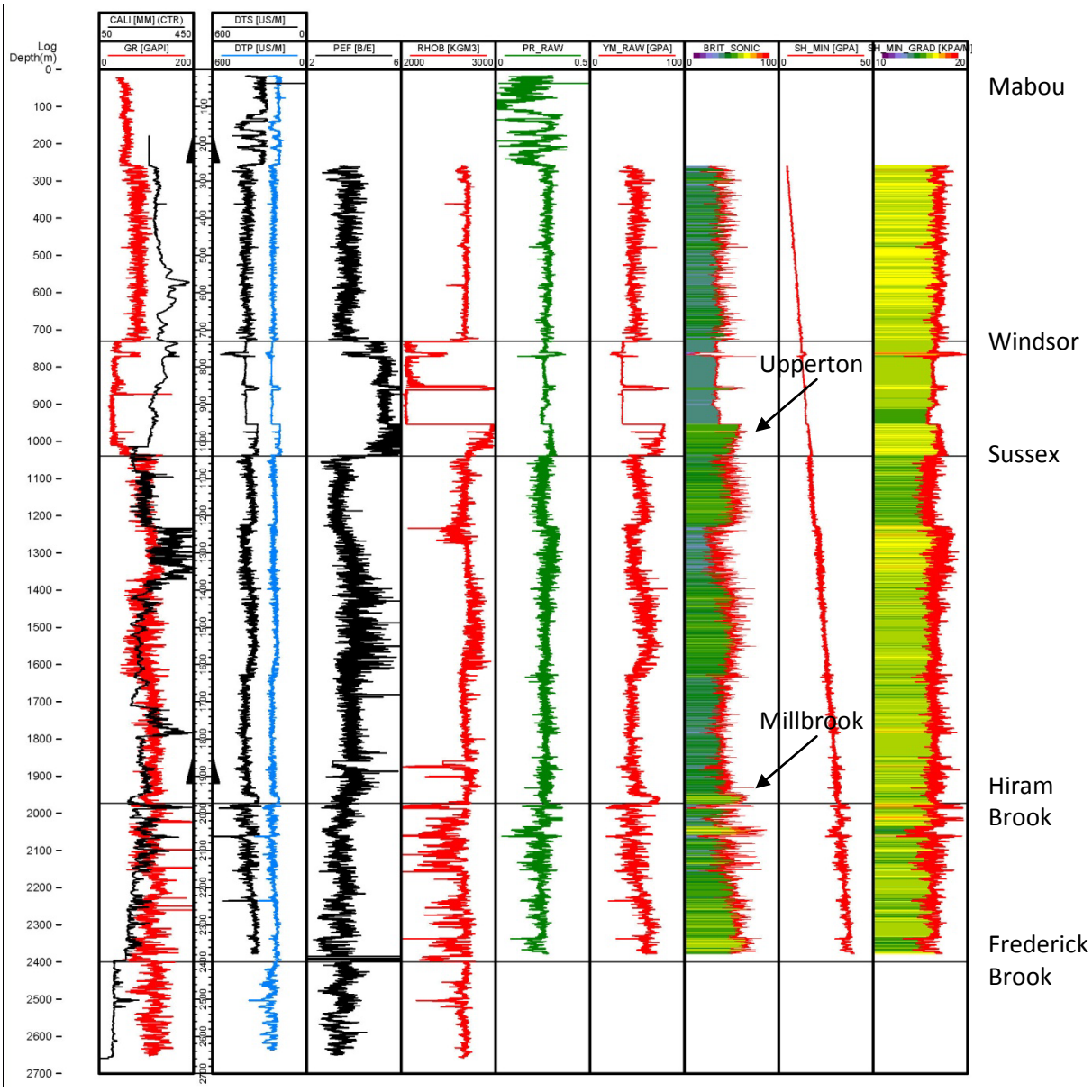

Figure 51 : Synthesis of the geomechanical properties estimated for the well P-66. YM_RAW : Young's modulus (E), expressed in GPa. PR_RAW : Poisson's ratio (υ), dimensionless; BRIT_SONIC : Acoustic brittleness index (0 to 100); SH_MIN : minimum horizontal principal stress, expressed in GPa. SH_MIN_GRAD : Gradient of Shmin, expressed in kPa/m. The Millbrook is a conglomeratic member at the base of the Sussex Group. The Upperton is an evaporite-rich formation (gypsum and anhydrite) at the base of the Windsor Group.

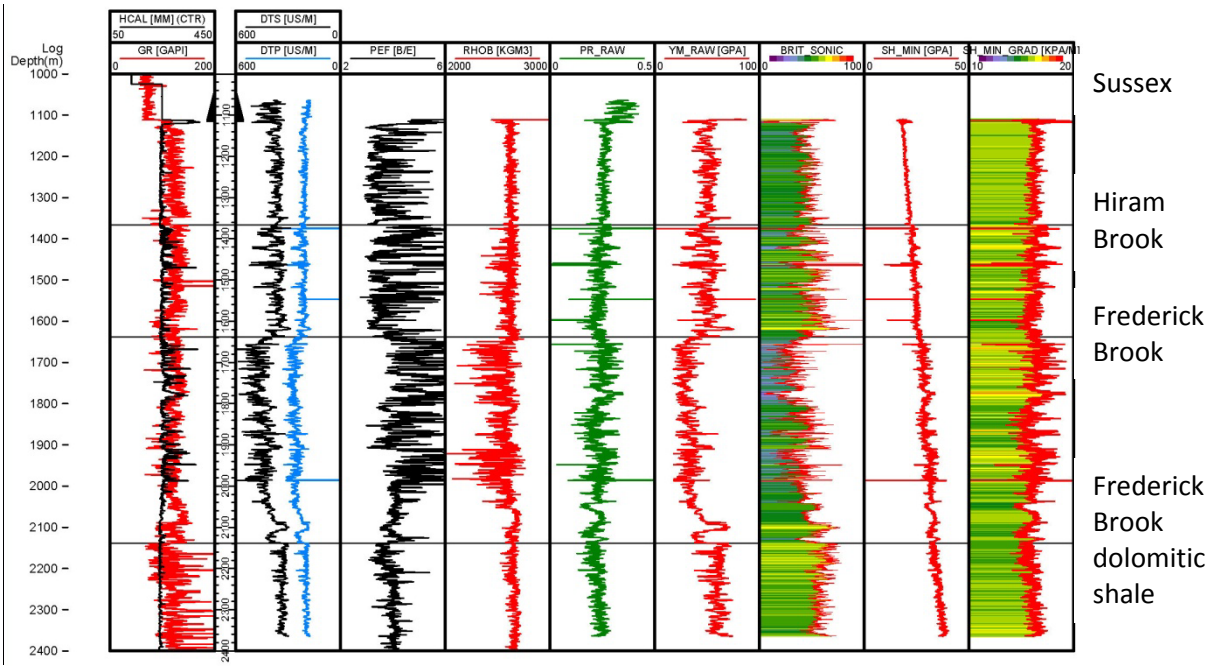

Figure 52 : Synthesis of the geomechanical properties estimated for the well G-41. YM_RAW : Young's modulus (E), expressed in GPa. PR_RAW : Poisson's ratio (υ), dimensionless; BRIT_SONIC : Acoustic brittleness index (0 to 100); SH_MIN : minimum horizontal principal stress, expressed in GPa. SH_MIN_GRAD : Gradient of Shmin, expressed in kPa/m.

The contact between the Sussex and Windsor groups is very contrasted, mainly due to the presence of the Upperton (gypsum and anhydrite) and/or Macumber (limestones and conglomerates) formations at the base of the Windsor Group, which confers to the base of the Windsor Group a more fragile and resistant characteristic than the upper part of the Sussex Group. The salt interval is absent in the well G-41 from the Elgin area. Most of the Windsor Group consists, above the Upperton and Macumber formations, of homogeneous halite layers that are more ductile and less resistant compared to the basal units of the Windsor Group. Finally, the Mabou Group is more fragile and brittle than the underlying salt layers.

Moreover, the geomechanical contrasts defined above from three representative wells for the McCully gas field and for the Elgin area are comparable to those which are recognized for narrower stratigraphic intervals in the other studied wells (figures 47 to 49).

The presence of layers of halite in the Windsor Group, the thickness of the underlying Sussex Group and the strong geomechanical contrasts identified in the Hiram Brook Member would make it most difficult for fractures induced in the Frederick Brook Member to propagate up to surface. However, the propagation of fractures into the Hiram Brook Member remains possible. The abundance and the role of natural fractures remain to be evaluated, but the Windsor Group is not prone to maintain open the natural fractures where salt layers are present, as is the case in the McCully field. In addition, the existence of a slightly overpressured reservoir in the Hiram Brook Member immediately above the

Frederick Brook Member, is a direct indicator of the absence of an hydraulic connection between the surface and the Frederick Brook Member under natural conditions (before hydraulic fracturing).

6. Conclusions and recommendations

This study allowed to establish the geomechanical properties of the Frederick Brook Member (Albert Formation, Horton Group) and its cover succession, based on the petrophysical log records available from oil and gas wells, at the scale of the well and at the regional level, for the McCully gas field and the adjacent area of Elgin.

The Young's modulus, the Poisson's ratio, two brittleness indexes (acoustic and mineralogic) as well as the intensity of the minimum horizontal principal stress were studied. The wells coverage, initially restricted to those wells with a complete suite of logs, has been extended by calculating synthetic parameters for some wells whose datasets were incomplete, and their representativeness has been verified by comparing the log results with independent laboratory data.

At the scale of the individual well the results highlight the presence of clear geomechanical contrasts between the Frederick Brook Member and the overlying Hiram Brook Member, as well as within the cover succession above these two units. In the context of hydraulic fracturing these geomechanical contrasts translate into the existence of barriers that may limit the propagation of hydraulic fractures outside the Frederick Brook Member.

At the regional scale it has been possible to recognise the same geomechanical contrasts than those documented at the scale of the individual well and to confirm the homogeneity of the geomechanical properties within the McCully gas field and between this field and the Elgin area. The latter stands out however, by the absence of evaporite deposits in the Windsor Group.

Further work is recommended in order to better understand the role played by natural fractures – if present – in the possible migration paths through the cover succession of the shale. To this end it is particularly recommended to :

- Review the characteristics of the natural fractures in the Frederick Brook Member and its cover succession, using the geological descriptions, the gas shows and the drilling breaks, the relative permeability logs (nuclear magnetic resonance), the image logs and the results from hydraulic fracturations and mini-frac tests made in the Frederick Brook and Hiram Brook members.
- Drill one or more observation wells out of the limits of drill pads, following the subsurface of the deviated wells that underwent hydraulic fracturation program in the Frederick Brook Member, so as to highlight the migration or the absence of migration of fluids in the geological medium away from the surface casings. The interpretation of selected seismic lines, or at least a good understanding of the trajectory of the faults at depth, appears a necessary prerequisite for the location of these additional observation wells.

Acknowledgements

The different datasets collected by the operator of the McCully gas field and in the Elgin area, Corridor Resources, proved to be very complete and remarkably useful for the realization of this geomechanical study. In particular, the diversity and quality of the wireline logs recorded in the wells allowed to approach the geomechanical parameters of the McCully gas field under different and complementary angles, and to validate the conclusions of the study using several independent datasets.

The author wishes to thank Denis Lavoie (GSC-Quebec) for the critical review of this report. The author also wishes to thank Christine Rivard (GSC-Quebec, coordinator of the project), Denis Lavoie (GSC-Quebec) and the staff of the Department of natural resources, Geological surveys branch of New Brunswick, for facilitating access to the public data needed for this work.

This project was made with the financial support of Natural Resources Canada through financial contributions to the Earth Sciences Sector and the Energy Sector in the scope of its Program for Energy Research and Development (PERD).

References

ASTM, 2015a. Standard test methods for compressive strength and elastic moduli of intact rock core specimens under varying states of stress and temperatures. American Society for Testing and Materials, standard D7012, 9p.

ASTM, 2015b. Standard test method for laboratory determination of pulse velocities and ultrasonic elastic constants of rock. American Society for Testing and Materials, standard D2845, 8p.

Barree, R.D., Gilbert, J.V., Conway, M., 2009. Stress and rock property profiling for unconventional reservoir stimulation. Society of Petroleum Engineers, SPE-118703-MS, 18p.

Core Lab, 2005. Rock mechanics testing and analysis performed on core plugs from the Corridor/PCS McCully G-67 well, McCully, New-Brunswick. Core Lab Technical Services Report HOU-050811, confidential report prepared for Corridor Resources, December 19, 2005, 21p.

Corridor Resources, 2015. Corporate Presentation. Corridor Resources, December 2015. 28p. See website https ://corridor.ca/wp-content/uploads/2014/05/2015-12-Corporate-Presentation.pdf (accessed online on November 6, 2016).

Corridor Resources, 2016. McCully development map with gathering system and gas plant. One map. See website http ://www.corridor.ca/wp-content/uploads/2014/05/McCully-Devel_Map_JUN2010_ dimmed.jpg (accessed online onon March 30, 2016).

Durling, P., Martel, T., 2001. Seismic stratigraphy and structural setting of the McCully gas field. Atlantic Geology, v.37, no 1, p.109.

Eaton, B.A., 1969. Fracture gradient prediction and its application in oilfield operations. Journal of Petroleum Technology, v. 246, p.1353-1360.

Glorioso, J. C., Rattia, A., 2012. Unconventional reservoirs : basic petrophysical concepts for shale gas. Society of Petroleum Engineers, SPE 153004, 38 pages.

Grieser, B., Bray, J., 2007. Identification of production potential in unconventional reservoirs. Society of Petroleum Engineers, SPE 106623, 6 pages.

Hinds, S.J., St. Peter, C.J., 2006. Stratigraphy and structure of the Moncton Subbasin in the Urney–Waterford area, Maritimes Basin, New Brunswick : implications for the McCully Natural Gas Field. *In* Geological Investigations in New Brunswick for 2005. Edited by G.L. Martin, New Brunswick Department of Natural Resources; Minerals, Policy and Planning Division, Mineral Resource Report 2006-3, p.73-102.

Hinds, S., St. Peter, C., 2016. The McCully gas field project. Department of natural resources Geological surveys branch, New Brunswick, 17p. See website http ://www2.gnb.ca/content/dam/gnb/

Departments/en/pdf/Minerals-Minerales/McCully_Gas_Field_Project-e.pdf (accessed online on March 30, 2016).

Keighley, D., Noftall, A., 2014. A bulk geochemical database of fine-grained sedimentary rock from the Albert Formation, Horton Group, Carboniferous, southern New Brunswick. Department of Earth Sciences, University of New Brunswick. Program of Energy Research and Development (PERD), Geological Survey of Canada, 54p.

Keighley, D., St. Peter, C., 2015. Selected Core from the Albert Formation (Mississippian), Moncton Basin, Southern New Brunswick. Search and Discovery Article #10729, 14p.

Lavoie, D., Pinet, N., Dietrich, J., Hannigan, P., Castonguay, S., Hamblin, A.P., and Giles, P., 2009. Petroleum resource assessment, Paleozoic successions of the St. Lawrence Platform and Appalachians of eastern Canada. Geological Survey of Canada, Open File 6174, 273p.

Martel, T., 2013. Pitfalls in assessing lacustrine shale versus marine shale prospects. Search and Discovery Article #41188, 30p.

New Brunswick Department of Natural Resources, 2008. Bedrock Geology of New Brunswick, Minerals, Policy and Planning Division. Map NR-1 (2008 Edition). Scale 1 :500 000.

Séjourné, S., 2015a. Étude géomécanique de la Formation de Macasty et de sa couverture dans un puits pétrolier et gazier (Pétrolia/Corridor Chaloupe No. 1), Île d'Anticosti, Québec. Geological Survey of Canada, Open file 7892, 52p.

Séjourné, S., 2015b. Étude géomécanique régionale de la Formation de Macasty et de sa couverture d'après les puits pétroliers et gaziers de l'Île d'Anticosti, Québec. Geological Survey of Canada, Open file 7907, 114p.

Séjourné, S., 2016. Étude des données géomécaniques de laboratoire des carottes d'un puits pétrolier et gazier (Talisman, Saint-Édouard No 1), région de Saint-Édouard, Québec. Geological Survey of Canada, Open file 7983, 54p.

Séjourné, S. 2017. Étude géomécanique du Shale d'Utica et de sa couverture d'après les puits pétroliers et gaziers de la région de Saint-Édouard-de-Lotbinière, Québec. Commission Géologique du Canada, Dossier Public 8196 (*in press)*, 55p.

St. Peter, C.J., Johnson, S.C., 2009. Stratigraphy and structural history of the late Paleozoic Maritimes Basin in southeastern New Brunswick, Canada. New Brunswick Department of Natural Resources; Minerals, Policy and Planning Division, Memoir 3, 348p.

Wilson, P., 2003. Stratigraphy, evaporite structure, and tectonic history in the McCully area, southern New Brunswick : Preliminary results. New Brunswick Department of Natural Resources; Minerals, Policy and Planning Division, Mineral Resource Report 2003-4, p.101-121.

Zoback, M. D., 2007. Reservoir geomechanics. Cambridge University Press, 449 pages.

Appendix I :

Detail of the wells and depth of the stratigraphic units

– Wells –

B-58, C-29, C-48, C-57, C-67, C-75, C-82, D-48, D-57, D-66, D-67, DeM1, E-38, E-57, E-67, F-58, G-36, G-41, G-67, H-28, H-76, I-47, I-67, J-38, J-47, J-65, J-66, J-67, J-76, K-48, K-57, K-66, L-37, L-38, L-41, M-59, M-66, McC1, N-11, N-66, O-66, P-47, P-56, P-66, P-67 and P-76

Some of the measured and vertical depths indicated in this appendix have been adjusted from the original well files in the course of the present study.

UWI	Well Name	KB (m)	Total Measured Depth (m)	Stratigraphic Unit	Unit Measured Depth (m)	Unit Vertical Depth (m)
B-58	Corridor McCully B-58-2425	105	2487	MABOU	0	0.0
				WINDSOR	1276	1275.3
				SUSSEX	1415	1414.2
				HIRAM BROOK	2280	2278.1
C-29	Corridor McCully I-39-2425/C-29	164	2990	MABOU	30	30.0
				WINDSOR	1558.93	1458.9
				SUSSEX	1860	1683.7
				HIRAM BROOK	2821	2439.3
C-48	Corridor McCully G-48-2425/C-48	57.8	2528	HIRAM BROOK	2184	2096.1
C-57	Corridor/PCS McCully N-57-2425/C-57	32.8	2916	HIRAM BROOK	2392	1935.8
				FREDERICK BROOK	2897	2432.3
C-67	Corridor / PCS McCully F-67-2425/C-67	34.8	2475	MABOU	30	30.0
				WINDSOR	1042	1031.8
				SUSSEX	1166	1151.4
				HIRAM BROOK	2160	2122.5
				FREDERICK BROOK	2465	2426.3
C-75	Corridor/PCS McCully C-75-2425	49	3159	MABOU	10	10.0
				WINDSOR	652	651.9
				SUSSEX	936	935.9
				HIRAM BROOK	1992	1990.9
				FREDERICK BROOK	2280	2278.6
C-82	Corridor/Globex Case Settlement C-82-2424	76.8	2123	WINDSOR	974	973.9
				SUSSEX	1045	1044.9
D-48	EOG Corridor McCully D-48-2425	36	2650	WINDSOR	911	898.6
				SUSSEX	1282	1262.7
				HIRAM BROOK	2083	2063.4
				FREDERICK BROOK	2548	2523.2
D-57	Corridor / PCS McCully B-67-2425/D-57	28	2582	MABOU	30	30.0
				WINDSOR	767	759.6
				SUSSEX	1089	1035.4
				HIRAM BROOK	2110	1943.8
				FREDERICK BROOK	2552	2381.5
D-66	Corridor McCully O-76-2425 / D-66	29.6	3300	MABOU	30	30.0
				WINDSOR	1000	944.6
				SUSSEX	1210	1097.5
				HIRAM BROOK	2449	2009.4
				FREDERICK BROOK	3095	2637.7

UWI	Well Name	KB (m)	Total Measured Depth (m)	Stratigraphic Unit	Unit Measured Depth (m)	Unit Vertical Depth (m)
D-67	Corridor/PCS McCully O-76-2425/D-67	30	2576	HIRAM BROOK	2561	2271.8
				FREDERICK BROOK	2754	2463.0
DeM1	Corridor/Columbia Will DeMille 1	216.3	2644	MABOU	10	10.0
				WINDSOR	354	354.0
				SUSSEX	576	576.0
				HIRAM BROOK	1392	1385.6
				FREDERICK BROOK	2018	1939.9
				DAWSON SETTLEMENT	2598	2445.8
E-38	Corridor McCully L-38-2425 / E-38	60.2	3203	MABOU	30	30.0
				WINDSOR	1070	1065.3
				SUSSEX	1445	1427.0
				HIRAM BROOK	2250	2190.8
				FREDERICK BROOK	2960	2897.4
E-57	Corridor / PCS McCully N-57-2425/E-57	30.2	2673	MABOU	30	30.0
				WINDSOR	1015	960.9
				SUSSEX	1273	1197.4
				HIRAM BROOK	2203	2059.4
				FREDERICK BROOK	2621	2475.1
E-67	Corridor/PCS McCully F-67-2425/E-67	37.3	4133	MABOU	30	30.0
				WINDSOR	1109.71	1093.6
				SUSSEX	1237.66	1218.5
				HIRAM BROOK	2185	2147.3
				FREDERICK BROOK	2529	2488.4
				FREDERICK BROOK DOLOMITE	3025.6	2982.2
				MCQUADE BROOK	3722	3675.8
F-58	Corridor McCully F-58-2425	67.2	3751	MABOU	30	30.0
				WINDSOR	1377	1376.3
				SUSSEX	1497	1496.3
				HIRAM BROOK	2498	2490.7
				FREDERICK BROOK	2753	2745.4
				FREDERICK BROOK DOLOMITE	3213	3203.5

UWI	Well Name	KB (m)	Total Measured Depth (m)	Stratigraphic Unit	Unit Measured Depth (m)	Unit Vertical Depth (m)
G-36	Corridor South Branch G-36-2425	164.4	2622	MABOU	30	30.0
				WINDSOR	620	616.2
				SUSSEX	840	830.1
				HIRAM BROOK	1388	1370.3
				FREDERICK BROOK	2125	2106.5
				FREDERICK BROOK DOLOMITE	2566	2545.0
G-41	Corridor Green Road G-41-2426	128.2	2422	MABOU	145	145.0
				WINDSOR	812	811.7
				SUSSEX	885	884.7
				HIRAM BROOK	1367	1364.6
				FREDERICK BROOK	1638	1629.8
				FREDERICK BROOK DOLOMITE	2138	2111.3
G-67	Corridor/PCS McCully F-67-2425/G-67	34.8	2555	MABOU	30	30.0
				WINDSOR	1064	1054.7
				SUSSEX	1208	1193.4
				HIRAM BROOK	2184	2137.3
				FREDERICK BROOK	2530	2479.8
H-28	EOG Corridor McCully H-28-2425	96.7	3260	MABOU	30	30.0
				WINDSOR	885	884.8
				SUSSEX	1345	1344.7
				HIRAM BROOK	2433.8	2433.3
H-76	Corridor/PCS McCullyO-76-2425/-H-76	30	2910	MABOU	30	30.0
				WINDSOR	979	970.4
				SUSSEX	1130	1115.7
				HIRAM BROOK	2354	2262.8
				FREDERICK BROOK	2869	2774.0
I-47	Corridor McCully G-48-2425/I-47	57.7	3693	HIRAM BROOK	2335	2085.1
I-67	Corridor/PCS McCully N-57-2425/I-67	30.4	2821	MABOU	30	30.0
				WINDSOR	1126.5	1045.8
				SUSSEX	1373	1245.3
				HIRAM BROOK	2394	2135.5
				FREDERICK BROOK	2787	2527.9

UWI	Well Name	KB (m)	Total Measured Depth (m)	Stratigraphic Unit	Unit Measured Depth (m)	Unit Vertical Depth (m)
J-38	Corridor McCully L-38-2425/J-38	60.2	3169	MABOU	30	30.0
				WINDSOR	1029	955.7
				SUSSEX	1442	1304.9
				HIRAM BROOK	2637	2379.7
				FREDERICK BROOK	3150	2890.6
J-47	Corridor McCully G-48-2425/J-47	57.5	2959	MABOU	30	30.0
				WINDSOR	1135	992.5
				SUSSEX	1596	1326.3
				HIRAM BROOK	2546	2048.6
				FREDERICK BROOK	2932.8	2386.4
J-65	EOG Corridor McCully J-65-2425	58.3	3006	MABOU	12	12.0
				WINDSOR	740	739.9
				SUSSEX	912	911.9
				HIRAM BROOK	1880	1879.9
				FREDERICK BROOK	2322	2321.7
				DAWSON SETTLEMENT	2898	2896.7
J-66	Corridor / PCS McCully M-66-2425/J-66	27.7	2600	MABOU	25	25.0
				WINDSOR	819	765.2
				SUSSEX	1106	1006.8
				HIRAM BROOK	2197	1919.8
				FREDERICK BROOK	2560	2278.7
J-67	Corridor/PCS McCully F-67-2425/J-67	34.5	2658	MABOU	30	30.0
				WINDSOR	1167	1119.4
				SUSSEX	1312	1252.7
				HIRAM BROOK	2325	2240.1
				FREDERICK BROOK	2586	2499.6
J-76	Corridor McCully O-76-2425/J-76	30	3029	MABOU	30	30.0
				WINDSOR	1008	1004.8
				SUSSEX	1147	1138.6
				HIRAM BROOK	2629	2566.7
				FREDERICK BROOK	2869	2804.9
K-48	Corridor McCully G-48-2425/K-48	57.5	2686	MABOU	38	38.0
				WINDSOR	1246.1	1226.1
				SUSSEX	1465	1434.9
				HIRAM BROOK	2362	2295.6
				FREDERICK BROOK	2738	2668.9

UWI	Well Name	KB (m)	Total Measured Depth (m)	Stratigraphic Unit	Unit Measured Depth (m)	Unit Vertical Depth (m)
K-57	Corridor McCully N-57-2425/K-57	49.7	2659	MABOU	30	30.0
				WINDSOR	991	982.2
				SUSSEX	1237	1223.1
				HIRAM BROOK	2130	2099.8
				FREDERICK BROOK	2645	2604.9
K-66	Corridor/PCS McCully M-66-2425/K-66	27.7	2485	MABOU	30	30.0
				WINDSOR	867	866.4
				SUSSEX	1064	1053.4
				HIRAM BROOK	2089.5	1966.2
				FREDERICK BROOK	2448	2323.1
L-37	Corridor McCully D-48-2425/L-37	39	2128	MABOU	30	30.0
				WINDSOR	960	959.2
				SUSSEX	1283	1282.2
				HIRAM BROOK	2180	2179.2
L-38	Corridor McCully G-48-2425/L-38	57	3133	MABOU	30	30.0
				WINDSOR	1355	1158.3
				SUSSEX	1685	1402.5
				HIRAM BROOK	2680	2138.8
L-41	Apache Corridor Green Road B-41-2326/L-41	129	2301	MABOU	145	145.0
				WINDSOR	813.5	812.7
				SUSSEX	883	882.1
				HIRAM BROOK	1376.5	1370.4
				FREDERICK BROOK	1687	1660.3
M-59	Apache Corridor WillDemille G-59-2426/M-59	163	2735	MABOU	30	30.0
				WINDSOR	293	293.0
				SUSSEX	331	331.0
				HIRAM BROOK	1082	1081.5
				FREDERICK BROOK	1711	1709.5
M-66	Corridor / PCS McCully M-66-2425/M-66	28	2509	MABOU	30	30.0
				WINDSOR	875.5	875.3
				SUSSEX	1036.5	1036.1
				HIRAM BROOK	2151	2120.3
				FREDERICK BROOK	2511.2	2480.2
McC1	PCS/Corridor McCully 1	28.1	2657	MABOU	0	0.0
				WINDSOR	732	730.9
				SUSSEX	1034	1032.2
				HIRAM BROOK	1972	1962.8
				FREDERICK BROOK	2381	2371.5

UWI	Well Name	KB (m)	Total Measured Depth (m)	Stratigraphic Unit	Unit Measured Depth (m)	Unit Vertical Depth (m)
N-11	Corridor Mapleton N-11-2326	196.7	814	MABOU	30	30.0
N-66	Corridor/PCS McCully O-76-2425/N-66	29	2364	HIRAM BROOK	2419	2296.8
O-66	Corridor/PCS McCully B-67-2425/O-66	27.9	2556	MABOU	30	30.0
				WINDSOR	759	757.7
				SUSSEX	1053	1029.4
				HIRAM BROOK	2076	1960.3
				FREDERICK BROOK	2536	2419.7
P-47	Corridor McCully G-48-2425/P-47	56.8	3177	MABOU	30	30.0
				WINDSOR	1131	975.3
				SUSSEX	1637	1331.4
				HIRAM BROOK	2528	2094.5
P-56	Corridor/PCS McCully P-56-2425	69	3182	MABOU	0	0.0
				WINDSOR	579	575.9
				SUSSEX	1039	1031.1
				HIRAM BROOK	1892	1883.0
				FREDERICK BROOK	2768	2715.5
P-66	Corridor/PCS McCully 2/A-67-2425/P-66	28	2431	MABOU	30	30.0
				WINDSOR	730.57	709.9
				SUSSEX	1039	1005.1
				HIRAM BROOK	1973.11	1907.3
				FREDERICK BROOK	2400	2330.5
P-67	Corridor/PCS McCully N-57-2425/P-67	32.8	2791	MABOU	30	30.0
				WINDSOR	1211	1124.4
				SUSSEX	1436	1308.5
				HIRAM BROOK	2548	2269.9
				FREDERICK BROOK	2778	2498.5
P-76	Corridor McCully O-76-2425 / P-76	29.3	2769	MABOU	30	30.0
				WINDSOR	1036.5	1014.5
				SUSSEX	1158	1132.4
				HIRAM BROOK	2386	2353.0
				FREDERICK BROOK	2536	2502.0

Appendix II :

Logs and geomechanical parameters calculated from the raw data

– Wells –

B-58, C-29, D-57, E-38, E-67, F-58, G-36, G-41, G-67, H-28, J-38, J-47, J-65, J-66, J-67, K-48, K-57, K-66, L-38, M-66, McC1, N-11, O-66, P-47, P-56 and P-66

B-58

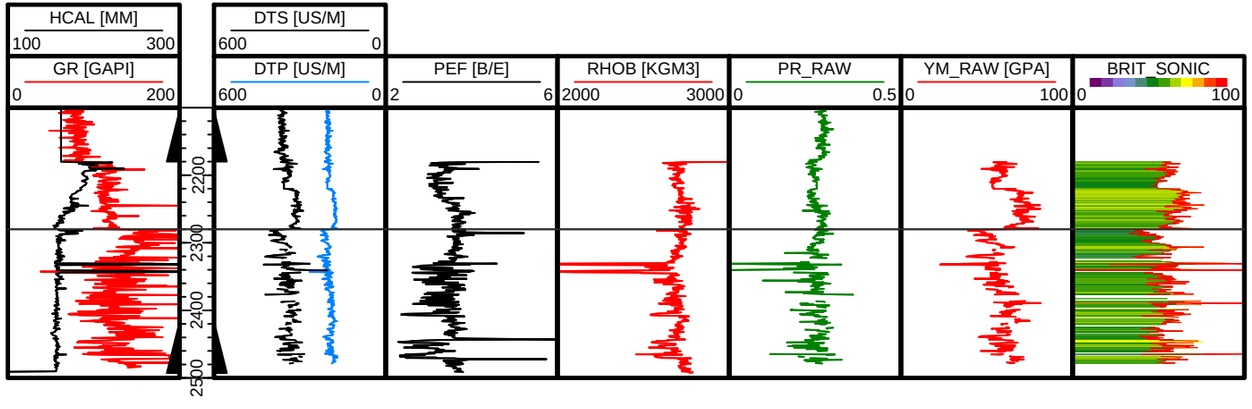

Log Depth(m)

2100 −

2200 −

2300 −

2400 −

2500 −

HIRAM_BROOK

Log Depth(m)

− 2100

− 2200

− 2300

− 2400

− 2500

HS=1

PETRA 8/8/2016 1:45:43 PM

C-29

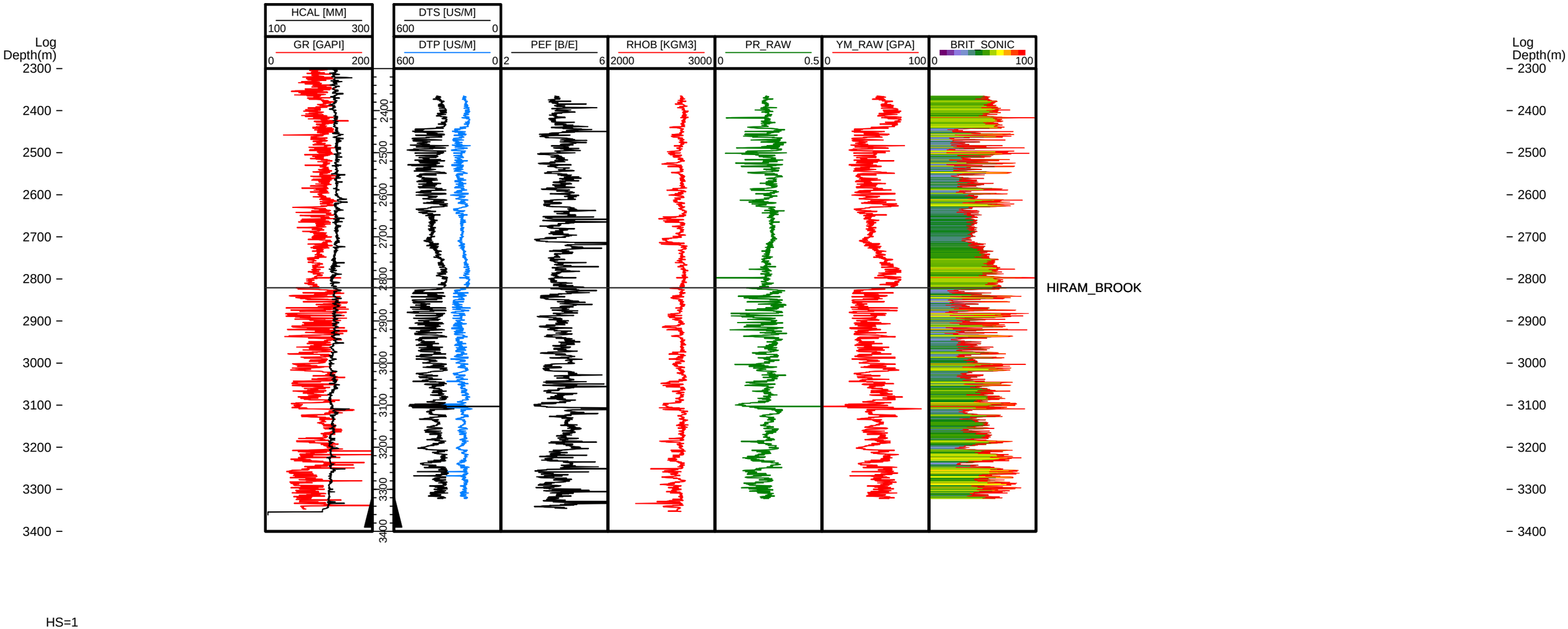

HS=1

PETRA 8/8/2016 1:46:29 PM

D-57

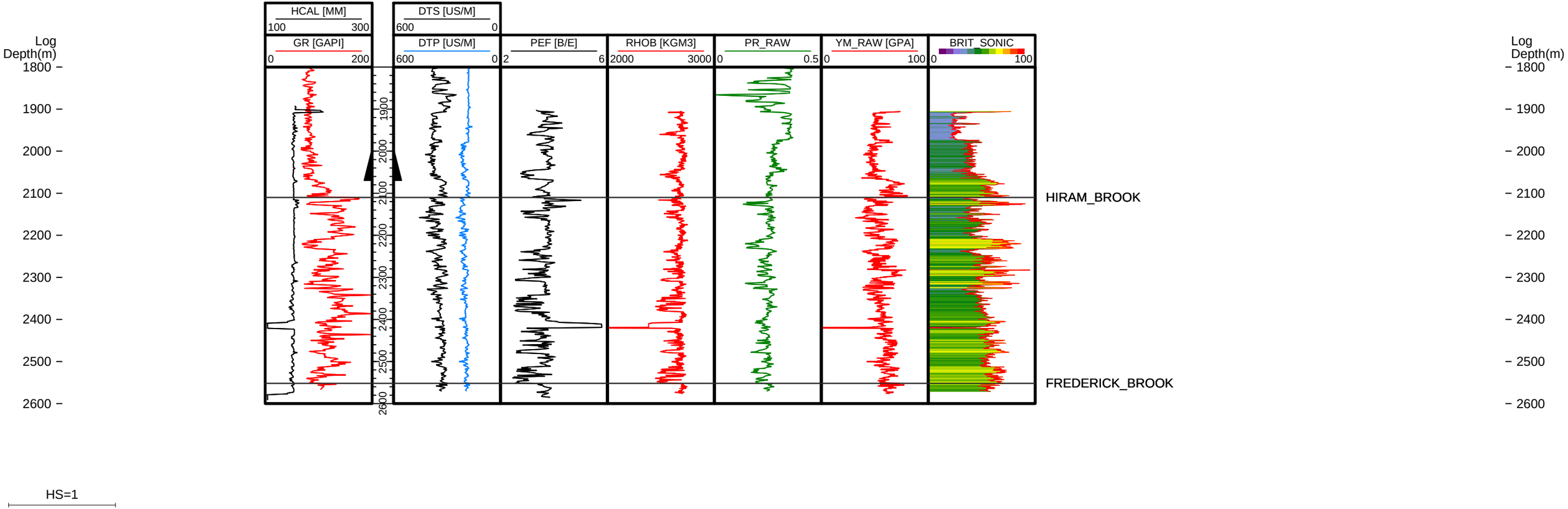

HS=1

PETRA 8/8/2016 2:08:51 PM

E-38

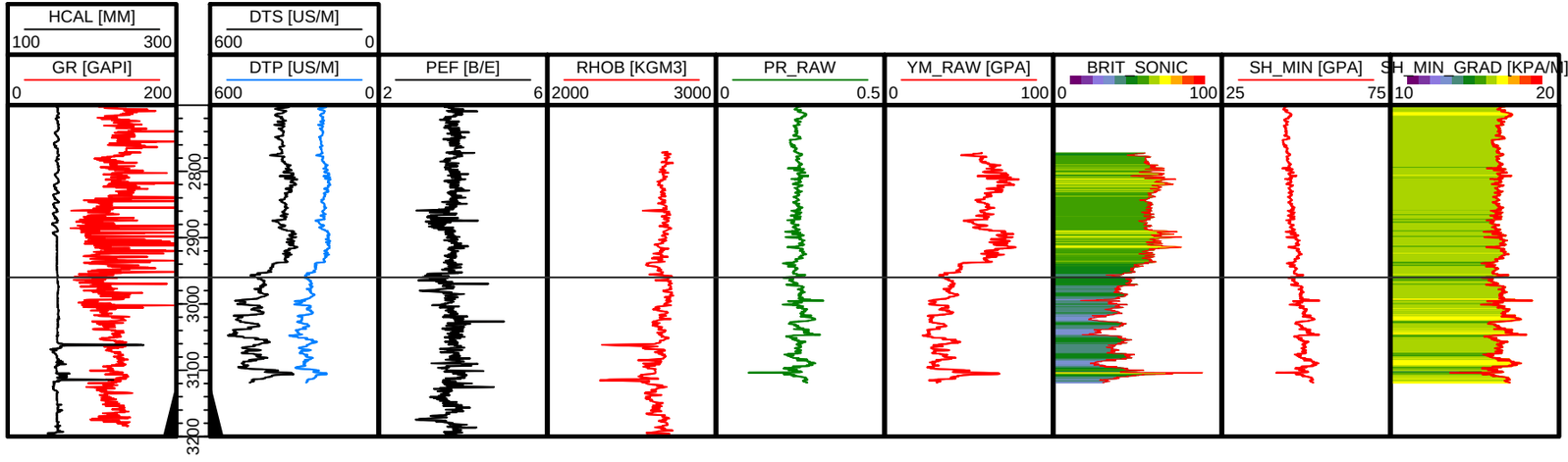

Log Depth(m)

2700
2800
2900
3000
3100
3200

Log Depth(m)

2700
2800
2900
3000
3100
3200

HS=1

PETRA 8/8/2016 1:30:20 PM

E-67

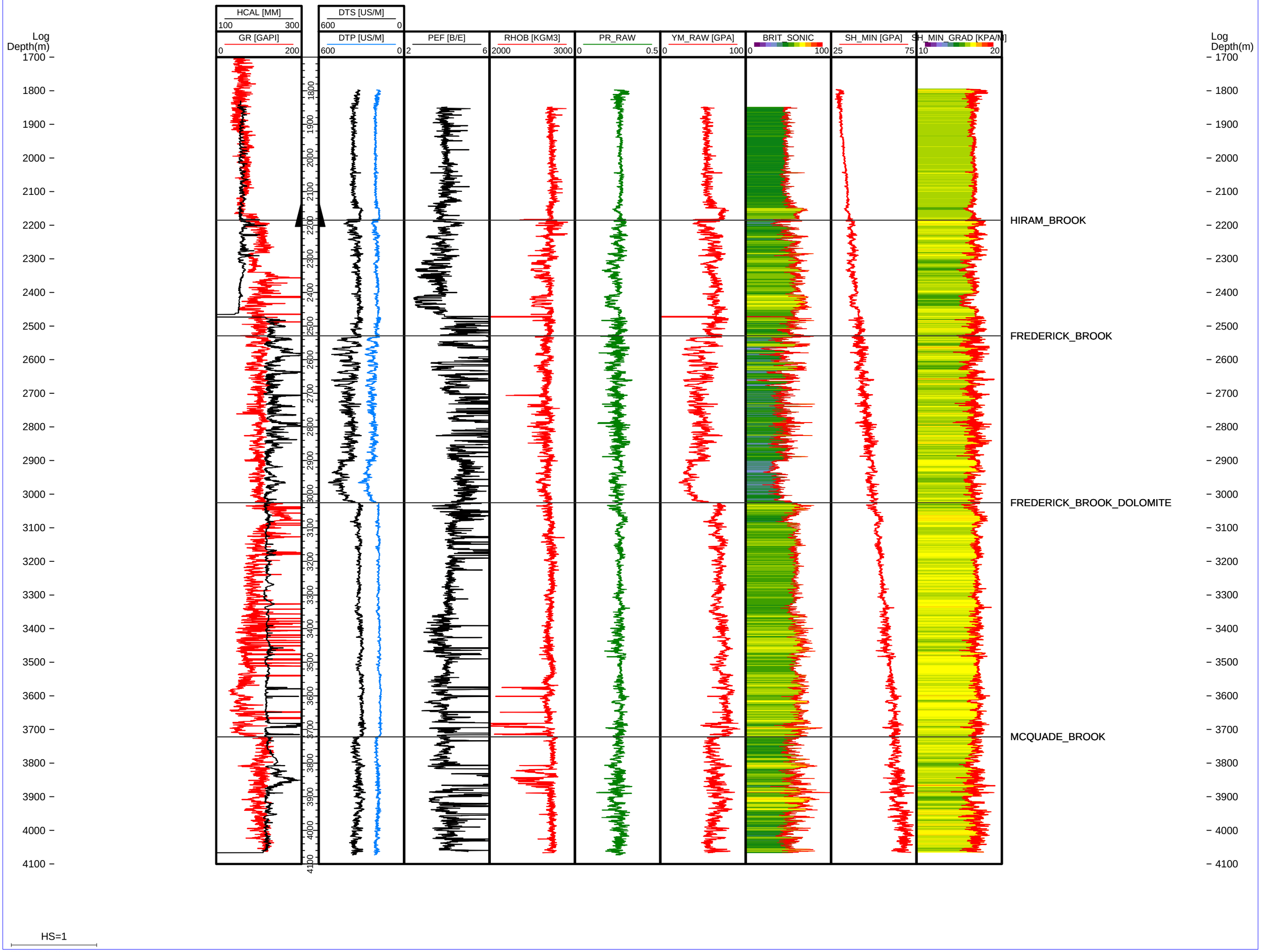
HCAL [MM]
100
300
DTS [US/M]
600
0
GR [GAPI]
0
200
DTP [US/M]
600
0
PEF [B/E]
2
6
RHOB [KGM3]
2000
3000
PR_RAW
0
0.5
YM_RAW [GPA]
0
100
BRIT_SONIC
0
100
SH_MIN [GPA]
25
75
SH_MIN_GRAD [KPA/M]
10
20
Log Depth(m)
1700
1800
1900
2000
2100
2200
2300
2400
2500
2600
2700
2800
2900
3000
3100
3200
3300
3400
3500
3600
3700
3800
3900
4000
4100
HIRAM_BROOK
FREDERICK_BROOK
FREDERICK_BROOK_DOLOMITE
MCQUADE_BROOK

HS=1

F-58

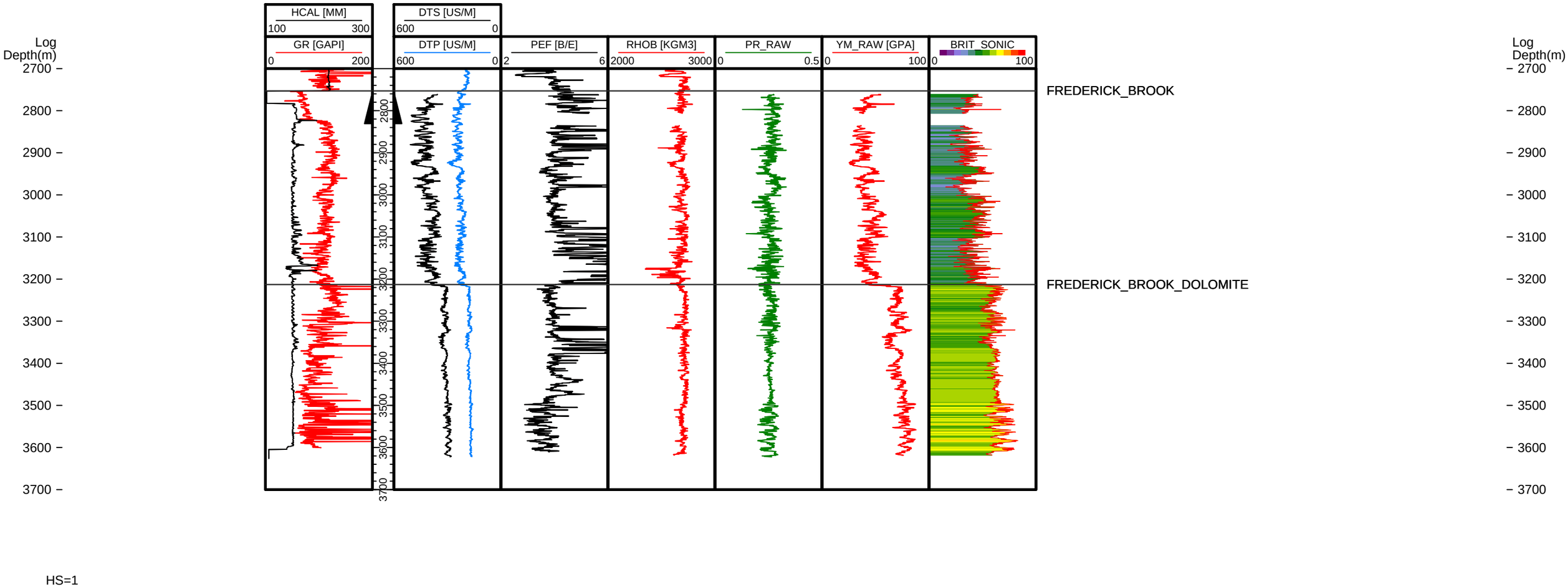

PETRA 8/8/2016 1:48:48 PM

G-36

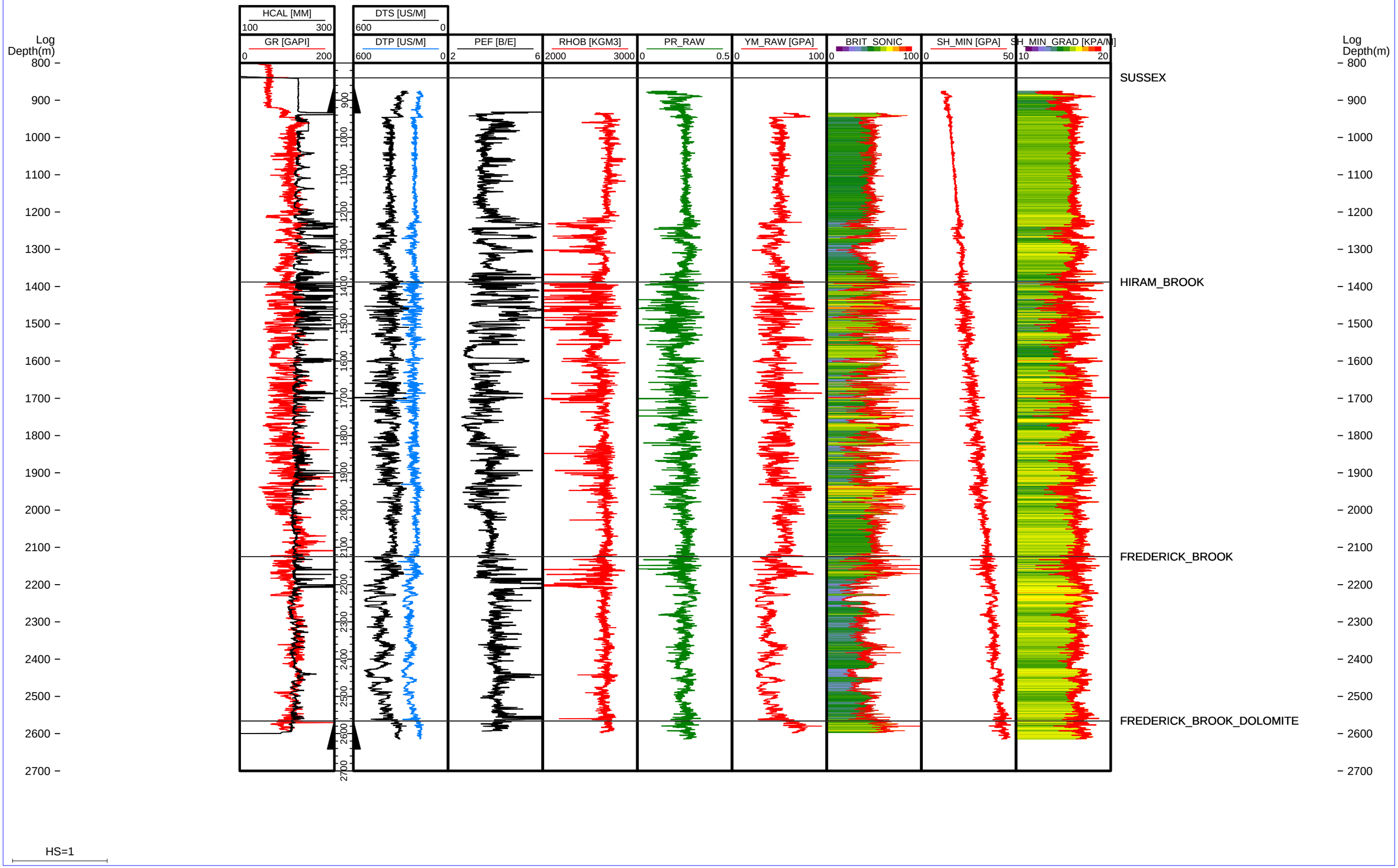

HS=1

PETRA 8/8/2016 1:31:46 PM

G-41

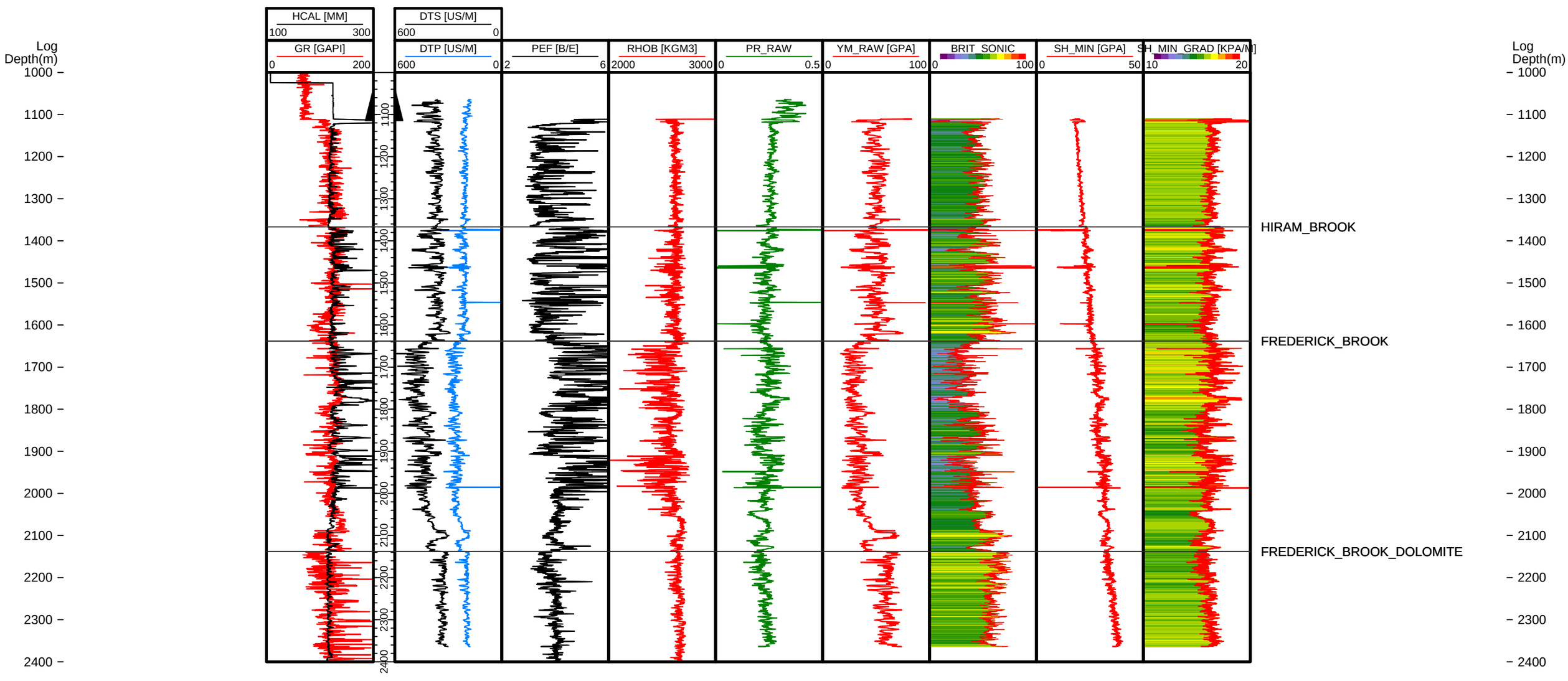

HS=1

PETRA 8/8/2016 1:32:58 PM

G-67

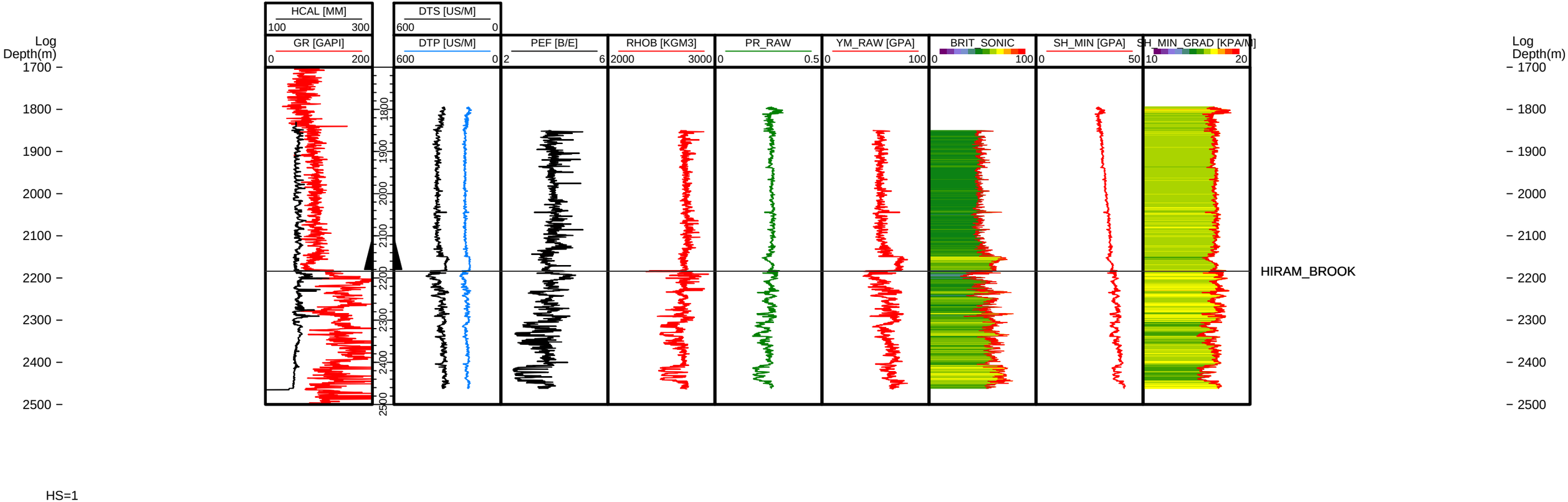

HS=1

PETRA 8/8/2016 1:34:05 PM

H-28

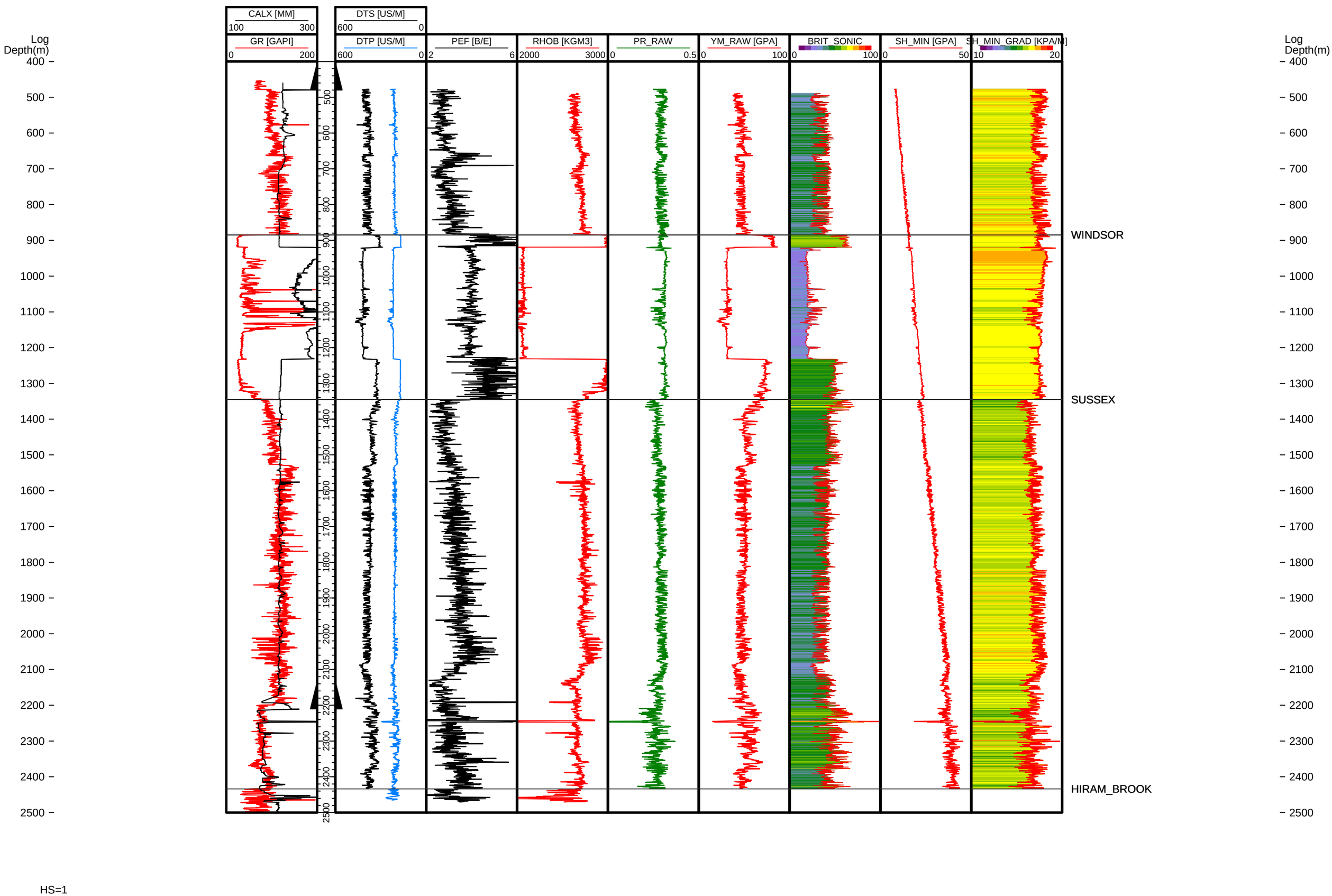

HS=1

PETRA 8/8/2016 1:36:43 PM

J-38

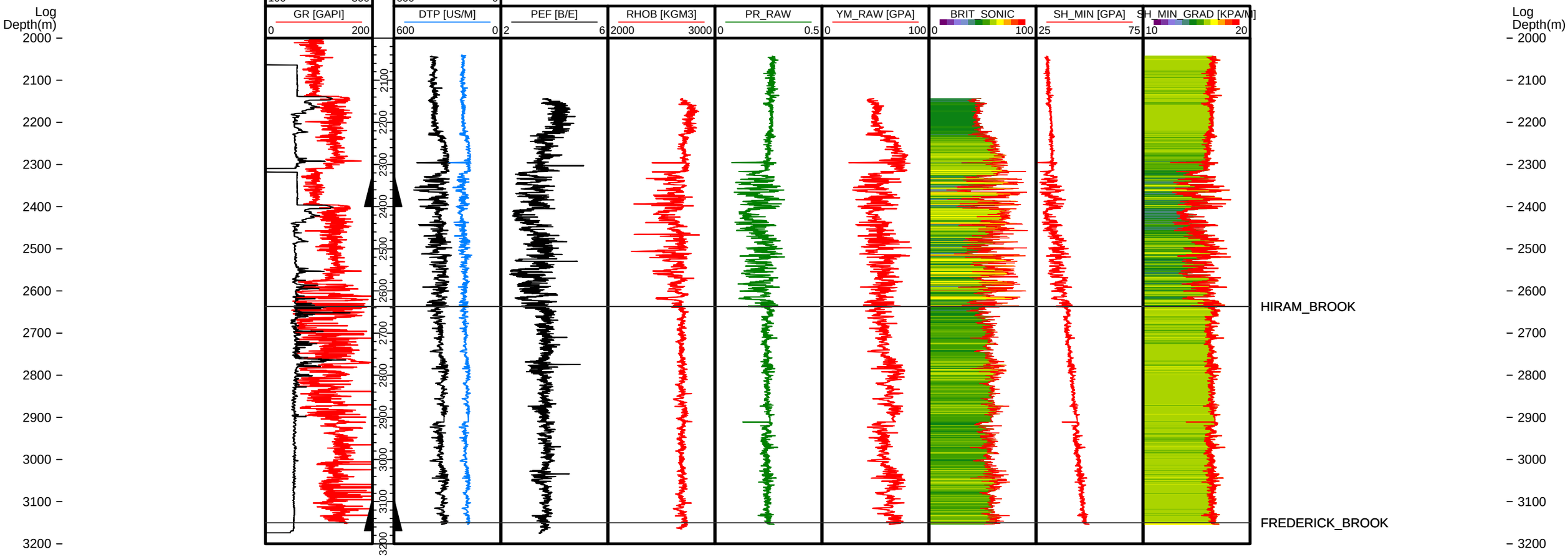

HS=1

PETRA 8/8/2016 1:39:12 PM

100

J-47

HCAL [MM] 100 300
DTS [US/M] 600 0
GR [GAPI] 0 200
DTP [US/M] 600 0
PEF [B/E] 2 6
RHOB [KGM3] 2000 3000
PR_RAW 0 0.5
YM_RAW [GPA] 0 100
BRIT_SONIC 0 100
SH_MIN [GPA] 0 50
SH_MIN_GRAD [KPA/M] 10 20

Log Depth(m)

1700 1800 1900 2000 2100 2200 2300 2400 2500 2600 2700 2800 2900 3000 3100 3200 3300 3400 3500 3600

HIRAM_BROOK

FREDERICK_BROOK

HS=1

PETRA 8/8/2016 1:40:28 PM

J-65

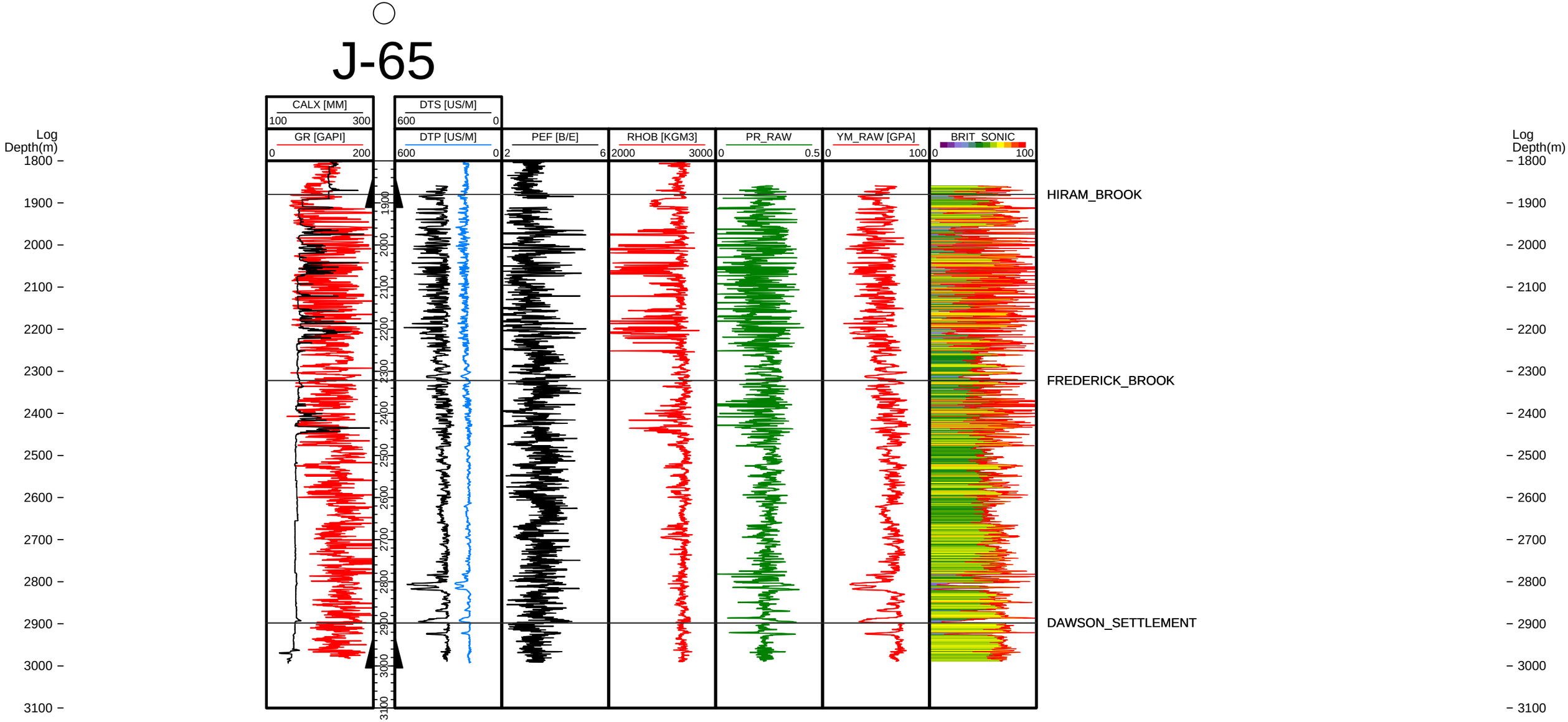

HS=1

PETRA 8/8/2016 1:50:13 PM

J-66

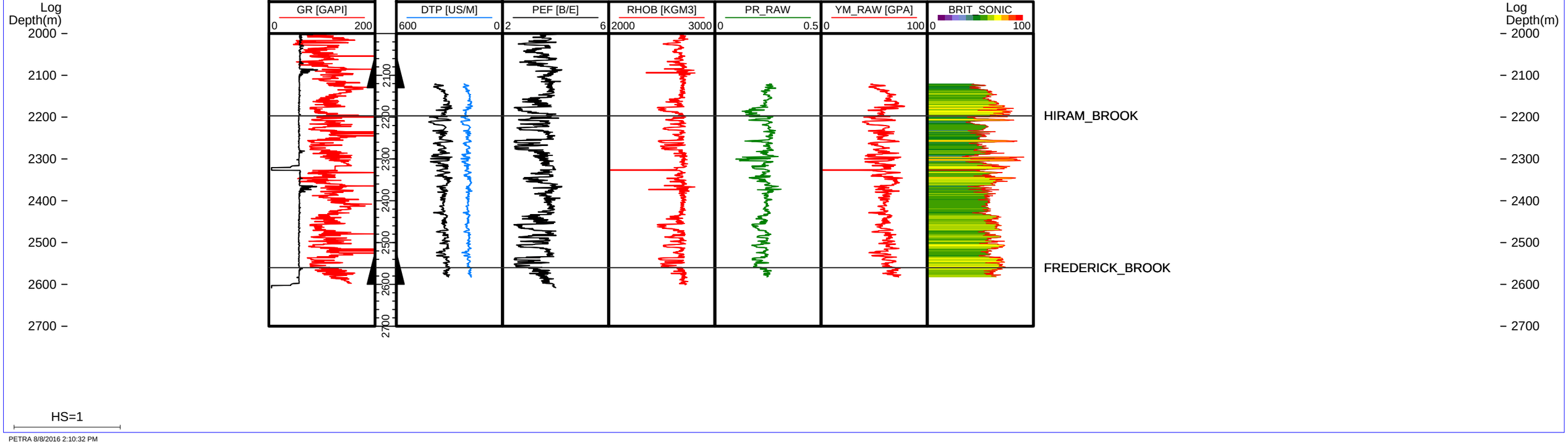

HS=1

PETRA 8/8/2016 2:10:32 PM

J-67

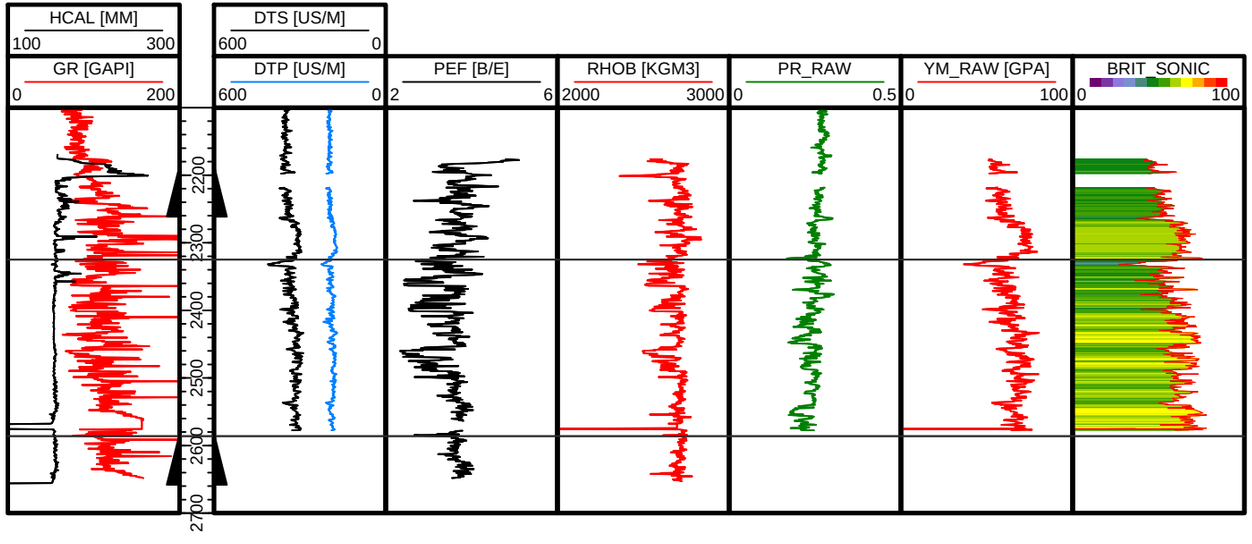

Log Depth(m)

2100 – 2200 – 2300 – 2400 – 2500 – 2600 – 2700

HIRAM_BROOK

FREDERICK_BROOK

Log Depth(m)

2100 – 2200 – 2300 – 2400 – 2500 – 2600 – 2700

HS=1

K-48

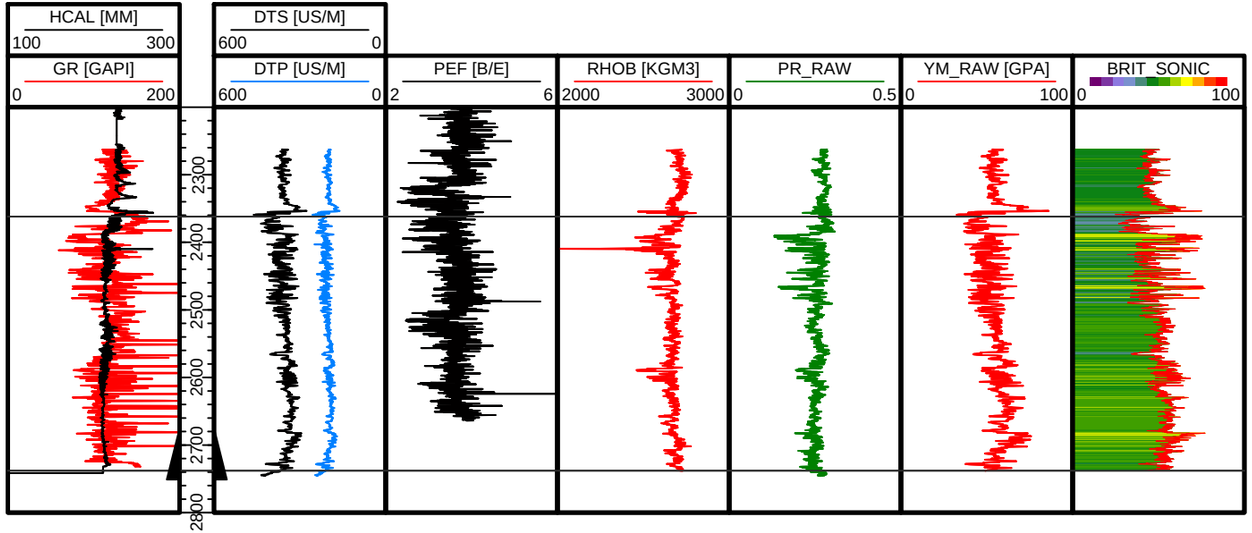

Log Depth(m)

2200
2300
2400
2500
2600
2700
2800

HIRAM_BROOK

FREDERICK_BROOK

Log Depth(m)

2200
2300
2400
2500
2600
2700
2800

HS=1

K-57

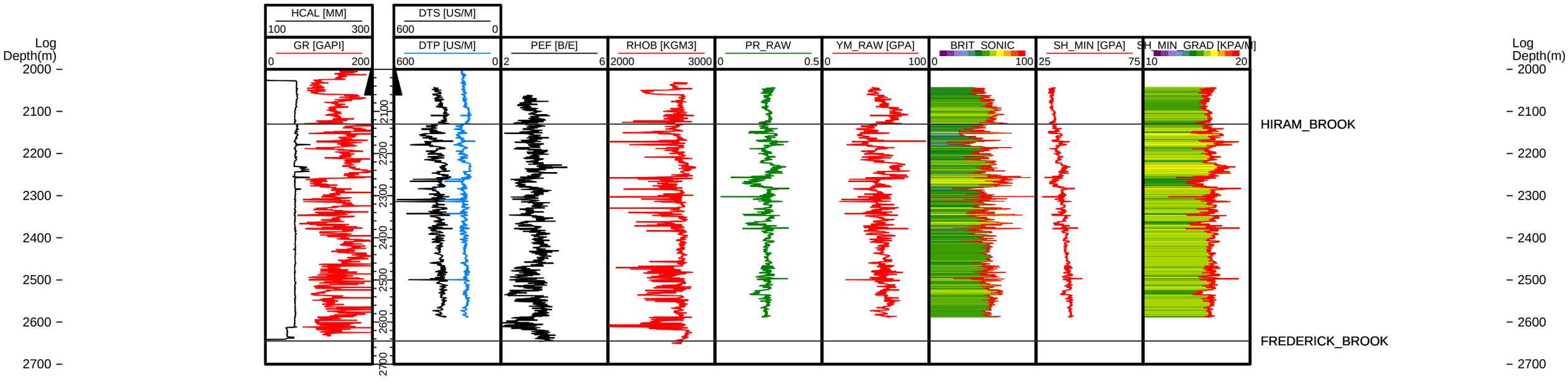

HS=1

PETRA 8/8/2016 1:41:39 PM

K-66

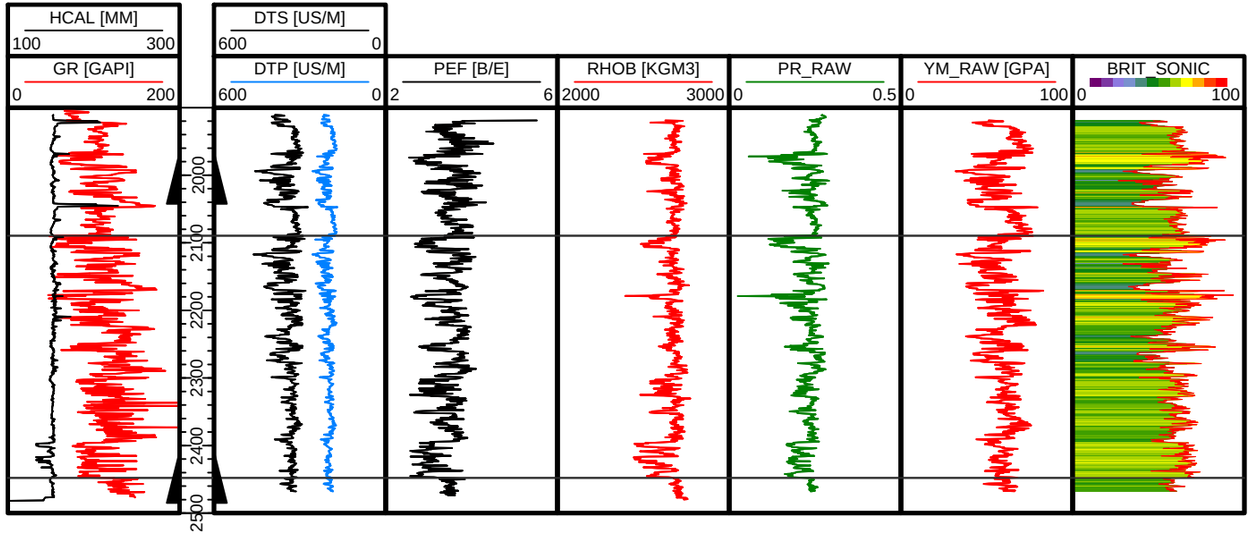

Log Depth(m)

1900
2000
2100
2200
2300
2400
2500

HIRAM_BROOK

FREDERICK_BROOK

Log Depth(m)

1900
2000
2100
2200
2300
2400
2500

HS=1

L-38

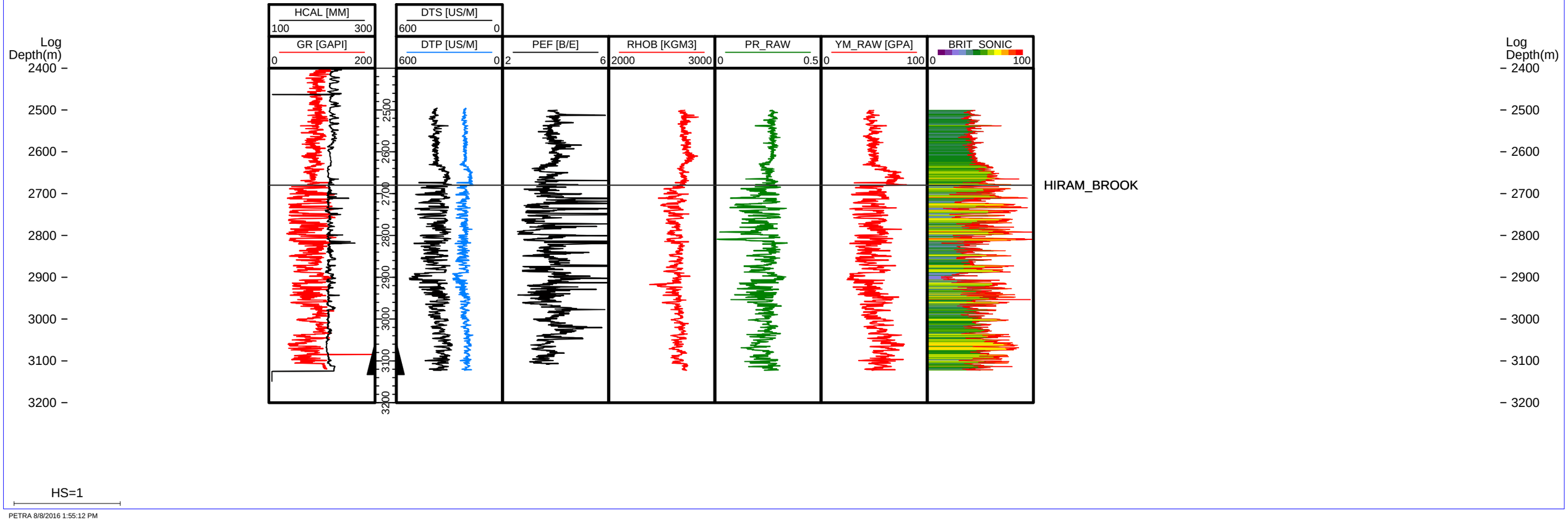

HS=1

PETRA 8/8/2016 1:55:12 PM

M-66

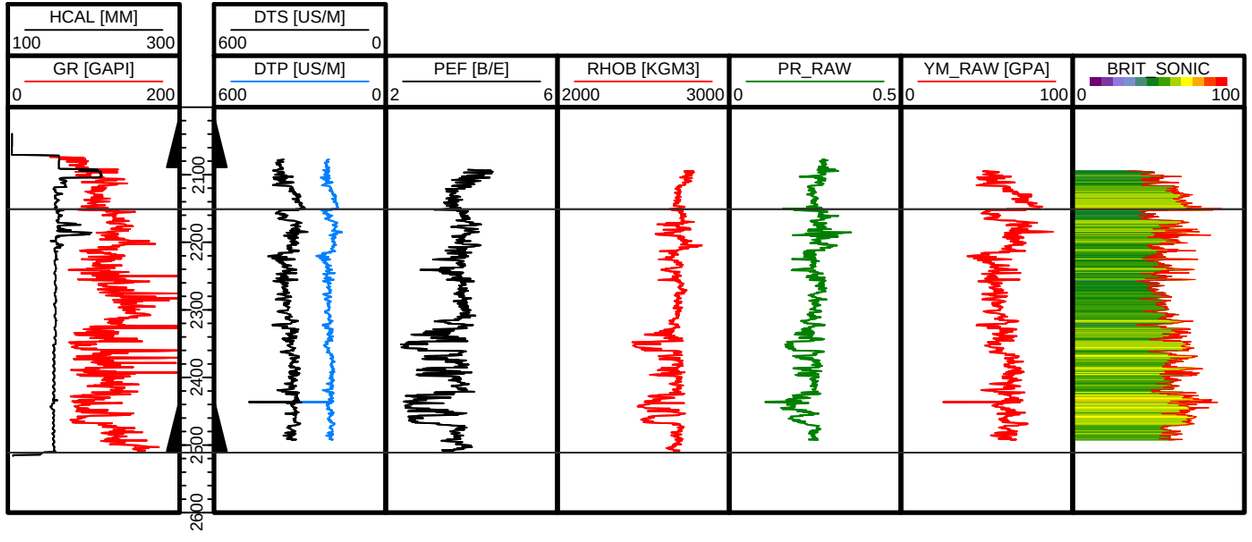

Log Depth(m)

2000
2100
2200
2300
2400
2500
2600

HIRAM_BROOK

FREDERICK_BROOK

Log Depth(m)

2000
2100
2200
2300
2400
2500
2600

HS=1

PETRA 8/8/2016 2:12:54 PM

McC1

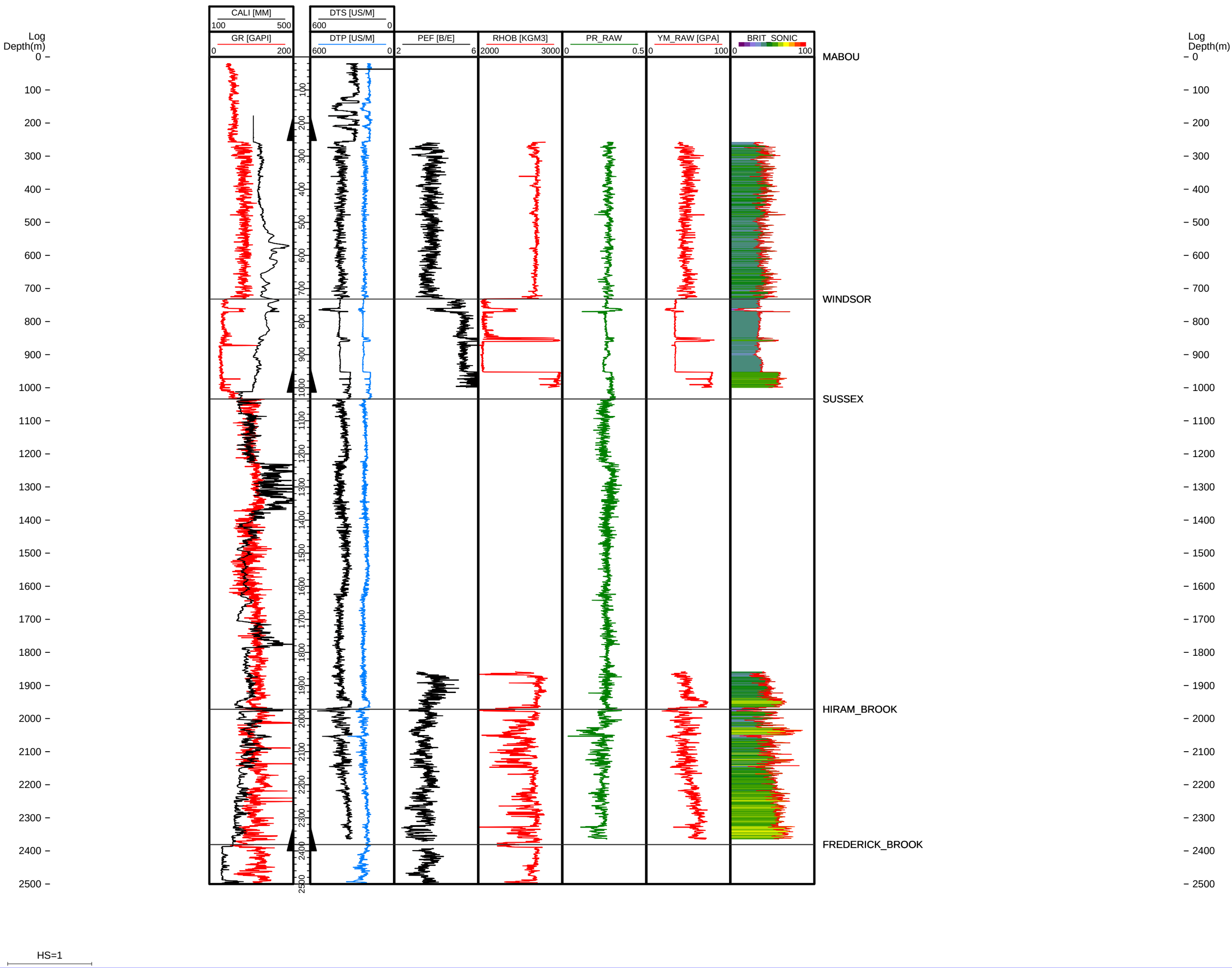

HS=1

PETRA 8/8/2016 2:15:41 PM

N-11

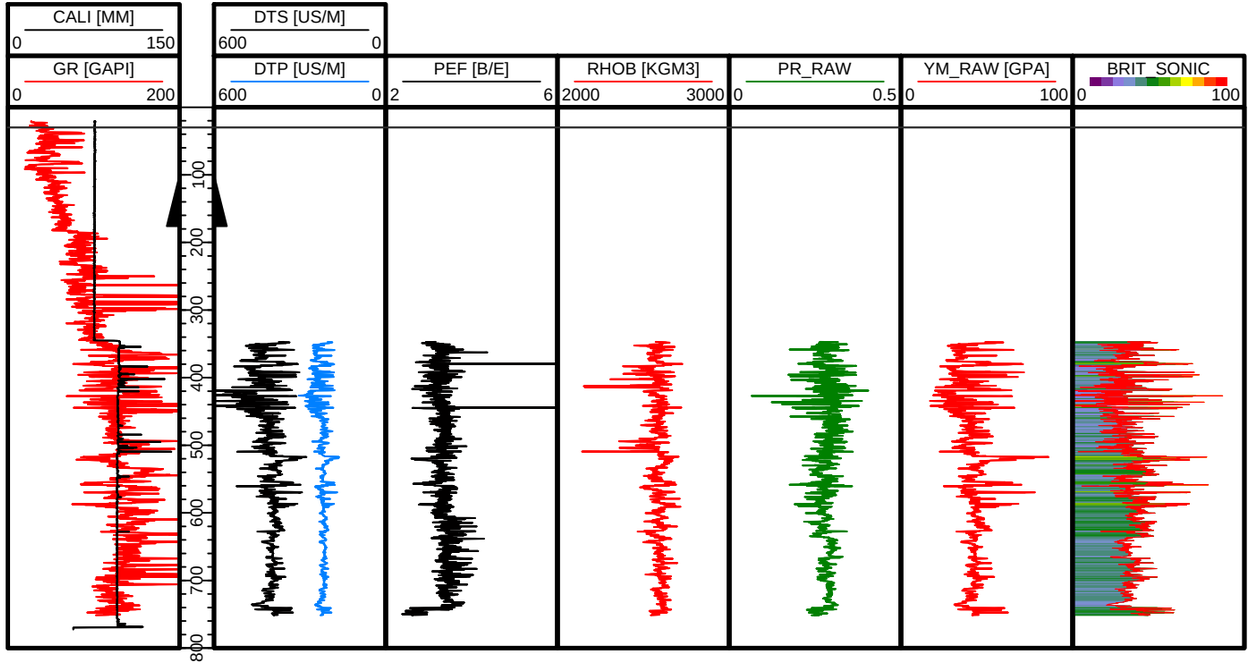

Log Depth(m)

0
100
200
300
400
500
600
700
800

Log Depth(m)

0
100
200
300
400
500
600
700
800

HS=1

PETRA 8/8/2016 1:59:42 PM

O-66

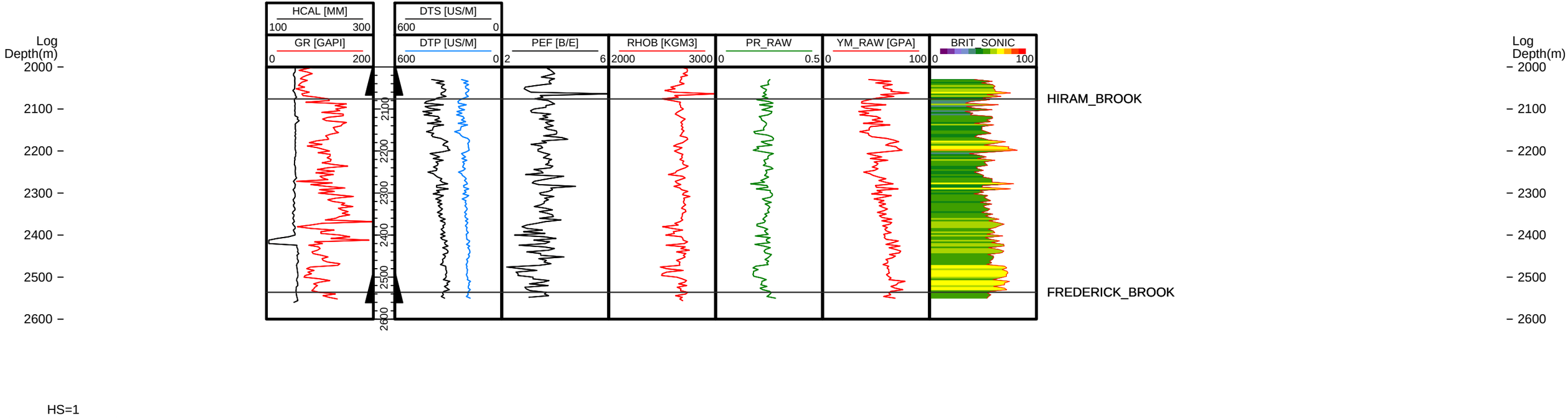
HCAL [MM]
100
300
DTS [US/M]
600
0
GR [GAPI]
0
200
DTP [US/M]
600
0
PEF [B/E]
2
6
RHOB [KGM3]
2000
3000
PR_RAW
0
0.5
YM_RAW [GPA]
0
100
BRIT_SONIC
0
100
Log Depth(m)
2000
2100
2200
2300
2400
2500
2600
HIRAM_BROOK
FREDERICK_BROOK
Log Depth(m)
2000
2100
2200
2300
2400
2500
2600
HS=1

P-47

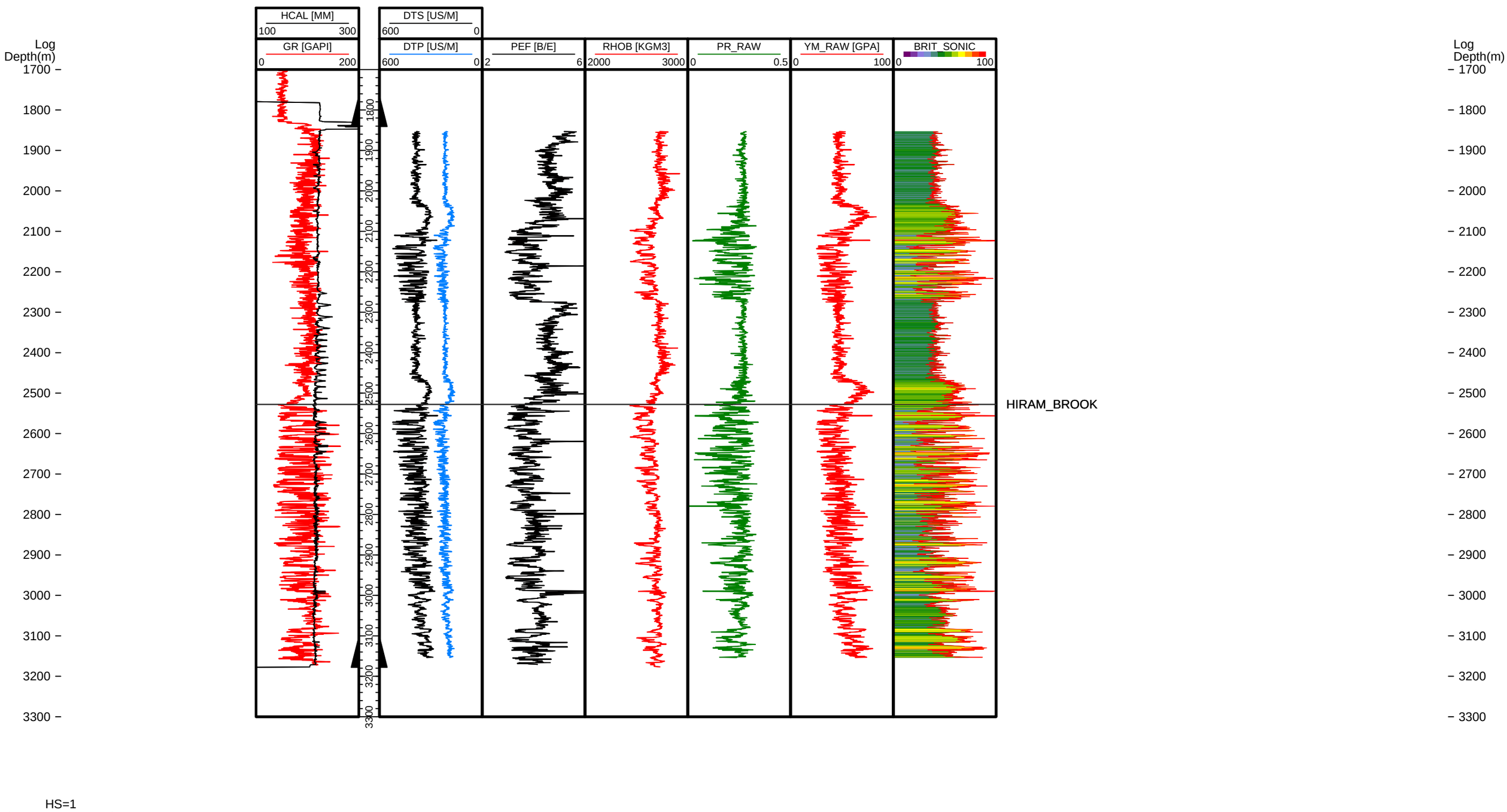

HS=1

PETRA 8/8/2016 2:01:11 PM

P-56

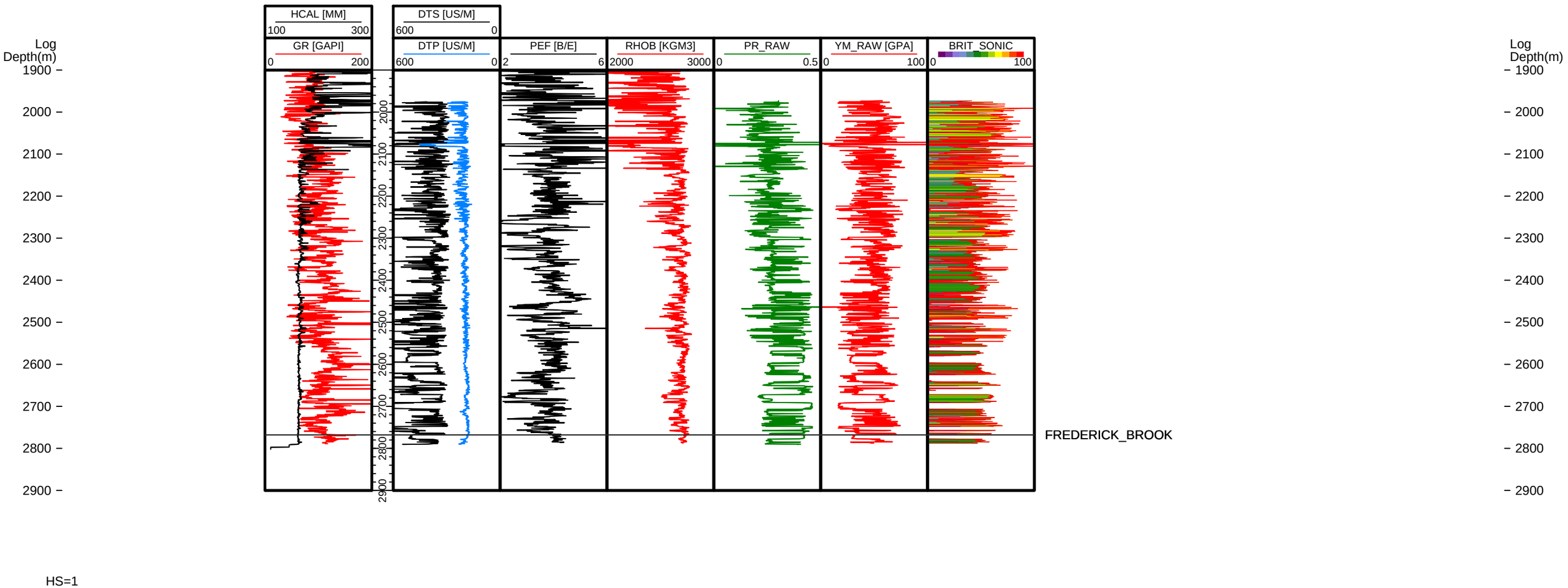

HS=1

PETRA 8/8/2016 2:01:51 PM

P-66

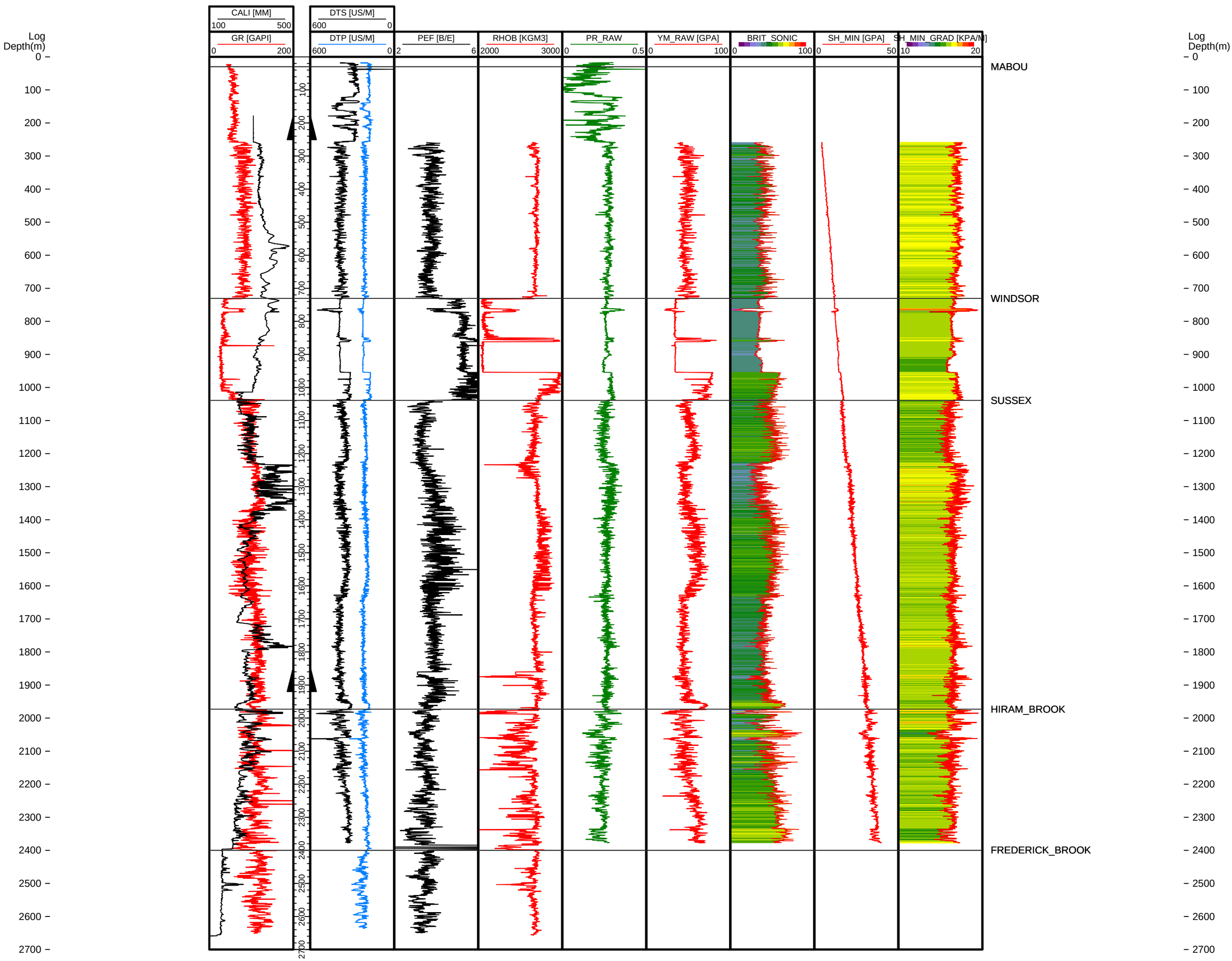

HS=1

PETRA 8/8/2016 1:43:23 PM

Appendix III :

Logs and geomechanical parameters calculated from a synthetic S wave

– Wells –

C-75, D-66, DeM1, J-65 and M-59

C-75

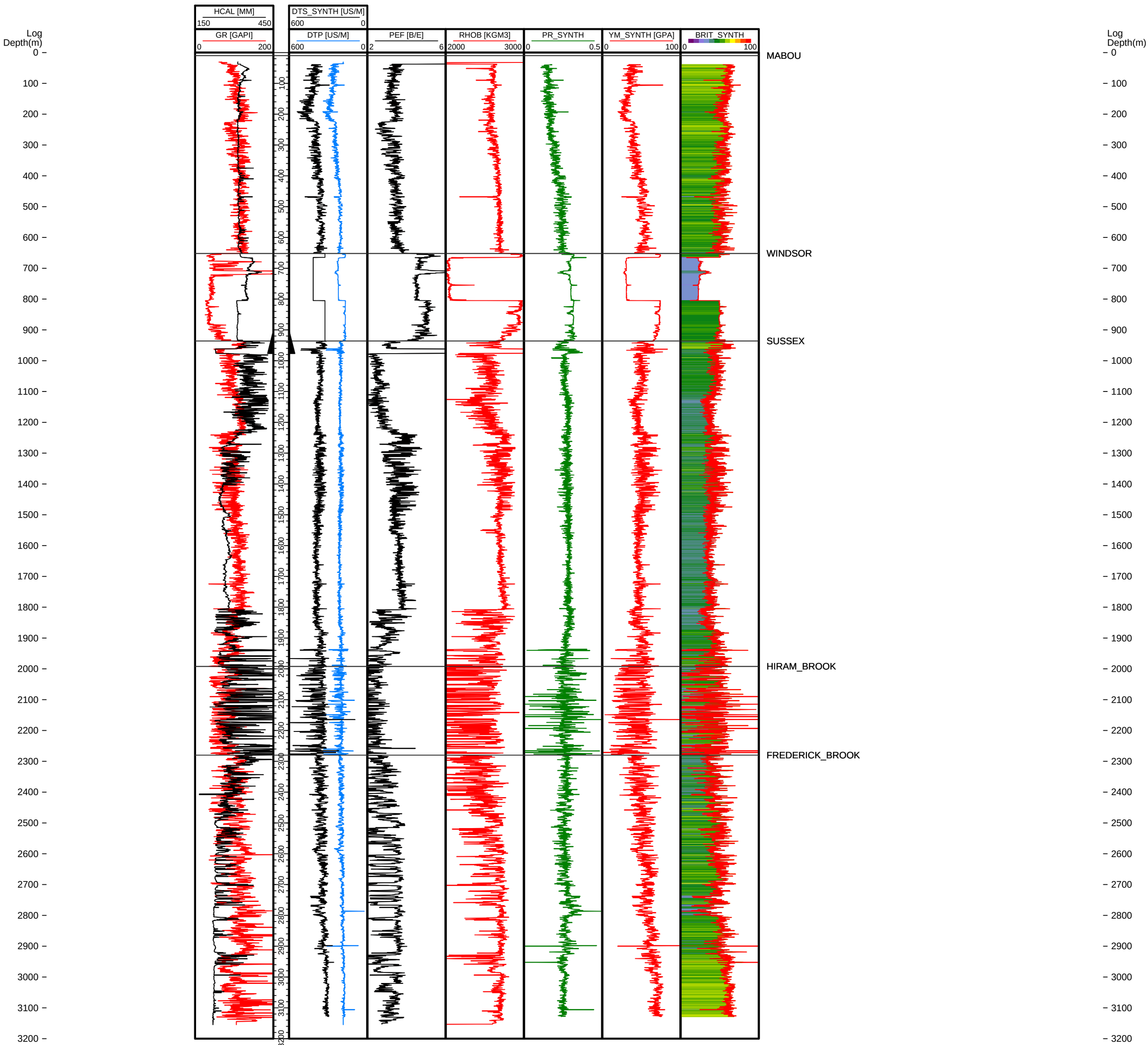
HCAL [MM]
150
450
GR [GAPI]
0
200
DTS_SYNTH [US/M]
600
0
DTP [US/M]
600
0
PEF [B/E]
2
6
RHOB [KGM3]
2000
3000
PR_SYNTH
0
0.5
YM_SYNTH [GPA]
0
100
BRIT_SYNTH
0
100
Log Depth(m)
MABOU
WINDSOR
SUSSEX
HIRAM_BROOK
FREDERICK_BROOK

HS=1

D-66

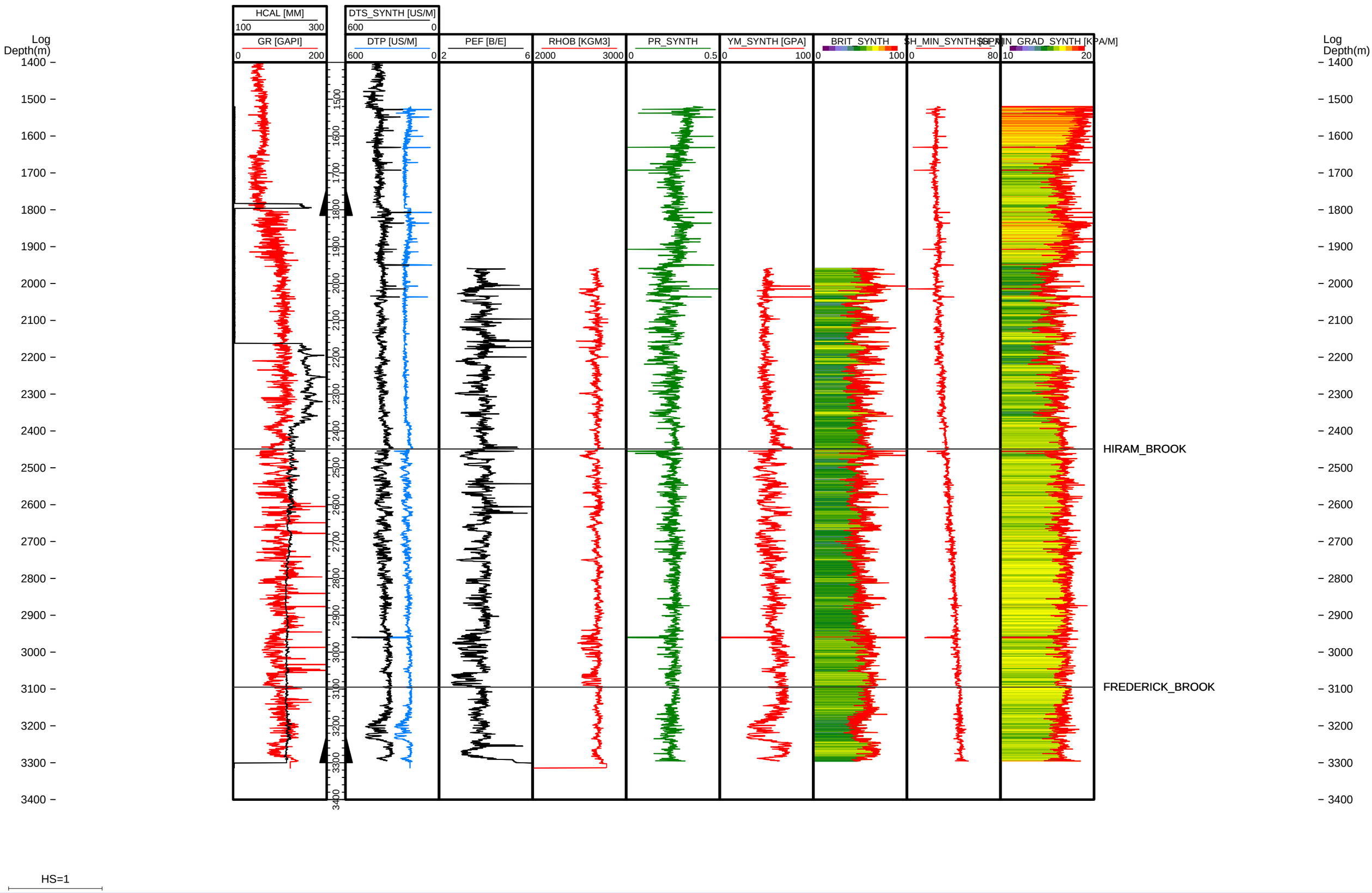
HCAL [MM]
100 300
DTS_SYNTH [US/M]
600 0
GR [GAPI]
0 200
DTP [US/M]
600 0
PEF [B/E]
2 6
RHOB [KGM3]
2000 3000
PR_SYNTH
0 0.5
YM_SYNTH [GPA]
0 100
BRIT_SYNTH
0 100
SH_MIN_SYNTH [GPA]
0 80
MIN_GRAD_SYNTH [KPA/M]
10 20
Log Depth(m)
1400
1500
1600
1700
1800
1900
2000
2100
2200
2300
2400
2500
2600
2700
2800
2900
3000
3100
3200
3300
3400
HIRAM_BROOK
FREDERICK_BROOK

HS=1

DeM1

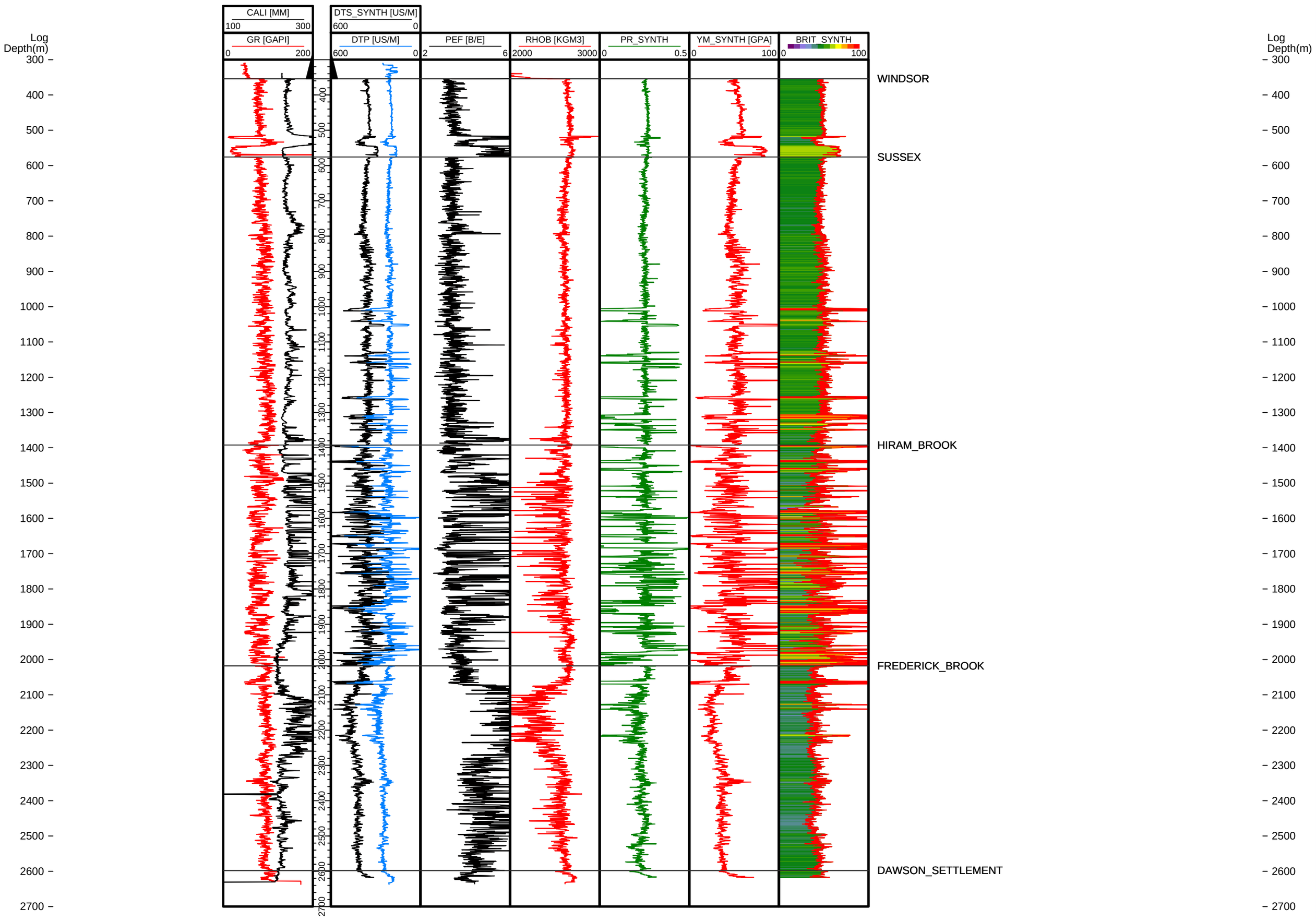

HS=1

PETRA 8/8/2016 3:49:47 PM

J-65

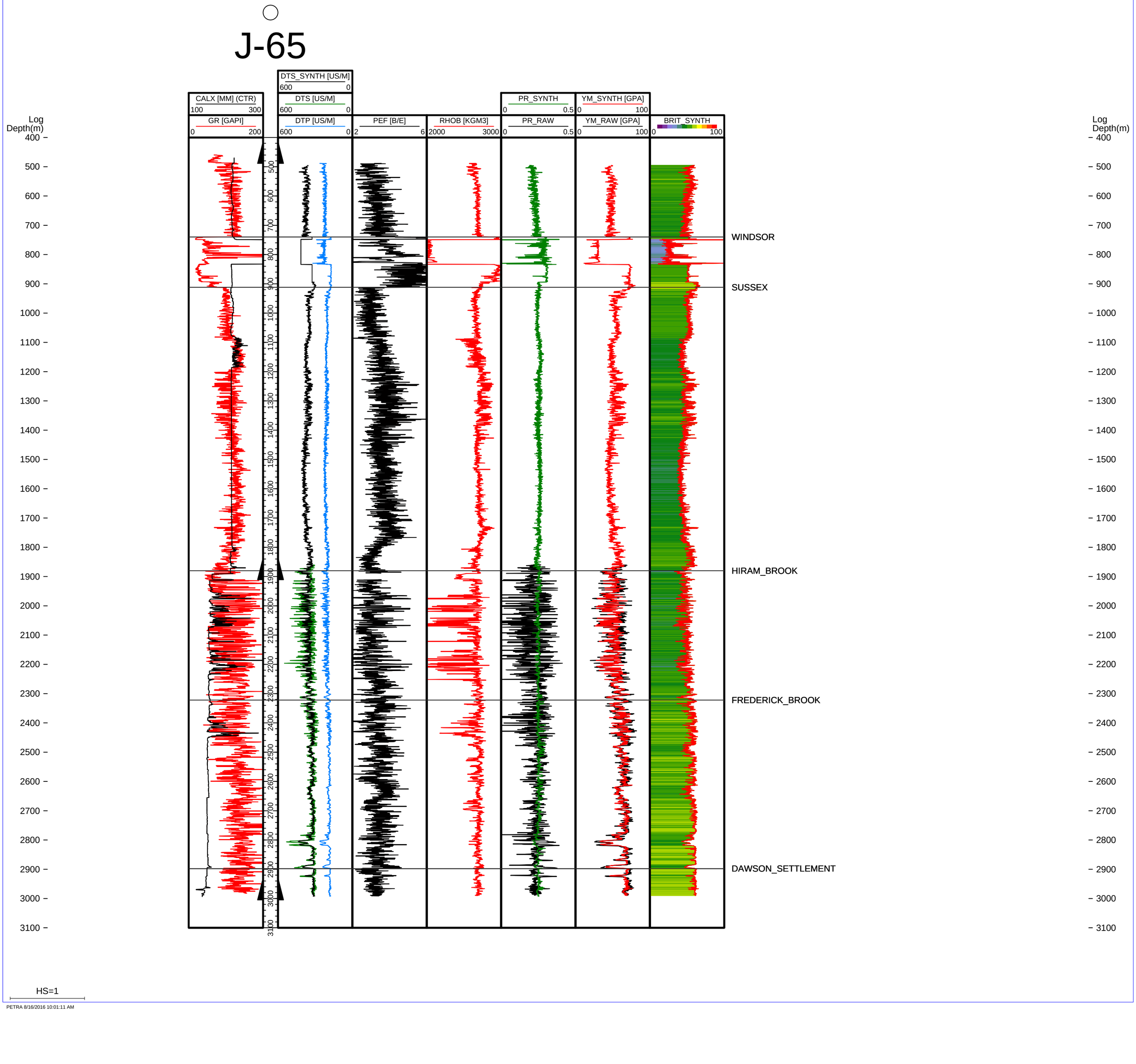

HS=1

PETRA 8/16/2016 10:01:11 AM

M-59

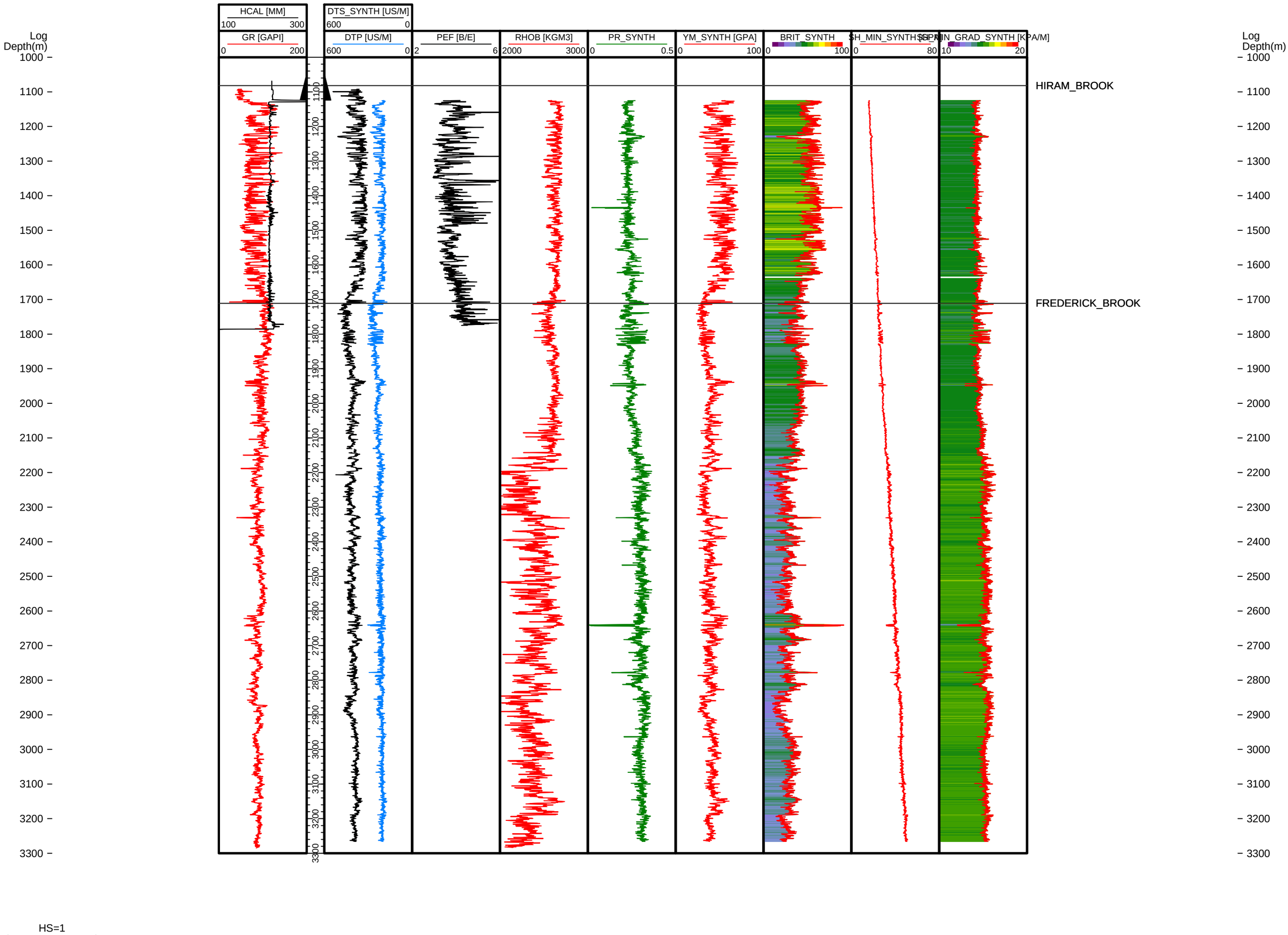
HCAL [MM]
100 300
GR [GAPI]
0 200
DTS_SYNTH [US/M]
600 0
DTP [US/M]
600 0
PEF [B/E]
2 6
RHOB [KGM3]
2000 3000
PR_SYNTH
0 0.5
YM_SYNTH [GPA]
0 100
BRIT_SYNTH
0 100
SH_MIN_SYNTH [GPA]
0 80
MIN_GRAD_SYNTH [KPA/M]
10 20
Log Depth(m)
HIRAM_BROOK
FREDERICK_BROOK
1000
1100
1200
1300
1400
1500
1600
1700
1800
1900
2000
2100
2200
2300
2400
2500
2600
2700
2800
2900
3000
3100
3200
3300

HS=1